Technical Report

TR-10-28

Design analysis report for the canister

Heikki Raiko, VTT

Rolf Sandström, Materials Science and Engineering, KTH

Håkan Rydén, Magnus Johansson
Svensk Kärnbränslehantering AB

April 2010

Svensk Kärnbränslehantering AB
Swedish Nuclear Fuel
and Waste Management Co

Box 250, SE-101 24 Stockholm
Phone +46 8 459 84 00

ISSN 1404-0344
SKB TR-10-28

Design analysis report for the canister

Heikki Raiko, VTT

Rolf Sandström, Materials Science and Engineering, KTH

Håkan Rydén, Magnus Johansson
Svensk Kärnbränslehantering AB

April 2010

Contents

1 Introduction

1.1 Purpose and scope

This design analysis report (DA) is the summary of the mechanical analyses of the canister. **The main effort is put into the analyses for repository conditions,** although the DA also covers analysis of loads during lifting of the canister via the copper lid**. Other loads that the canister may be subjected to during handling in the facilities or during transportation to the final repository remain to be specified and analysed.** The overall purpose of the report is to demonstrate compliance with specified design requirements for the mechanical integrity of the canister in a KBS 3 repository utilized with the reference design as specified in /SKB 2009/. The report is written with the only purpose to be a reference report to the production line report for the canister section verification of reference design.

The relevant loading types are defined in the updated design premises report /SKB 2009/. The design premises report defines the following:

- *The canister shall withstand an isostatic load of 45 MPa, being the sum of maximum swelling pressure and maximum groundwater pressure.*
- *The canister is surrounded by a buffer with a density less than 2,050 kg/m^3, corresponding to swelling pressures up to 15 MPa.*
- *The copper corrosion barrier should remain intact after a 5 cm shear movement at a velocity of 1 m/s for buffer material properties of a 2,050 kg/m^3 calcium bentonite, for all locations and angles of the shearing fracture in the deposition hole, and for temperatures down to 0°C. The insert should maintain its pressure-bearing properties against isostatic loads.*

The canister may be subjected to asymmetric loads during different phases in the repository evolution. This could temporarily occur due to uneven water saturation in the buffer and lack of straightness of the deposition hole. Permanent asymmetric loads may occur due to an uneven buffer density distribution after water saturation in combination with lack of straightness of the deposition hole. Pessimistic assessment of asymmetric loads are useful for confirmation of the isostatic load case but have too low probability to be considered to coincide with the shear load case.

The design basis cases also depend on the time scale considered. For times longer than 100,000 years the recommendations referenced in /SKB 2009/ state that: "*A strict quantitative comparison of calculated risk in relation to the criterion for individual risk in the regulations is not meaningful. The assessment of the protective capability of the repository should instead be based on reasoning on the calculated risk together with several supplementary indicators of the protective capability of the repository such as barrier functions, radionuclide fluxes and concentrations in the environment.*"

The accumulated likelihood of the occurrence of detrimental events like large earthquakes and major ice sheets increases with time. The detrimental effects of some continuous processes, like canister corrosion, also increase with time. In /SKB 2009/ it is stated that a strict application of the risk criterion is relevant in a 100,000 year time scale. However, as also stated the principle of best available technique (BAT) applies over the one million year assessment time. Therefore, the one million year time scale was considered when the design premises where developed.

This does, however, not mean that the repository must be designed to withstand all loads identified in the safety assessment in a one million year perspective. The design must be such that the requirements on risk and BAT are met and this may well be compatible with the occurrence of some detrimental effects on the barriers during the assessment period.

The expected environmental conditions used for design verification of the canister are presented in 2.2. In there, all the possible processes are discussed and the relevant load processes are identified. Accordingly, the mechanical loads are then processed in a series of loading, strength and fracture resistance analyses and finally summarised in this report. The flowchart of the activities done in the design analysis is shown in Figure 1-1.

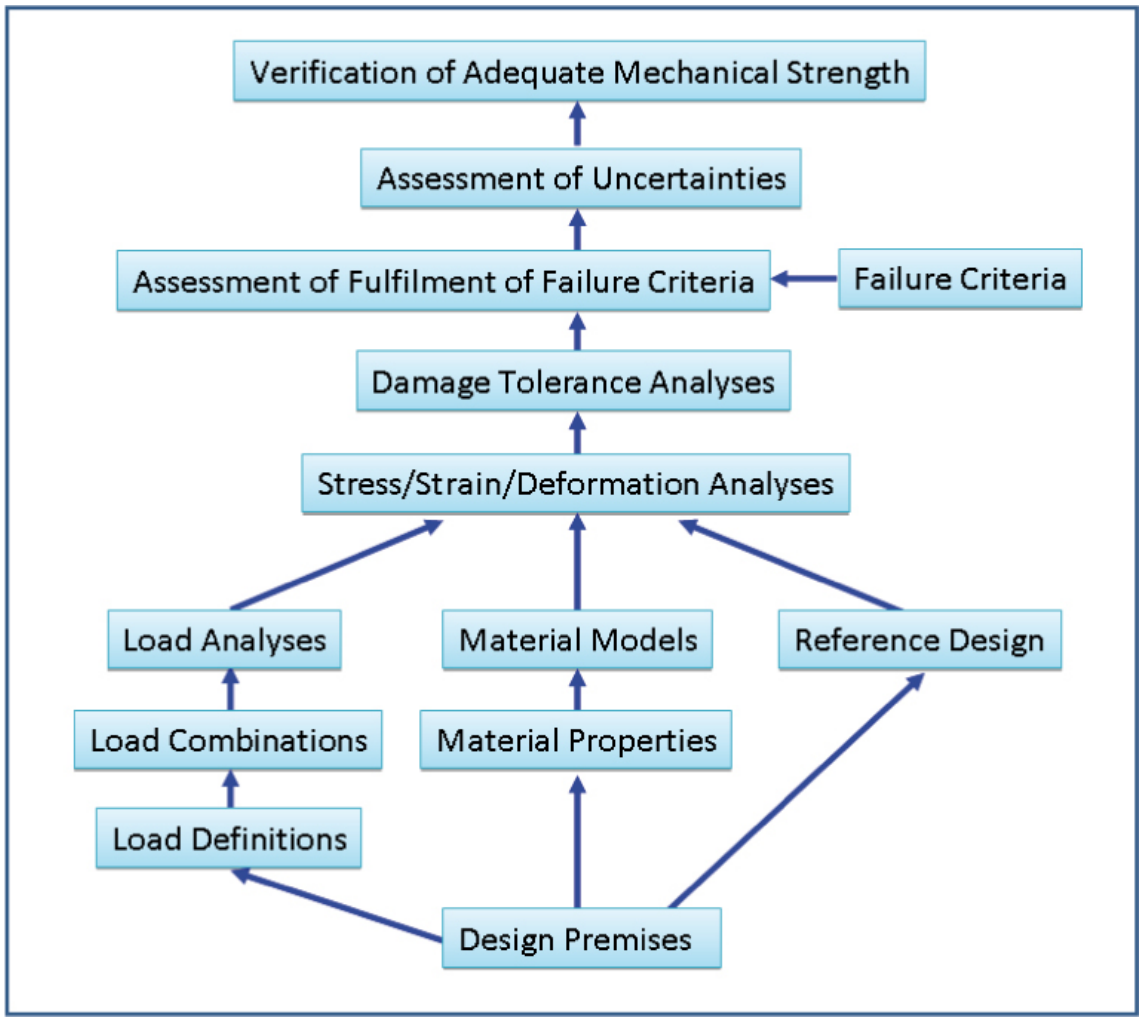

Figure 1-1. *The relations between design premises, initial data, modelling, results and assessment in the canister design analysis. The same scheme is valid for all load cases.*

The main safety function of the canister is to ensure a prolonged period of complete containment of radionuclides. This safety function rests first and foremost on the mechanical strength of the canister insert and the corrosion resistance and mechanical endurance of the copper surrounding it.

The canister will be subjected to mechanical loads during both handling and in the final repository. It is essential that it will maintain its barrier function during and after application of these loads. This report gives an account for the verifying calculations to give evidence that the design verification of the reference canister is sufficient.

The analyses presented in this report cover mechanical strength aspects of the canister design. Consideration of the chemical integrity and other possible degradation mechanisms like radiation embrittlement are given in the references listed in /SKB 2009/.

1.2 The canister in general

The canister is designed to keep the spent nuclear fuel isolated from the surrounding environment for at least 100,000 years. Details of the material properties used, and the canister design, are given in Section 4 and 5 in this report. A short summary is given below.

1.2.1 Canister design

The canister consists of two main components; a load bearing insert with channels for the spent fuel and an outer corrosion barrier. The materials are chosen based on respective component functions. The material selected for the corrosion barrier is Cu-OFP (oxygen free copper doped with 30–100 ppm phosphorus) that has excellent corrosion resistance under repository conditions and high ductility which will maintain its integrity under the loads that are expected in the repository. The material in the insert is nodular cast iron with good casting properties and sufficient mechanical strength for the application. The casting process makes it possible to fill the void space between the fuel channels thus avoiding the risk for criticality even in the case of water filling of the canister. The design of the canister allows that a load bearing steel lid can be easily mounted during the encapsulation process and that the canister can be sealed by joining the copper lid to the copper shell by Friction Stir Welding (FSW).

Within the Swedish nuclear programme two main types of fuel elements exist, BWR- and PWR-elements. These are geometrically different which results in the need for two different designs of the insert as shown in Figure 1-2. The channels in the inserts are made by using steel tubes. To complete the insert a steel lid is bolted to the top after the fuel elements have been put in place.

1.2.2 Canister materials

The materials for the canister need to be well characterised, easy to manufacture and available in adequate quantities. The insert shall be strong enough to withstand both external pressure and bending loads. On the other hand the insert must be ductile enough to tolerate imposed strains. Geometric stress concentrations and material imperfections caused by possible material defects must not lead to failure. The copper shell shall maintain its isolation and containment of the radioactive contents of the canister for a very long period. Presumably, the corrosion resistance and the mechanical endurance must be especially high.

Pure copper is a natural element that has shown in nature (natural analogies) that it can survive in comparable circumstances for millions of years. The copper's capacity for deformation and strain is also excellent and that is why it has been selected for the material of corrosion shield of the canister.

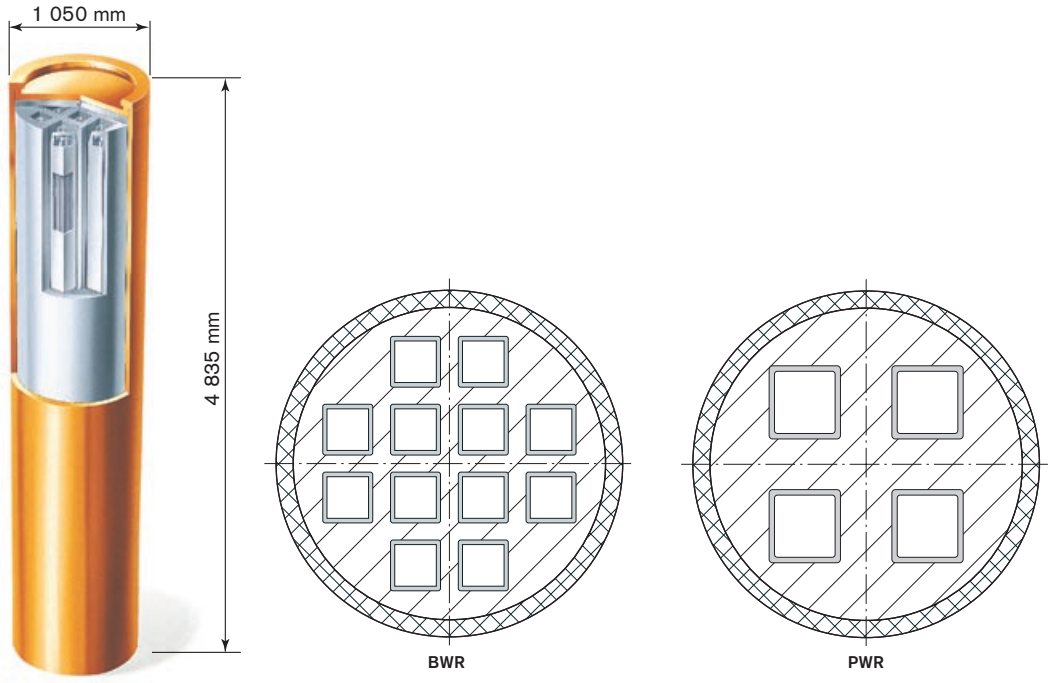

Figure 1-2. *Left: general design of the canister showing the insert and the copper shell. Right: the difference between BWR- (left) and PWR-inserts (right).*

The copper is high conductivity oxygen free copper micro alloyed with 30–100 ppm phosphorus to improve the creep properties /Andersson-Östling and Sandström 2009/**.** The main features of the copper specification are as follows: the material for copper canisters shall fulfil the specification in EN 1976:1998 for the grades Cu-OFE or Cu-OF1 with the following additional requirements for the allowable amounts of some elements: O < 5 ppm, P 30–100 ppm, H < 0.6 ppm, S < 8 ppm. In addition, the grain size of the copper is limited to < 800 µm to ensure sufficient creep properties. However, from a quality control point of view the grain size is currently limited to < 360 µm to avoid excessive attenuation in ultrasonic testing (this latter requirement is still under evaluation).

The cast iron material composition of the insert is specified only for the content of copper to avoid risk for radiation embrittlement. The content of copper shall therefore not exceed 0.05%. During the development of the casting process for the nodular cast iron inserts the standard requirements in EN 1563 grade EN-GJS-400-15U have been used regarding mechanical properties. Some additional requirements for mechanical properties, material testing and microstructure are defined in /SKB 2009/ and in /SKB 2010/.

The steel lid of the insert is made of structural steel plate according to EN 10025 S355J2G3 or similar grade with at least the same tensile strength and ductility, in the as-hot-rolled or normalised condition. Formally the lid steel is specified in more detail in /SKB 2010/.

The square tubes used in the welded cassette to form the openings for fuel elements in the insert are made of standard type hollow steel sections made either of cold formed steel plates (with longitudinal weld) or by hot formed steel (seamless tubes). The material for hot formed VKR (RHS) square hollow sections shall fulfil the requirements in EN 10210-1 S355J2H concerning chemical composition and mechanical properties (R_{eL}, R_m, A_5). And, alternatively, the material for cold formed KKR square hollow sections shall fulfil the requirements in EN 10219-1 S355J2H concerning chemical composition and mechanical properties (R_{eL}, R_m, and A_5).

The material for steel plates and flat bars used as spacers in the cassette (within the cast iron insert) shall fulfil the requirements in EN 10025 S235JRG2 or similar.

2 Loads

Loads will be introduced to the canister during handling, during operation as well as in the repository after deposition. The majority of the loads associated with the canister arise from anticipated conditions in the repository. These loads, which will affect the canister during its entire lifetime, are presented in Section 2.2.

Before the canister reaches its final position in the repository it will be lifted a number of times through the lifting shoulder of the copper lid. This must be done safely without any risk of rupture in the copper shell. The operational handling loads are presented in Section 2.1.

In addition to the loads that affect the entire canister some loads that occur during manufacturing of the canister and the canister components might be of interest. This especially applies to loads causing residual stresses in the components as they might influence the properties of the canister. Residual stresses in the copper shell can be created both during hot forming (this can be avoided by controlling the forming temperature) as well as during machining. For the insert residual stresses appear during the solidification and cooling process after casting.

2.1 Operational handling loads

The canister shall be so designed and handled that the postulated operational conditions during encapsulation, storing, transport and deposition will not cause any damage or change in properties that may affect the canister's ability to isolate its contents from the outside environment for the period of analysis.

During normal operation, the canister is lifted a few times from the lifting shoulder of the copper lid. The gripping is made with a special device that gives a secured grip and a widely distributed surface load, so that the contact pressure does not exceed the copper strength. The payload of the gripper is the total weight of the canister and the contents. For lifting operations an additional dynamic factor is added according to the lifting device design verification practice and respective standards. In addition to normal operation, some effects of disturbances are also analysed, such as operation of emergency braking system of the lifting device in the canister installation vehicle. A design verification analysis of the copper shell, especially the lid, is presented in 6.2.8. The analysis also covers the weakening effect of possible material imperfections in the load carrying area.

The governing load cases for the lifting operation of the canister are, according to /SKBdoc 1206868/:

1. While the canister is being lowered at a speed of 0.033 m/s, an emergency stop of the winch occurs, leading to deceleration of the canister to a standstill within 0.5 s. The retardation leads to increased load on the canister. The load is calculated using basic equations of motion, where velocity $v = 0.033$ m/s, time $t = 0.5$ s, mass $m = 27{,}600$ kg and acceleration of gravity $g = 9.81$ m/s^2. This gives a force of $F = 273$ kN acting on the copper shell.
2. The winch lowering the canister is assumed to be faulty leading to lowering with a higher velocity equivalent to a free fall with $v = 11.80$ m/s. While the faulty winch is lowering the canister, an emergency stop occurs, leading to the same consequence as for load case 1, above. The load the copper shell is subjected to is defined according to the same equations, where now $v = 11.80$ m/s, $t = 0.5$ s, $m = 27{,}600$ kg and $g = 9.81$ m/s^2. This gives a force of $F = 922$ kN acting on the copper shell.

The handling and transportation system for the canister shall be designed in such way that the canister surface is not unacceptably damaged during handling and transport operations. The effects of possible local surface deformations such as scratches or bruises are assessed and discussed later in this report, in Section 6.2.9.

2.2 General loads in the repository

Mechanical **external loads** in the repository come from the natural environment and from the behaviour of the bentonite buffer.

The bentonite swelling pressure component can be somewhat unevenly developed and distributed. This is especially true during the beginning of the wetting phase, but also in saturated condition if the dimensions of the deposition hole and the density of the bentonite are varying. In earlier load specifications the unevenly distributed swelling loads were based on overly-conservative assumptions. They were not realistic, using extremely rigid supports; further the restraints assumed in the load specification were mechanically unfeasible in reality. The canister inside the bentonite buffer is loaded and supported by the bentonite that has the same swelling properties on the spots of postulated load and on the spot of postulated support or reaction force. Thus the maximum pressure acting on the canister surface inside the bentonite buffer is limited to the sum of hydrostatic pressure and the swelling pressure. Furthermore, the vector sum of loads and supporting reaction forces has to be statically in balance. A load scheme for uneven swelling of the buffer material that influences the canister, based on these specifications, is given in /SKBdoc 1206894/.

The main scenario for the canisters during the first tens of thousands of years is that the external hydrostatic pressure load is about 4 MPa and the bentonite swelling pressure is about 10 MPa, evenly distributed corresponding to a nominal density of 2,000 kg/m^3 and the temperature is 10 – 70°C. The maximum swelling pressure of bentonite depends on the chemical content of it. Originally, after installation the bentonite is sodium bentonite with the maximum swelling pressure of about 11 MPa and then later, after the sodium ions have been exchanged and replaced with calcium ions, which may occur in calcium-rich ground water, the maximum swelling pressure may be as high as 15 MPa. This ion-change is possible, but it takes a very long time. Thus the maximum swelling pressure has different values depending on time. This condition, with a total of 15 MPa external pressure, could be named as the “normal operation condition” of the canister in early periods, while analyses concerning the total isostatic load during glaciation or later use the higher assumption for swelling pressure. All the particular load cases that are analysed and summarised in this report represent some kind of upset condition.

One load case that will occur and affect all canisters in the repository is the glacial pressure load. This is associated with periods of time when a thick layer of ice covers the area where the repository is located.

In very rare cases, the canister can be loaded due to shear type rock movements, if the shear plane happens to intersect the deposition hole and the shear amplitude is large enough.

Some processes taking place inside the canister may cause **internal loads** in the canister structure. This may be from, for example, gas production from corrosion processes or from radioactive decay of the fuel. These are handled as a part of the long-term safety assessment and are shown to be negligible. Also, thermal stresses from the behaviour of the bi-metallic canister structure generate potential internal loads, as do the possible residual stresses in the material originating from manufacture. The exact definition of the gap and gap tolerances between the insert and the copper shell guarantees that the loose structures do not load each other by thermal deformation loads during thermal evolution. The effect of residual stresses is discussed more in Section 6.2.10 for FSW-welds in copper and in Section 7.3.1 for cast iron.

Table 2-1 describes the evolution of the canister in repository in relation to time, temperature, saturation, bentonite swelling, hydrostatic pressure and earthquake induced rock shear load cases. Loads affecting the copper shell or cast iron insert are considered separately.

Table 2-1. The canister loads extracted from postulated repository evolution. Loads that may act simultaneously shall be combined. Coloured boxes correspond to the possible periods for the load case (1…5) in question. Clarifying comments in Table 2-1 are given in italic letters.

Repository evolution phase **Years after closure of the repository**		**Water saturation** **0–100 y.**	**Temperate** **100 y.–20 ky.**	**Permafrost** **20 ky.–50 ky.**	**Glacial** **50 ky.–60 ky.**	**Subsequent permafrost and glacial periods** **60 ky. → 1 My.**
Canister temperature (°C)		**< 125/100 (Fe/Cu)**	**20 < T < 125/100**	**0 < T < 20**	**0 < T < 20**	**0 < T < 20**
Load #)	**Deformation rate**					
1) Asymmetric loads due to uneven water saturation and imperfections in deposition hole geometry. No simultaneous hydrostatic pressure. Uneven water saturation effects will decay later and be replaced by permanent loads 2) and 3) acting in saturated condition.	**Insert** Static	Water saturation effects are assumed to reach their maximum. Load 1) can create bending loads				
	Copper shell Creep or static	Load 1) can create compressive loads				
2) Permanent asymmetric loads due to uneven bentonite density and imperfections in deposition hole geometry.	**Insert** Static		Bending loads from load 2) and compressive isostatic loads from load 3)	Loads 2) and 3) are expected to act throughout the analysis period →		
3) Ground water hydrostatic pressure + even isostatic swelling pressure of bentonite.	**Copper shell** Creep or static		Uneven pressure loads from load 2) and isostatic loads from load 3)	Loads 2) and 3) are expected to act throughout the analysis period →		
4) Glacial pressure (additional isostatic pressure, only during glacial period).	**Insert** Static				Load 4) will cause additional isostatic pressure on insert	*Permafrost and glacial conditions are to reappear*
	Copper shell Creep or static				Load 4) will cause additional isostatic pressure on shell	
5) Shear load due to rock displacement. Amplitude is 5 cm, shear velocity 1 m/s.	**Insert** Short-time forced displacement				*Load 5) is primarily expected in pre- or post-glacial periods*	
	Copper shell Short-time forced displacement				*Load 5) is primarily expected in pre- or post-glacial periods*	

2.2.1 Asymmetric loads on the canister due to uneven water saturation of the buffer

This is identified as load case 1 in Table 2-1. During this first period the development in the near zone of the canister is of interest. Due to groundwater inlet in the deposition hole the bentonite will slowly saturate. Depending on where in the deposition hole the water will intrude, local swelling can occur and create temporary stresses in the canister. These swelling effects are analysed in combination with geometric imperfections of the deposition hole. The duration of this period will differ depending mainly on the rock geo-hydrology.

The reference bentonite quality MX-80 is a commercially sold sodium bentonite from Wyoming, USA. It is produced by American Colloid Co. and is a blend of several natural sodium dominated bentonites, dried and milled to millimetre-sized grains. In contact with calcium ions the sodium ions will be exchanged and after completed equilibrium MX-80 will become calcium converted MX-80 (called MX-80Ca).

The thermal evolution (time history of typical temperature in the near-field of canisters) will go in parallel with the swelling effects and reach its maximum after about 10 years and then slowly decay. For the canister the maximum temperature is less than 125°C and for the bentonite it is less than 100°C. From a fracture mechanics point of view the worst case is the lowest temperature. The temperature expectations are given in /SKB 2009/.

In order to analyse the complex problem of water inflow versus swelling, a simple approach is used whereby an upper bound estimate for the swelling distribution is defined and analysed. Results are summarized in Section 6.1.1. The full study for uneven swelling loads for disposal canisters is given in /SKBdoc 1206894/.

The load case below is the result of simplified assumptions during the complicated wetting phase and is probably conservative. Figure 2-1 illustrates the assumed uneven water flow distribution into the buffer from a vertical water-bearing fracture. The resulting swelling pressure on the canister may in the worst case be a triangular load distribution that in combination with a banana shaped hole described in the next section yields load case 1.

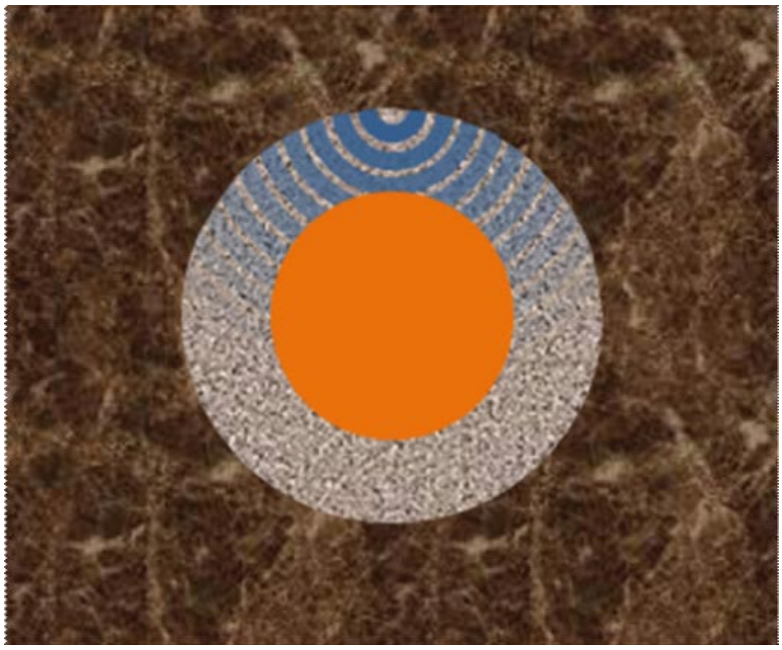

Figure 2-1. *Illustration of the wetting from an axial fracture in the bedrock intersecting the deposition hole. The wetting and resulting swelling pressure decreases with distance from the fracture. The water-feeding fracture can be long in axial direction.*

2.2.2 Asymmetric loads on the canister after buffer saturation

The uneven swelling pressure caused by uneven wetting is successively equalised, and ultimately the entire repository is water saturated. Finally the pressure will be the sum of the bentonite swelling pressure and the water pressure. These are the load cases 2 and 3 in Table 2-1. While the water pressure will be isostatic the bentonite density variations in combination with imperfections in the deposition hole can give an asymmetric pressure, which is considered to be permanent. In the same way as in the water saturation case, the worst situation for the canister in terms of swelling distribution is defined and analysed. As the start of the period in relation to the water saturation period end is not well defined, it is assumed that the insert temperature can be up to 125°C and that this temperature coincides with maximum swelling effects. In practice, when bentonite is saturated and the gap between buffer and canister has vanished, the thermal conductivity over the material interfaces and in the bentonite is increased and the maximum temperature in the canister surface is decreased by about 20°C, if compared to conditions before wetting. The actual temperature is expected to fall below 20°C much later under this period.

In order to evaluate the stresses in the most unfavourable case, an investigation of these cases has been done. Results are reported in Section 6.1.2. The full study for all asymmetric loads for disposal canisters is given in /SKBdoc 1206894/.

There are several factors that may affect the rock contour after drilling of the bore hole. The most important ones are the following:

- The inclination of the hole may differ from vertical.
- The deposition hole can be curved (banana shaped).
- There may be rock fall out caused by e.g. spalling.
- There may be a change in diameter due to change of bore crown etc.

Since the load case is only sensitive to factors that cause a difference in buffer density at the same horizontal section a change in borehole diameter will not cause bending loads like the case described. Neither will an inclined deposition hole since it will only make the canister tilt. There must be force equilibrium in the horizontal direction, which means that a rock fall out on one side of the deposition hole is not severe, since the canister will get displaced or tilt unless the rock fallout is local at the central part of the canister.

Two cases may yield a stress distribution that results in more severe bending of the canister:

- Case 1: Curved deposition hole.
- Case 2: Rock fall out at critical locations.

The two severe cases are thus a curved deposition hole with rock fallout at places that accentuate the shape as illustrated in Figure 2-2. The resulting swelling pressure on the canister may in the worst case be a rectangular load distribution that in combination with a banana shaped hole and rock fall out yield load case 2.

The most critical stresses on the copper shell may proceed from uneven vertical stresses caused by vertical density gradients in the buffer, which causes shear stresses on the copper. The worst case comes from a high buffer density of calcium converted MX-80 in the bottom of the deposition hole in combination with unconverted MX-80 in the upper part and the highest possible axial density gradient caused by rock fallout. This case leads to axial shear stresses on the copper shell that are linearly reduced from τ = 2.55 MPa to τ =0.573 MPa over the length 1.96 m. Figure 2-3 describes the load condition.

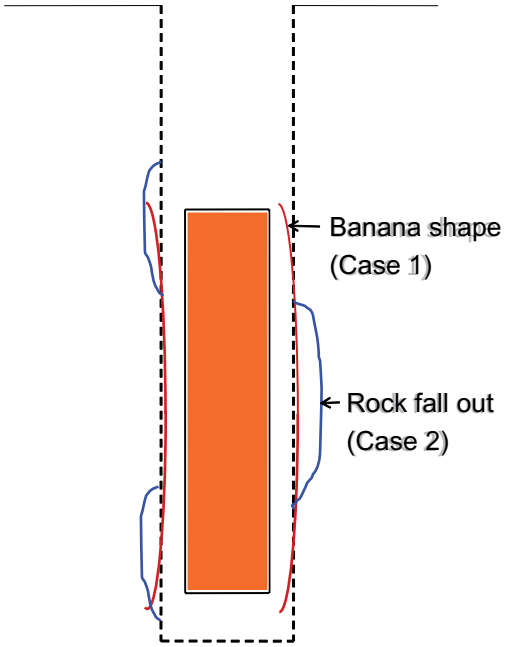

Figure 2-2. *Two severe cases of deformed rock contours. The read lines illustrate a curved (banana-shaped) hole and the blue lines illustrate rock fallouts that accentuate the banana shape.*

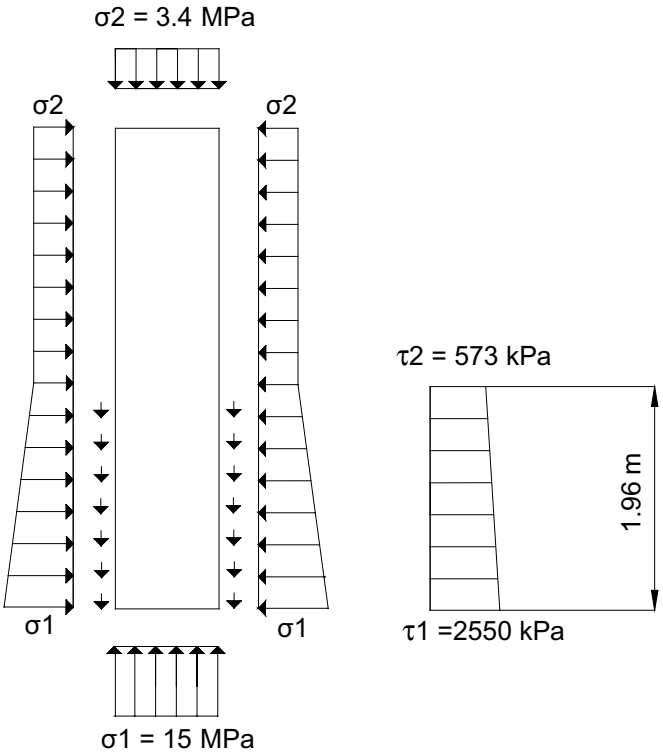

Figure 2-3. *The effect of variable swelling pressure on copper shell load and shear stresses /SKBdoc 1206894/.*

2.2.3 Isostatic pressure load

The nominal depth of the repository in Forsmark is 400 m. Thus the groundwater hydrostatic pressure is 4 MPa, when the glacial load is not present. The total pressure on the canister is the sum of the water pressure and the swelling pressure from the bentonite. The normal swelling pressure expected from sodium bentonite MX-80 at the maximum density 2,050 kg/m^3 is 11 MPa. This is the load case 3 in Table 2-1. The combination of these pressures is "the normal operation condition". The total maximum isostatic pressure load is then 15 MPa /SKB 2009/. The higher value of bentonite swelling pressure 15 MPa is used as an upper conservative limit after conversion to calcium bentonite, and this is the case after a very long time; see the glacial period in the next sub-section.

2.2.4 Glacial pressure load

During the glacial period the pressure will increase further. Despite that the climate scenario predicts that the maximum ice thickness will occur later, it is assumed that a maximum pressure of 45 MPa will occur during the first glacial period. The temperature at repository level will fall but stay over 0°C. This is the load case 4 in Table 2-1.

The postulated ice sheet during glacial period may cause an increase of 28 MPa to the groundwater pressure in Forsmark, if the ice sheet is conservatively suggested to float on the groundwater surface according to /SKB 2009/. The bentonite swelling pressure is strongly dependent on the final density of the buffer. Also the salinity of the absorbed water has a minor effect on swelling. The specified final density for the buffer is 1,950–2,050 kg/m^3. This leads to a swelling pressure (in case of calcium bentonite) of 6–15 MPa, respectively, according to /Börgesson et al. 2010/ where the swelling pressure dependencies are discussed more thoroughly. The swelling pressure dependencies are discussed more thoroughly in Section 2.2. Theoretically the maximum isostatic pressure load 47 MPa, which is the enveloping sum of all pressure components (4+28+15=47 MPa) named above, can affect the canister.

However, laboratory measurements have shown that at such high water pressures the total pressure is not the sum of the water pressure and the swelling pressure but considerably lower. On this reason 45 MPa is taken as the design pressure for the canister in /SKB 2009/.

Asymmetric loads due to density variations in combination with imperfections in the deposition hole are not analysed in combination with the glacial pressure load. This is judged as conservative for tensile loads as described in Section 6.1.2.

During this period shearing of the bedrock is also possible and in rare cases could lead to a load case 5) in Table 2-1 where canisters are subjected to shearing forces.

2.2.5 Rock shear load

The permafrost period does not normally lead to any additional significant effects except that temperature will continue to slowly fall. However, in the transition to the ensuing glacial period, shearing of the bedrock is possible and could, in rare cases, lead to that canisters are subjected to shearing forces.

According to /SKB 2009/ the corrosion barrier of the canister should remain intact after a 5 cm shear movement at 1 m/s for all locations and angles of the shearing fracture in the deposition hole. The buffer material properties used in the calculations should conservatively correspond to properties of calcium converted MX-80 at the density of 2,050 kg/m^3. The insert should maintain its pressure-bearing properties to isostatic load also after the rock shear. Further information of the rock shear load case is given in the design premises /SKB 2009/.

This case is not combined with the asymmetric loads described in Section 2.2.2 since these loads are extreme values that are considered to have a low probability of occurrence. The combination would then be the combination of two events with low probability. The effect of hydrostatic ground water pressure and the symmetric swelling pressure are, however, combined with the rock shear load case. The rock shear load is also analysed in combination of glacial pressure load in two scenarios: the glacial load is preceding and thus simultaneous with the rock shear and in the second scenario the rock shear is preceding the glacial load. Both scenarios are analysed in /Hernelind 2010/. The

temperature during rock shear is assumed to be the least favourable in the low end, 0°C, because the fracture toughness of the cast iron insert decreases with temperature. This is the load case 5 in Table 2-1.

2.2.6 Subsequent permafrost and glacial-period loads

The post-glacial period means going back to temperate and subsequent permafrost and glacial conditions and does not lead to any new load cases or combinations. The safety assessment shall, however, cover the time period extended up to 10^6 years.

3 Mechanical failure criteria for the canister

The overall safety function of the canister is to provide containment and isolation of the spent nuclear fuel. This is interpreted to be fulfilled as long as the copper barrier is nowhere breached. The ultimate aim of the analysis of the canister's response to any mechanical load is, therefore, to determine whether the load leads to penetration of the copper shell, in which case the canister is considered as *failed*.

In the evaluation of mechanical load cases, the copper shell will be considered as disrupted, if the mechanical conditions in the shell itself exceed certain failure criteria directly associated with its rupture. The direct rupture criteria are specified below. The mechanical or structural conditions in the insert exceeding failure criteria associated with its structural collapse or severe weakening are also specified below. In the latter case the damaged insert is assumed to lead to loss-of-integrity in the copper shell as well.

The nature of the induced mechanical conditions in both the copper shell and the insert will depend on the nature of the mechanical load, i.e. on the load case under consideration. Static loads could either be associated with direct mechanical effects such as gross plastic collapse and/or excessive crack growth or excessive long term creep elongation.

Due to the different functions and material properties, different failure criteria are required for the shell and the insert in various load conditions.

It is thus necessary to develop a complete *set of failure criteria* that cover mechanical alterations associated with all conceivable load cases for both the shell and the insert. In principle, the consequences of any load case should be tested against all failure criteria. However, in practice, a specific load condition and ambient conditions will be much more sensitive to only some of the failure criteria than to others.

3.1 Load cases and associated mechanical processes

The following mechanical load phenomena have been assessed to be relevant for the integrity of the canister in repository conditions:

- Bentonite buffer swelling effects during wetting and saturation, as well as after saturation.
- Isostatic loads associated with hydrostatic pressures under temperate climate conditions and increased pressures under glacial conditions.
- Shear loads associated with rock displacements in fractures intersecting deposition holes.

Possible loads and load combinations are considered in more detail in Section 2 in this report. Table 2-1 in Section 2, gives an overview of the relevant mechanical load cases and the ambient conditions, under which they are expected to occur.

This report also assesses the effects the postulated handling loads of the canister in encapsulation plant and possible scratches or dents during transport; see Sections 6.2.8 and 6.2.9. The effect of residual stresses from the manufacturing process is also discussed in 6.2.10 and 7.3.1. Both of these shall be limited in a way that they are not threatening to the canister integrity in the long term.

3.2 Mechanical failure processes

3.2.1 Copper shell

The following processes could potentially lead to mechanical failure of the copper and must be considered under the conditions given in Table 2-1:

- Fracture due to excessive plastic deformation.
- Rupture due to creep deformation.

The following potential failure processes are excluded:

- Brittle failure.

Cu-OFP is so ductile that unstable crack growth is not relevant at repository temperatures. The fracture mechanics tests made on oxygen-free copper show that the cracks in the test specimen are blunted but not growing, see /SKBdoc 1187725/ . Unstable crack growth is consequently not necessary to consider in the design.

- Plastic instability (buckling) due to excessive plastic deformation requires special load cases that do not exist for the copper shell. As far as insert is supporting the copper shell, the shell cannot collapse inwards.
- Creep crack growth.

Creep tests on notched specimens at 20 and 75°C show that initially sharp notches are blunted due to the high ductility of Cu-OFP and creep crack growth cannot take place /Andersson-Östling and Sandström 2009/.

Even if residual stresses in copper and especially in the FSW-weld are discussed in this report, the full analysis of the process stress corrosion cracking as a failure process is not handled. Stress corrosion cracking is handled in context with other types of corrosion processes as a part of the long-term safety assessment.

3.2.2 Insert

The following processes could lead to mechanical failure of the cast iron insert under the conditions given in Table 2-1:

- Plastic collapse (buckling).

In compressive stress condition the loss of stability may be involved. Effects that may contribute to buckling tendency are low yield strength, geometric inaccuracy, non-symmetry of the structure or load.

- Crack initiation or stable crack growth.
- Ultimate tensile strength is exceeded.

The following potential failure process is excluded:

- Brittle fracture.

Brittle fracture is possible only for brittle materials at low temperature. The tendency for brittle fracture depends on material quality, the amount of some foreign elements in the material and the ambient temperature. The brittle fracture of the insert is assessed not to be an issue. The fracture mechanics testing of the insert material at 0°C temperature showed that all the test samples had a stable behaviour during testing conditions /SKBdoc 1207576/. In addition, a series of high loading rate tests were conducted and the results showed that the static fracture resistance curves are representative even for dynamic loads, and the higher loading rate does not lower the fracture resistance of this insert material at this temperature, /SKBdoc 1203550/.

3.3 Failure criteria

3.3.1 Copper shell

Relevance and criteria for potential failure mechanisms in the copper shell:

- Fracture due to excessive plastic deformation.

  This failure mode can best be represented by the reduction in area, which is 80 to 90% for Cu-OFP and FSW welds in the material /Andersson-Östling and Sandström 2009/. Very large deformations of the order of the reduction in area are needed to initiate this type of failure. The design criterion is that the effective strain should not exceed 80%. If the reduction in area in a tensile test is at least 80%, this means that the material can stand an effective strain of 80% (true strain 1.6).

- Rupture due to creep deformation.

  Creep tests for parent metal and friction stir welds of Cu-OFP for defect free material have given a creep elongation of 30% or more in the temperature interval 75 to 175ºC. Multiaxial creep tests that have been performed at 75°C demonstrate that Cu-OFP is not notch sensitive and that the creep rupture time can be estimated to be 100 times longer than in uniaxial tests for the same net section stress. Local strains of 30% can appear without crack initiation /Andersson-Östling and Sandström 2009/. The creep rate is essentially controlled by the effective stress since the creep exponent is a high as 65. The factor with the deviatoric stress plays only a secondary role since it enters the creep rate only to the first order.If creep rupture would occur during the conditions in the repository it would show a ductile behaviour.

  To initiate creep rupture a spatially constant stationary effective stress must have been established across a section of the canister. The design criterion is that such a stationary stress should not exceed the uniaxial rupture stress. The safety factor is chosen to be 1.2 after considering the flatness of the rupture curve.

3.3.2 Insert

The failure criteria for the iron insert are classified as follows:

- Plastic collapse (buckling).

  This criterion is used for external pressure loading cases of the insert.

  Plastic collapse is the first and most common failure mode for an externally pressure loaded thick wall shell that is inside supported by bulkheads. This phenomenon can be accounted for in the analyses by using large deformation theory in the numerical models, when external pressure load cases are analysed. It can be analysed and assessed according to the plastic collapse method described in ASME Code, Section III, Divisions 1 and 2 /ASME 2008a/. The Code requires that the operational load shall be less than 2/3 of the limit load, which means, in other words, that the required safety factor against (global) collapse load is 1.5. This criterion is used for load controlled cases, in other words, for external pressure load cases.

  The interpretation of this criterion is given so that, **for basic dimensioning**, the plastic collapse load is determined for the load case of isostatic pressure, say p_L, and then the maximum allowable isostatic pressure in the design is taken to be $2\,p_L/3$. In other words, a safety factor 1.5 is used for collapse load analyses for design pressure load.

  In analysis of components used in the Swedish nuclear industry, acceptance criteria are usually adopted from the ASME code /ASME 2008a/. In the design analysis report the criteria for plastic analysis described in ASME III, Div 1, NB-3228.3, /ASME 2008a/ is used.

  The purpose with the method described in NB-3228.3 is to show that the applied load does not exceed 2/3 of the calculated plastic analysis collapse load and if this can be shown then the limits of General Membrane Stress Intensity (NB-3221.1), Local Membrane Stress Intensity (NB-3221.2), and Primary Membrane Plus Primary Bending Stress Intensity (NB-3221.3) need not be satisfied at a specific location /ASME 2008a/.

  In ASME III, Div 1, NB-3213.25, /ASME 2008a/, the definition of a plastic analysis collapse load can be found. The following criterion for determination of the collapse load shall be used. A load–deflection or load–strain curve is plotted with load as the ordinate and deflection or strain as

the abscissa. The angle that the linear part of the load–deflection or load–strain curve makes with the ordinate is called θ. A second straight line, hereafter called the collapse limit line, is drawn through the origin so that it makes an angle $\phi = \tan^{-1}(2 \tan \theta)$ with the ordinate. The collapse load is the load at the intersection of the load–deflection or load–strain curve and the collapse limit line. *This is also, more clearly, shown in ASME VIII, Div 2, 6-153, using Figure 6-153, /ASME 2004/, which shows how to determine this collapse load (please, note that this is given in ASME 2004).*

- Crack initiation or stable crack growth.

  This criterion is used for all types of loading of the insert.

  In the case of the external pressure load case, when the load controls the stresses and causes **primary stresses**, the damage tolerance analysis is made using K_{Ic}-data that is based on crack initiation, not for limited stable crack growth like $J_{2\,mm}$. The safety factor used for K_I-parameter is $\sqrt{10} = 3.16$, which is the ASME Code requirement for normal operational loads. This means that crack initiation is not allowed during pressure type of loading.

  When doing a damage tolerance analysis of components with cracks, different approaches may be used concerning method of analysis and decision of safety factors in the assessment. In Sweden, the Swedish Radiation Safety Authority (SSM) has published a handbook /Dillström et al. 2008/. In this handbook, a procedure is described which can be used both for assessment of detected cracks or crack-like defects and for defect tolerance analysis.

  – The method utilized in this procedure is based on the R6-method. This is also the method chosen for the damage tolerance analysis of the insert in the case of an external pressure load case (R6, option 1 failure assessment curve). In the case of a displacement controlled load, i.e. a rock shear load, the damage tolerance analysis is based on a *J*-integral analysis.
  – Within the SSM-procedure, a deterministic safety evaluation system is defined (which is not present in the original version of the R6-method). When choosing safety factors for nuclear applications, the objective has been to retain the safety margins expressed in ASME, Sect. III, Ref /ASME 2008a/, and XI, Ref /ASME 2008b/. For ferritic steel components $SF_K = 3.16$ (normal/upset load event) and $SF_K = 1.41$ (emergency/faulted load event) as defined in the SSM-handbook (when using a *J*-integral analysis, SF_J should be used, where $SF_J = (SF_K)^2$). These safety factors are taken from ASME XI, Div 1, IWB-3612 (acceptance criteria based on applied stress intensity factor). ASME XI, Div 1, IWB-3611 (acceptance criteria based on flaw size) is not allowed to be used according to the Swedish Radiation Safety Authority.
  – Doing a damage tolerance analysis, using these safety factors, does not imply that one needs to fulfil other code requirements within the ASME code (regarding inspection, fabrication etc). The only purpose is to use established safety factors for nuclear applications (within Sweden) when doing a damage tolerance analysis.
  – In Sweden, the aspect ratio chosen for postulated (initial) defects is mainly related to the assumed damage mechanism. When no damage mechanism is known, an aspect ratio (length/depth) of 6 could be used for surface defects. In the damage tolerance analysis for the insert, different assumptions regarding the aspect ratio has been used (both for surface and subsurface defects). The purpose has been to show that it is possible to introduce reasonable sized defects without jeopardising the integrity of the reference canister.
  – Regarding annual frequency of occurrence of the loading conditions and implicit conditional probability of failure in the event of the service loading, it is believed that this is fulfilled and also conservative. To quantify this, a more refined investigation may be needed.

Initiation of crack growth can be allowed for special load cases, but reasonable safety margin shall be applied for stable crack growth. This means for ex. that the calculated fracture parameter *J* may be higher than the J_c that corresponds to the initiation of crack growth but the dimensioning value could be $J_{2\,mm}$ that corresponds to the stable crack growth of 2 mm, which is very moderate in a massive iron structure of typical dimension of 1 metre. Reasonable small crack growth can be allowed, because limited local crack growth does not lead to global rupture.

In the case of a **displacement controlled load**, like the rock shear, the influenced stresses are secondary in character. The stable crack growth criterion is then taken as $J(a) < J_{2mm}/2$, where $J(a)$ is the calculated J-integral parameter value of the postulated crack, $J_{2\,mm}$ is the J-integral value corresponding to 2 mm stable crack growth and 2 is the safety factor. Safety factor 2 for a low-probability load case (under postulated emergency or faulted condition) is taken according the ASME Boiler and Pressure Vessel Code, ASME XI, Division 1, Article IWB-3600, /ASME 2008b/.

Safety factor 2 for J-integral is equivalent for safety factor $\sqrt{2}=1.41$ for K_I-parameter, which is primarily used in ASME Code. This discrepancy in safety factors comes from the relation between J and K_I as follows: $(K_I)^2 = J^*E/(1-\nu^2)$, where E is Young's modulus and ν is Poisson's ratio. This means that $J \sim K_I^2$. The justification for classification of the shear load case as a low probability case is based on /SKB 2009/ where it is calculated that 4 canisters may be subjected to shearing of magnitude of 5 cm or more. This gives a probability of <1/1,000.

The allowable amount of crack growth is assessed from the fracture resistance curves (R-curves), which are defined by fracture mechanical testing at respective temperature. These curves give the relation between stable crack growth and the respective J-integral. In this assessment we are describing the phenomena as a limited stable crack growth in a ductile material.

- Ultimate tensile strength is exceeded.

  This criterion is used for the exceptional displacement controlled loading of the insert.
  In the insert material test data the typical true-stress value in static (low deformation rate, at +20°C) uni-axial test is 270 MPa at yield and the ultimate tensile stress 456 MPa according to /SKBdoc 1207576/.

  This direct ultimate stress criterion is used for displacement controlled loads that lead to secondary stresses as described in the following. In 3D-stress state, the equivalent stress is defined as the von Mises effective stress. The effective stress σ_{vM} (von Mises stress) is generally in 3 dimensions

  $$\sigma_{vM} = \{1/2[(\sigma_x-\sigma_y)^2 + (\sigma_y-\sigma_z)^2 + (\sigma_z-\sigma_x)^2] + 3\,(\tau_{xy}^2 + \tau_{yz}^2 + \tau_{zx}^2)\}^{-1/2} \quad \text{(Eq. 3-1)}$$

  where σ_i and τ_{ij} are the respective stress and shear components at a point expressed in any positively-defined orthogonal coordinate system.

  For rock shear case that is an exceptional load case that will possibly hit only a few canisters during a very long period of time, this type of effective stress criterion is used. The load, rock shear, is a displacement controlled load that means that the consequent stresses are secondary in character. High secondary stresses and possible local material damage are not critical, because the driving force (forced displacement) decreases with the onset of local yielding in the material.

  Thus we can set an **engineering type stress criterion for displacement controlled secondary stresses** that the effective stress may be, at maximum, the stress corresponding to half of the strain at the lower limit of the ultimate elongation (A_5) in uniaxial tensile testing with 90% reliability (12.6%, see Section 4.1.1). The stress in the actual stress-strain curve of the insert iron corresponding a half of the 12.6% elongation is 395 MPa. Figure 3-1 shows the relation of the allowable effective stress in comparison to ultimate tensile stress (UTS). The stress-strain curve is the multi-linear elastic-plastic relation used in the FEM-analyses. It can be seen that the stress work density utilised at the allowable stress level is less than a half of that at failure.

This means, in other words, that we set a requirement of a safety factor of 2 against the ultimate strain for the effective stress. The rock shear case in ASME Service Conditions (load classification) is Level C or D condition, for which the Code does not set any direct requirement for the secondary stresses, according to Figure NB-3224-1 in /ASME 2008a/. The selected engineering type stress criteria are clearly stricter in this case than the ASME practise.

Uniaxial uniform elongations for the insert material are $12.6 < A_5 < 14.8$ using 90% confidence in test data. Elongation measured in the uniaxial tensile tests could be used as a measure for maximum allowable strain, but multi-dimensional strain condition should be taken into account. However, such a criterion for strains with a general acceptance is not available. Thus we use the effective stress criteria (von Mises), as given above, instead of equivalent plastic strain (PEEQ in ABAQUS terms).

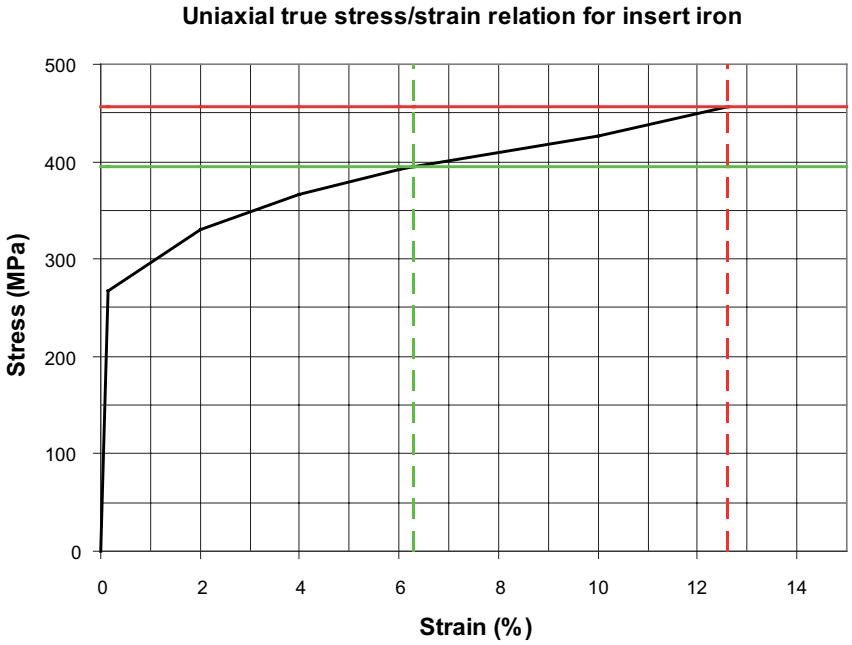

Figure 3-1. *The ultimate strength is 456 MPa (red lines) and the corresponding strain is 12.6% with the reliability of 90% according to the material testing. The maximum allowable effective (von Mises) stress (green lines) is set in a way that the respective strain is half of the strain (A_5) corresponding to the ultimate tensile strength (UTS=456 MPa). The green lines are at 6.3% and 395 MPa. The basic curve is the average tension test results (true stress) in 20°C with standard test (no strain-rated).*

3.3.3 Summary of failure criteria relevance

The failure criteria relevance for iron and copper are summarised in Table 3-1. Brittle fracture in actual operating temperatures has been avoided by the adequate fracture resistance properties of the both materials. Iron and copper are very dissimilar metals, thus different type of failure criteria are needed.

Table 3-1. Summary of failure criteria relevance.

Failure criteria	Iron insert	Copper shell
Plastic collapse (buckling)	Yes (for primary stresses)	–
Crack initiation or stable crack growth	Yes (for all load types)	–
Ultimate tensile strength is exceeded	Yes (for secondary stresses)	–
Fracture due to excessive plastic deformation	–	Yes
Creep	–	Yes
Brittle fracture	–	–

4 Material properties, models and constitutive equations

To perform the design analysis adequate materials data and materials models representing the canister materials are needed. This section gives an account for the materials data, how data for the analysis have been sampled and the combined model for plastic deformation and creep in copper.

4.1 Mechanical properties of canister materials

The mechanical properties of the canister structural materials to be used in the design analyses are based on a large amount of test data from demonstration-manufacture tests, reflecting the actual material properties. To handle the scatter in data, basic statistical measures have been used. The lower 90% confidence value is used as a standard value, when appropriate. This ensures that material properties are realistic and can be attained during production. However, for the stress-strain relationship for the cast iron, the average values taken from the test data are used for consistency. In different type of loading analyses, the conservative stress-strain relationship may vary between the higher and the lower. It is better strategy to put the required safety margin into the final results, in comparison of calculated fracture parameter value to the critical value.

It should be pointed out that values used in the calculations may differ from what is stated in the SKB materials specifications. For instance the critical *J*-value is not specified and the elongation values are higher, to give two examples. It needs to be stated that these specifications have been the starting point for SKB's development work and will be further developed in the future, in part because of results from this report.

The governing load cases, glacial isostatic pressure and/or rock slide shear deformation take place at temperatures that may be between 0°C and +20°C. Operational handling or transfer loads and asymmetric bentonite swelling loads take place in the ambient temperature range, from +20°C to +100°C that will be typically also the copper shell temperature. During the early years after disposal the canister insert may be, at maximum, some 25°C higher temperature than the copper shell, in other words, at +125°C. After water saturation of the bentonite buffer, the canister temperature will decrease markedly from the calculated maximum temperature due to better thermal conductivity between canister surface and the rock.

4.1.1 Properties of nodular cast iron and steel

The mechanical properties for the structural materials of the insert are given in Tables 4-1 to 4-4 for cast iron, steel in the lid, as well as cold formed and hot formed steel for the cassette hollow sections. Standard values for yield strength and ultimate strength are taken to mean the minimum required material test values based on standard-type uniaxial tension tests (EN 10002-1) with round samples and low strain rate tension tests.

For the most important components that comprise the canister, the insert and the shell, values of mechanical properties based on measurements of representative actual material test samples from manufacturing tests are given. These values are used in the analyses for the most severe load cases, the isostatic pressure under glacial period and the rock shear deformation. Strength values referenced in the tables below are mainly based on either tension or compression tests depending on load case type. The ultimate strength or the given stress/strain relationship is converted from uniaxial test result to a true-strain/true stress relation. Reports /SKBdoc 1207576, SKBdoc 1203550, SKBdoc 1173031, SKBdoc 1201865/ provide most of the test result details, on which the given engineering value is based.

Cast iron was widely investigated in conjunction with a probabilistic pressure test programme, /Nilsson et al. 2005/ and /SKBdoc 1207426/. Then a representative stress-strain curve was selected based on compressive testing. The curve and its origin is given in /Dillström et al. 2010/. For consist-

ency in the analyses the same compression data set is used in all reports using compression data for the cast iron, mainly /Dillström et al. 2010, SKBdoc 1177857, SKBdoc 1207429/. However, as stated in /SKBdoc 1207426, Dillström et al. 2010, appendix N/ this is a conservative approach since more recent data from manufactured inserts have showed better values. The selected curve is used anyway to show the strength of the insert.

Tension data used in analyses, mainly in rock shear analyses /Hernelind 2010/, is represented by the stress-strain data from series of stress-strain tests made both in +21°C and in 0°C using standard and elevated strain rate. The used data is taken from /SKBdoc 1201865/. The rock shear analysis used a strain-rate dependent material model, so the material stress-strain curve was presented for static and for strain rate 0.5/s case. Comparison with data from the serial manufacturing /SKBdoc 1207576, SKBdoc 1175208/ shows good agreement between the representation and actual measured values.

Based on results from standard type testing of material from top sections of inserts I53-I57 /SKBdoc 1207576/ the elongation at fracture for BWR-inserts can be evaluated and the 90% confidence interval calculated according to the methodology in /Dillström 2010/. This gives $12.6<A_5<14.9$ with 90% confidence. The engineering stresses are converted to true stresses thus they can be used directly as a material model for large-deformation and large-strains analyses. All model curves used for cast iron are given in Table 4-1.

The fracture toughness data measured for cast iron at 0°C is $88.1 \leq J_{2\,mm} \leq 93.5$ kN/m, when expressed as a *J*-parameter value. The number used for the damage tolerance analyses (88 kN/m) for the rock shear case is taken from the measured data with 90% confidence. See reference /Dillström 2010/ for further information about the evaluation of fracture toughness data measured for cast iron. The measured fracture toughness data is in more detail presented in /SKBdoc 1203550/. In probabilistic use of measured material data some data may be below the reference limit, but this is an approach that has been judged as necessary for a cast iron component of this size, where local unhomogeneity may have a large influence on a single point data. To use such a single lowest value as the reference limit value would be unnecessarily conservative as it is not representative for the properties of the whole insert. The lowest envelope value approach is normally used only when a very limited amount of data is available.

Since, in this case, quite a lot of data is available from fracture toughness testing, it is possible to use a statistical approach instead of using the lowest value. This has been done by using confidence interval, as recommended in the well-known R6-method (R6 uses 95% as confidence level). The same approach with confidence interval is used in the SSM-report 2009:26: “Tillämpning av stabil spricktillväxt vid brottmekanisk bedömning av defekter i sega material”, where the confidence level 90% is recommended for deterministic analysis (by implementing safety factors to the analysis, small local variations are considered to be negligible in the analysis).

For information and comparison it can be calculated that lower 95% confidence level for J_{2mm} would be 87.6 kN/m in comparison to 88.1 kN/m for 90% confidence.

In the case of an external pressure load, when the load controls the stresses and causes **primary stresses**, the damage tolerance analysis is made using K_{Ic}-data that is based on crack initiation, not for limited crack growth like $J_{2\,mm}$. The safety factor used for K_I-parameter is $\sqrt{10} = 3.16$, which is the ASME Code requirement for normal operational loads. The fracture toughness K_{Ic}-data measured for cast iron at 0°C is 78.0 MPa$\sqrt{m}$ with 90% confidence, when declared as stress intensity factor K_{Ic}-value. K_{Ic} = 78 MPa$\sqrt{m}$ is equivalent to J_c = 33 kN/m.

Iron is being investigated under long term loading conditions up to +125°C and preliminary tests do only show a creep behaviour that is logarithmic in nature. The preliminary tests show that the creep strain after long times, even at stress levels close to the yield of the material, is likely to be small or negligible at all tested temperatures. This is why the creep phenomenon in cast iron in repository condition is omitted in the following mechanical analyses. Reporting will be available later, when the testing is fully completed.

Table 4-1. Mechanical properties of the insert cast iron EN 1563 grade EN-GJS-400-15U (t= 60–200 mm) /SKBdoc 1207576, Dillström et al. 2010, Hernelind 2010/.

Property	Standard value (EN 1563)	Values used in static analyses	Values used in strain rate dependent shear case at 0°C and strain rate=0 *)
Yield strength in tension [MPa]	≥240	True stress [MPa]/ true strain [%] 0/0 267/0.160 330/1.998 366/4.000 392/6.000 427/9.998 456/15.005 480/49.990	True stress [MPa]/ plastic strain [%] 293/0 324/1 349/2 370/3 389/4 404/5 418/6 428/7 438/8 447/9 456/10 465/11 472/12 478/13 484/14 488/15 491/16
Yield strength in compression [MPa]	≥240	True stress [MPa]/ true strain [%] 0/0 270/0.1627 333/2 394/4 429/6 482/10 534/20 550/50 550/100	–
Ultimate strength [MPa] (in tension/compression)	≥370	456/534	456/534
Elongation at failure [%]		12.6<A_5<14.9 90% confidence	12.6<A_5<14.9 90% confidence
Fracture toughness, J-integral J_c [kN/m]	–	33 at 0°C 90% confidence in test data	33 at 0°C 90% confidence in test data
Fracture toughness, J-integral $J_{2\,mm}$ [kN/m]	–	88 at 0°C 90% confidence in test data	88 at 0°C 90% confidence in test data
Young's modulus E [GPa]		166	166
Poisson's ratio v [–]		0.32	0.32

*) The strain rate factor was defined according to the testing and a constant value of 1.08 was used at strain rate 0.5 s^{-1} and the values between static and the 0.5 s^{-1} were interpolated using the actual strain rate /Hernelind 2010/.

4.1.2 Properties of phosphorus doped copper

The standardised phosphorus doped copper grades that are closest to the one specified by SKB are the US alloys C10300 and C108000 /ASM handbook, 1990/. They are called oxygen free extra low phosphorus copper and oxygen free low phosphorus copper. They contain 10 to 50 respectively 50 to 120 ppm P. According to the SKB specification the P content should be in the interval 30 to 100 ppm to ensure sufficient creep ductility. The typical values for mechanical properties that are given are 69 MPa for the yield strength and 220 MPa for the tensile strength in soft condition, for the product form tube Φ 25×1.7 mm and a grain size of 50 µm. Both grades are given the same values. Since the canister material will have a coarser grain size, its mechanical properties can be expected to be somewhat lower. In the testing organized by SKB yield strength values from 40 to 75 MPa have been obtained at normal strain rates for tensile testing /Sandström et al. 2009/. According to /SKB 2009/ the P content should be in the interval 30 to 100 ppm to ensure sufficient creep ductility.

In the FEM-computations, model values for stress strain curves have been used. The model is described in Section 4.2. For the elastic modulus 120 GPa has been utilised. This is a compromise value for pure copper taken from ASM handbook /ASM handbook1990/, where values from 115 to 128 GPa can be found. For Poisson's ratio 0.308 has been used, again taken from ASM handbook.

4.2 Models for stress strain curves

4.2.1 Models for stress strain curves for iron and steels

The nodular iron is modelled with the von Mises plasticity material model. This is an elastic-plastic material model that contains the elastic part described by Young's modulus and Poisson's ratio and the plastic part that is defined by the yield surfaces (true stress versus plastic strain), which are interpolated between definition points in the FEM-programmes. The steel materials are modelled in the same way. This is very common way to model structural metallic materials. For cast iron, three separate models for stress strain relationship are used, depending on the character of deformation, static tension, static compression or strain-rate dependent deformation (in dynamic shear load case). The numerical values for the iron and steel models are given in Tables 4-1 to 4-4.

Table 4-2. Mechanical properties for the lid steel EN 10025 S355J2G3 (t= 40–63 mm) /Hernelind 2010/.

Property	Standard value (EN 10025)	Engineering stress [MPa]/ strain [%]	True stress [MPa]/ logarithmic strain [%]
Yield strength [MPa]	≥335	0/0	0/0
		335/0.1595	335/0.1593
		470/15	540/13.98
		470/20	564/18.2
Ultimate strength [MPa]	490–630	470	564
Elongation at failure [%]	19		
Young's modulus *E* [GPa]	210	210	210
Poisson's ratio *v* [–]	0.3	0.3	0.3

Table 4-3. Mechanical properties for the cold formed tube steel EN 10219-1 S355J2H (t= <16 mm) /SKBdoc 1177857, Hernelind 2010/.

Property	Standard value (EN 10219-1)	Engineering stress [MPa]/strain [%]	True stress [MPa]/logarithmic strain [%]
Yield strength [MPa]	≥335	0/0	0/0
		411/0.196	412/0.196
		509/15	587/14.3
		510/20	613/18.5
Ultimate strength [MPa]	470–630	510	613
Elongation at failure [%]	20	20	
Young's modulus *E* [GPa]	210	210	
Poisson's ratio *v* [–]	0.3	0.3	

Table 4-4. Mechanical properties for the hot formed *) tube steel EN 10210-1 S355J2H (t = 16 mm) according to Standard EN 10210-1.

Property	Standard value
Yield strength [MPa]	≥335
Ultimate strength [MPa]	470–630
Elongation at failure [%]	20
Young's modulus *E* [GPa]	210
Poisson's ratio *v* [–]	0.3

*) This is an alternative material (hot formed steel) for insert square tubes. The standard requirements of it are equal to that of the cold formed tubes given in Table 4-3.

4.2.2 Model for stress strain curves of copper

To model the deformation in the copper canisters, accurate data for creep and plastic deformation must be available as both these deformation processes may occur simultaneously. The ductility behaviour has hence been studied both with traditional creep tests and slow strain rate tensile tests (SSRTT). In the present section slow strain rate tensile data will be summarised for phosphorus micro-alloyed pure copper, Cu-OFP. The representation of creep data is described in the next section.

Slow strain rate tensile tests for cold deformed Cu-OFP have a characteristic appearance, Figure 4-1 /Yao and Sandström 2000/.

Tests have been carried out at 20 to 175ºC for strain rates between 10^{-7} and 10^{-3}. Two examples of results are shown in Figure 4-1.

In terms of engineering stresses the results have a simple form. After the elastic part the curves become essentially flat. A stationary value is reached. At 20ºC there is a slight work hardening that does not appear at higher temperatures. The behaviour of the curves is what would be expected at higher temperatures when the deformation is climb controlled. This behaviour can be described with the following equation

$$\frac{d\sigma(t)}{dt} = E\dot{\varepsilon}_{\text{tot}} - EB_N\sigma(t)^{n_N} \qquad \text{(Eq. 4-1)}$$

where σ is the stress, $\dot{\varepsilon}_{\text{tot}}$ the strain rate in the test, t the time, and E the elastic modulus. The last term is built up with Norton creep equation where B_N and n_N are constants. Equation 4-1 gives a uniaxial flow curve that can be used as hardening function in the multiaxial case. The values from the model (1) are illustrated in Figure 4-1. The stress level at the plateau in the flow curves has been found to be the same as the stress in a creep test giving a minimum creep rate that is the same as the strain rate in the tensile tests. The stress strain model for cold worked copper has so far been used to supplement the creep data at low temperatures. This will be discussed below in connection with Figure 4-4. In the future it is planned to be applied in FEM computations of cold worked material around indentations.

Annealed (annealed during hot working) copper, which is the condition that is going to be used in the canisters, has also been studied /Sandström et al. 2009/. Temperatures in the interval 20 to 175ºC and strain rates between 10^{-7} and 10^{-1} 1/s have been covered. Examples of curves are shown in Figure 4-2.

The curves for annealed copper are quite different from those of the cold worked material. There is significant work hardening and the "flat" region is much less pronounced. The SSRTT data for the cold worked material is close to the minimum strain rates in the creep tests as mentioned above. The strain rates for annealed material are higher. The dislocation barriers that are built up in the two types of tests can be expected to be different. It is likely that the dislocation barriers are broken down more efficiently in a strain controlled tests than in a stress controlled creep test. The difference in stationary stress level turns out to be 10%. The uniaxial flow curves for the annealed material can be represented by the following model

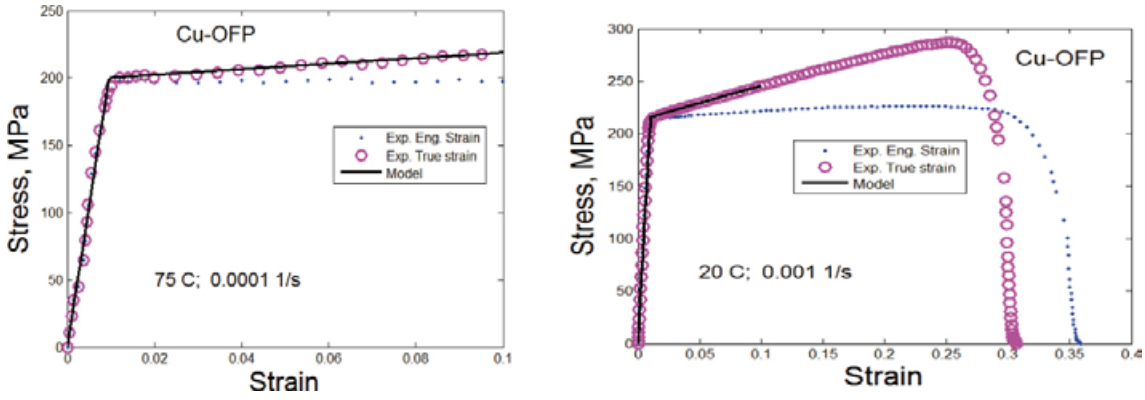

Figure 4-1. *Slow rate tensile tests for cold worked Cu-OFP at 75ºC, 0.0001 1/s, and 20ºC, 0.001 1/s /Yao and Sandström 2000/.*
Please, note different scale in the two figures.

$$\sigma = \sigma_y(\dot{\varepsilon}, T) + (\sigma_c(\dot{\varepsilon}, T)/1.1 - \sigma_y(\dot{\varepsilon}, T))(1 - e^{-\omega\varepsilon}) \quad \text{(Eq. 4-2)}$$

where σ_y is the yield strength, σ_c the creep strength, $\dot{\varepsilon}$ the plastic strain rate, and ω a constant. The factor 1.1 takes into account that the maximum flow stress is 10% lower than the value obtained from the creep model. Equation 4-2 is used in the FEM-modelling as hardening function. The strain rate and temperature dependence of the yield strength is illustrated in Figure 4-3.

As can be seen from Figure 4-3 the model values for $\sigma_y(\dot{\varepsilon}, T)$ can represent the observed values. An equation for $\sigma_y(\dot{\varepsilon}, T)$ is given in /Sandström et al. 2009/. The strain rate dependence is the same as in the creep model. At lower temperature when dislocation glide is controlling the deformation, the yield strength has the same temperature dependence as the shear modulus. On the other hand at higher temperatures when dislocation climb is controlling, the yield strength is related to the creep strength. Above 400ºC the deformation is completely governed by climb. At lower temperatures there is mixture between climb and glide. With the help of the creep model, which takes into account both climb and glide, the relative importance of the processes can be assessed. The resulting behaviour of the yield strength is the one illustrated in Figure 4-3.

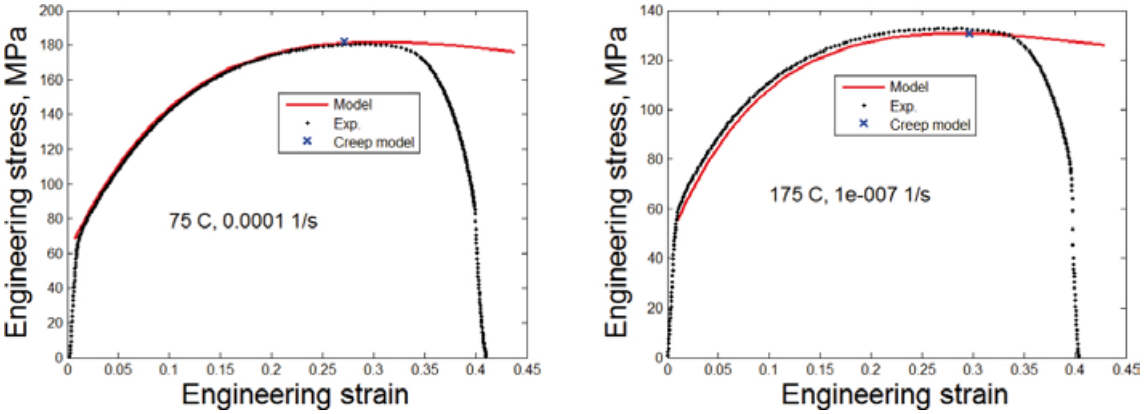

Figure 4-2. *Slow rate tensile tests for annealed Cu-OFP at 75ºC, 0.0001 1/s, and 175ºC, 0.0000001 1/s /Sandström et al. 2009/.*

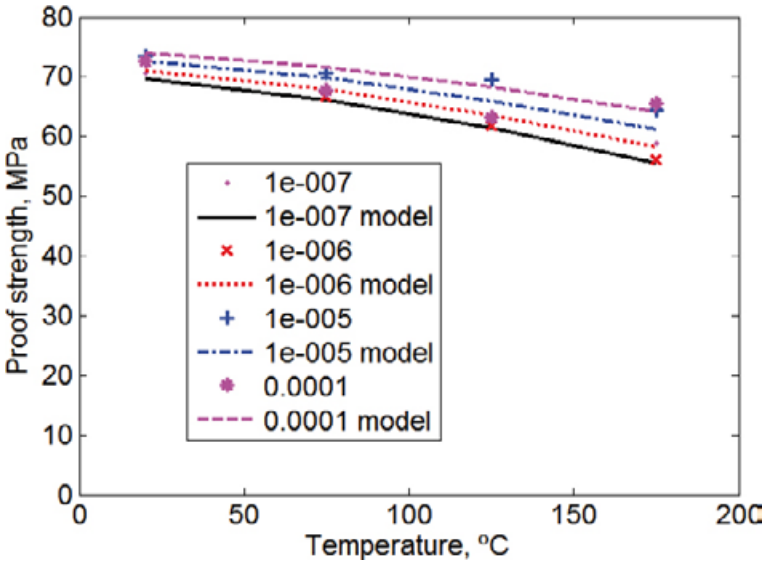

Figure 4-3. *Proof strength (yield strength) versus temperature for slow strain rate tensile tests. Values for four strain rates are shown from 1×10^{-7} to 1×10^{-4} 1/s. The lines are model values /Sandström et al. 2009/.*

4.3 Copper creep model

In the computations of creep deformation in the canister, models for the stationary and non-stationary creep rate have been used /Sandström and Andersson 2007, 2008/. These models are described in the present section. At high temperatures above half the melting point T_m, climb is believed to control the deformation in many types of metals including copper. For copper $T_m/2 \approx 400°C$.

It is believed that the deformation is glide controlled at lower temperatures. A difficulty with expressions for glide controlled deformation is that the values of the constants are not known. However, there are similarities between the equations for climb and glide control and such equations were combined into a unified model

$$\dot{\varepsilon}_{OFP} = \frac{2bc_L}{m}\frac{D_{s0}b\tau_L}{k_BT}\left(\frac{\sigma}{\alpha Gb}\right)^3 e^{\frac{\sigma b^3}{k_BT}} e^{-\frac{Q}{RT}\left[1-\left(\frac{\sigma}{\sigma_{i\max}}\right)^2\right]} / f_P = h(\sigma) \qquad \text{(Eq. 4-3)}$$

The interpretation and values of the parameters in Equation 4-3 are given in Table 4-5. Since Equation 4-3 is used a number of times below, a simplified expression $h(\sigma)$ is introduced.

Equation 4-3 is compared to experimental data in Figure 4-4.

In general an acceptable agreement is obtained between the model and the observation. The difficulty is in the transition between 175 and 215ºC, where the experiments show a sharp transition in slope whereas the model transition is more gradual.

To describe non-stationary creep an effective stress σ_{eff} is introduced in Equation 4-3 instead of the applied stress σ

$$\sigma_{eff} = \sigma - \sigma_i \qquad \text{(Eq. 4-4)}$$

where σ_i is an internal back stress. The same basic model for the back stress is used as for the flow curves in Section 4.2.

$$\sigma_i = \sigma_{i\max}\left(1 - e^{-\omega_c \varepsilon}\right) \qquad \text{(Eq. 4-5)}$$

However, the back stress during creep develops more slowly than the flow stress during tensile tests. Consequently, other parameter values have to be used. The constants $\sigma_{i\max}$ and ω_c are given in Table 4-5. The resulting equation for the non-stationary creep rate is

$$\dot{\varepsilon}_{\mathrm{OFPnon-stat}} = h((\sigma - \sigma_i)e^{-\varepsilon})g_{\mathrm{rate}} + h(\sigma e^{-\varepsilon}) \qquad \text{(Eq. 4-6)}$$

Table 4-5. Values of constants used in the model in Equation 4-3.

Parameter description	Parameter	Value
Burgers vector	b	$2.56 \cdot 10^{-10}$ m
Taylor factor	m	3.06
Boltzmann's constant	k_B	$1.381 \cdot 10^{-23}$ J/K
Shear modulus	G	G=4.75·10⁴–17T MPa, T in K
Dislocation line tension	τ_L	$7.94 \cdot 10^{-16}$ MN at RT
Coefficient for self diffusion	D_{s0}	$1.31 \cdot 10^{-5}$ m²/s
Activation energy for self diffusion	Q	198,000 J/mol
Strain hardening constant	c_L	57
Constant	α	0.19
Max back stress	$\sigma_{i\max}$	257 MPa
Influence of phosphorus	f_P	3,000 for T < 125ºC
Time at the start of primary creep	t_{init}	1 h
Time at minimum creep rate	t_{min}	$t_R/3$ where t_R is the rupture time
Parameter in g_{rate}	Φ_2	13.26–0.022T, T in K
Omega	ω_c	0.45
Ratio between initial and stationary creep rate	g_{rate}	$(t_{min}/t_{init})^{\phi_2(1+\phi_2)}$

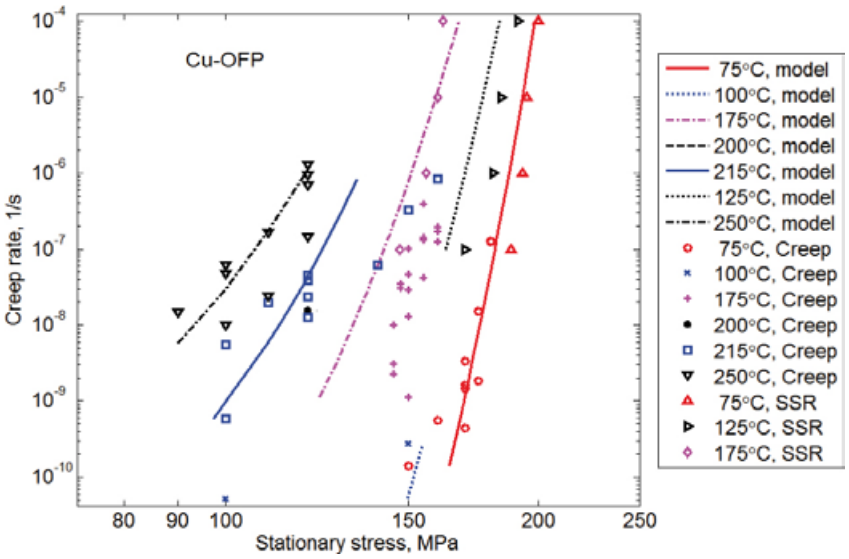

Figure 4-4. *Comparison of Equation 4-3 to creep data and slow strain rate (SSRTT) data Cu-OFP /Andersson-Östling and Sandström 2009/.*

g_{rate} takes into account the difference between the initial and the minimum creep rate, see Table 4-5. The creep rate is governed by the engineering stress, not the true stress. This is taken into account by the factor $e^{-\varepsilon}$. If the true stress would be used, which would seem natural, it would give an increase in the creep rate far beyond what is observed. This is referred to as retardation creep. It should be noticed that this is a substantial effect. All considered experimental data are in agreement with the effect. In Equation 4-6 the first and second terms represent primary and secondary creep, respectively.

Equation 4-6 is referred to as the Φ-model since the primary creep is handled with this model /Andersson-Östling and Sandström 2009/. Equation 4-6 is illustrated in Figure 4-5, where it is used to describe creep strain time curves at 75°C. There is a good general agreement with the observations. Due to the high creep ductility of the copper, the creep machines have to be reloaded several times during the tests. This is the cause of the cusps in the experimental data in Figure 4-5.

A comparison is also made to a basic model for primary creep /Andersson-Östling and Sandström 2009/ that does not involve any fitting parameters. The basic model is derived from Equation 4-1 for the flow stress curves. The basic model and Φ-model give similar results, which represents indirect support for the Φ-model. The basic model has been derived recently and only been used to a limited extent yet for FEM-computations of creep deformation in canisters.

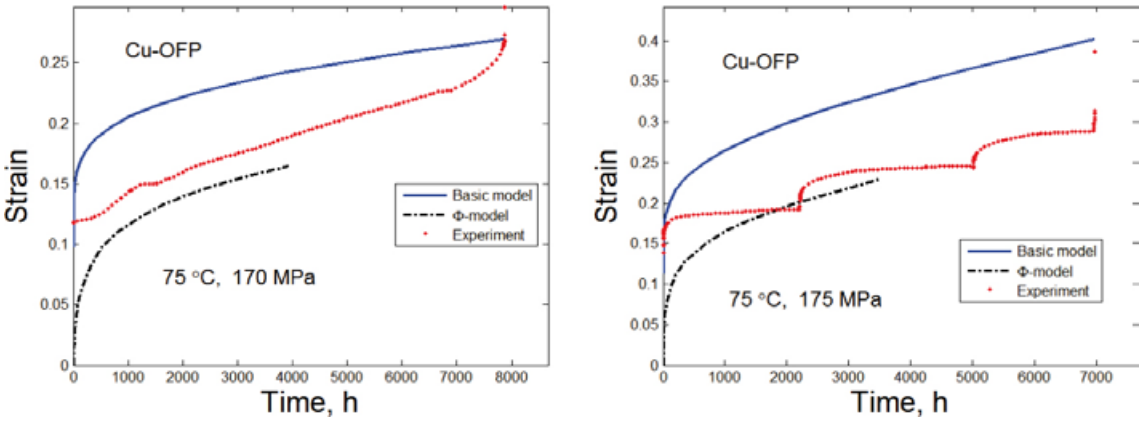

Figure 4-5. *Creep strain versus time curves for Cu-OFP at 75°C. A basic model and the Φ-model (Eq. 4-6) are compared to experimental data.*

4.4 The copper creep model for multiaxial stress states

The traditional way to transform a uniaxial creep model to multiaxial stress state is described in /Sandström and Andersson 2008/. When this way was used in FEM-computations some difficulties appeared. As a consequence three new approaches were developed and used /Jin and Sandström 2009a, b/. A summary is given in /Andersson-Östling and Sandström 2009/. The three approaches give essentially the same results. According to one of the approaches the starting equation is

$$\frac{d\varepsilon_{eff}^{p}}{dt} = h((\sigma_e - \sigma_i)e^{-\varepsilon_{eff}^{p}})g_{rate} + h(\sigma_e e^{-\varepsilon_{eff}^{p}}) \qquad \text{(Eq. 4-7)}$$

where ε_{eff}^{p} is the effective strain and σ_e the effective stress. With the help of Odqvist's equation, the individual components of the creep rate are obtained.

$$\frac{d\boldsymbol{\varepsilon}^{p}}{dt} = \frac{3}{2}\frac{d\varepsilon_{eff}^{p}}{dt}\frac{\boldsymbol{\sigma}'}{\sigma_e} \qquad \text{(Eq. 4-8)}$$

$\boldsymbol{\sigma}'$ is the deviatoric part of the stress tensor $\boldsymbol{\sigma}$. The back stress is now a scalar. It can be derived from the following equation, identifying the analogue with the uniaxial case

$$\sigma_i = \sigma_{i\,max}(1 - e^{-\omega_c \varepsilon_{eff}^{p}}) \qquad \text{(Eq. 4-9)}$$

4.5 Comparison to copper creep tests for notched specimens

The creep lifetime under multiaxial stresses for notched round bars has turned out to be much longer than for uniaxial specimens /Wu et al. 2009/. This demonstrates notch strengthening for the Cu-OFP material. If the rupture curves are extrapolated, the notch strengthening factor in time is greater than 100. Metallographic examination has shown that only limited number of pores and cavities are observed in ruptured specimens. This demonstrates that the local creep ductility is high.

Comparison to finite element modelling is illustrated in Figure 4-6. The Φ-model in Equation 4-7 and the basic model for primary creep are used.

Using the basic model, the observed strain is somewhat overestimated. In particular the initial strain is overestimated. With the Φ-model, Equation 4-7, on the other hand the strains are underestimated by a factor of three. Considering that the time difference to the uniaxial test results is more than a factor of 100, the comparison between the experiments and the simulation must be considered as satisfactory. These results give some validation of the multiaxial model formulation.

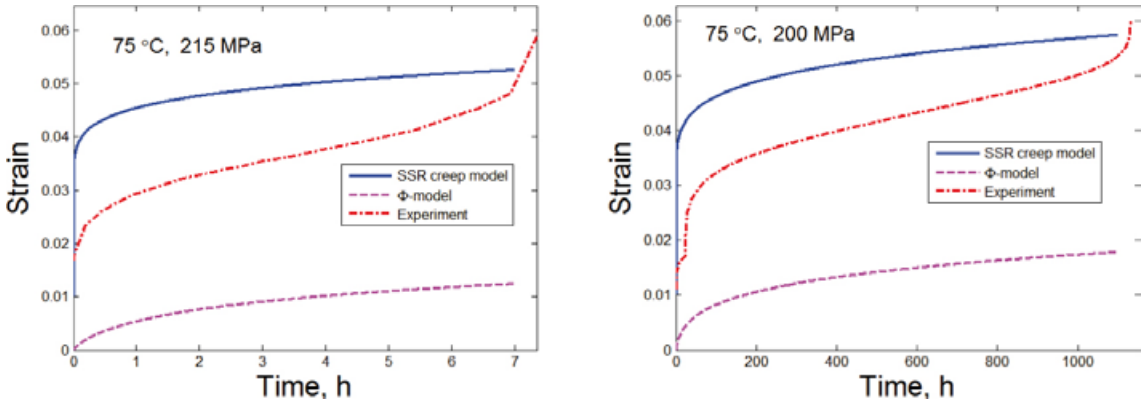

Figure 4-6. *Comparison between experimental data and FEM results for a notched creep specimen under a net section stress a) 215 MPa and b) 200 MPa. For the model marked SSR creep, the basic model was used for primary and secondary creep. For the curves marked Φ-model, Equation 4-7 was used. The initial strain on loading is included in the experimental data /Andersson-Östling and Sandström 2009/.*

4.6 Bentonite material model

As all mechanical loads on the canister is transferred through the bentonite buffer the material properties of bentonite gives important conditions for the design analysis of the canister. Table 4-6 gives an overview of which are the dominating bentonite properties in different load cases. For more information about bentonite data used in the analyses see /Börgesson et al. 2010/.

For FEM-analyses with the code ABAQUS the bentonite buffer is modelled with an elastic-plastic material model. The swelling pressure and the yield strength of the saturated bentonite are strongly dependent on the density of the bentonite. There are also different strength and swelling pressure estimates for Na and Ca bentonites.

The bentonite material model is based on laboratory testing and it is essentially different from material models for metals, because the stiffness and strength of bentonite depends strongly on the swelling pressure, which in turn depends on the density. Bentonite has two roles; it is a swelling load generating media and, on the other hand, it is a supporting and flexible substance.

The resulting stress-strain relations are shown in Figure 4-7. The dimensioning material model that is used in the calculations in /Hernelind 2010/ is the model of calcium converted MX-80 at water saturation and at the density ρ_m = 2,050 kg/m^3. The shear strength of bentonite is rate dependent. Different curves in Figure 4-7 correspond to different constant strain rates (in s^{-1}) according to strain rates named in the legend on the right side of the graph.

The density 2,050 kg/m^3 corresponds to swelling pressure 12.3 MPa and the elastic part of bentonite material model is described by the Young's modulus 462 MPa and the Poisson's rate 0.49 according to /Hernelind 2010/.

Table 4-6. Overview over dominating bentonite properties for different load cases.

Loads	Bentonite dominating property
1) Asymmetric loads due to uneven water saturation and imperfections in deposition hole geometry. No simultaneous hydrostatic pressure. Uneven water saturation effects will decay later and be replaced by permanent loads 2) and 3) acting in saturated condition.	Dry density, water absorption rate, degree of water saturation, swelling pressure
2) Permanent asymmetric loads due to uneven bentonite density and imperfections in deposition hole geometry.	Dry density, swelling pressure, pore water pressure
4) Glacial pressure (additional isostatic pressure, only during glacial period).	Dry density, swelling pressure, pore water pressure
5) Shear load due to rock displacement. Amplitude is 5 cm, shear velocity 1m/s.	Young's modulus, strain-rate dependent material model, von Mises stress at failure

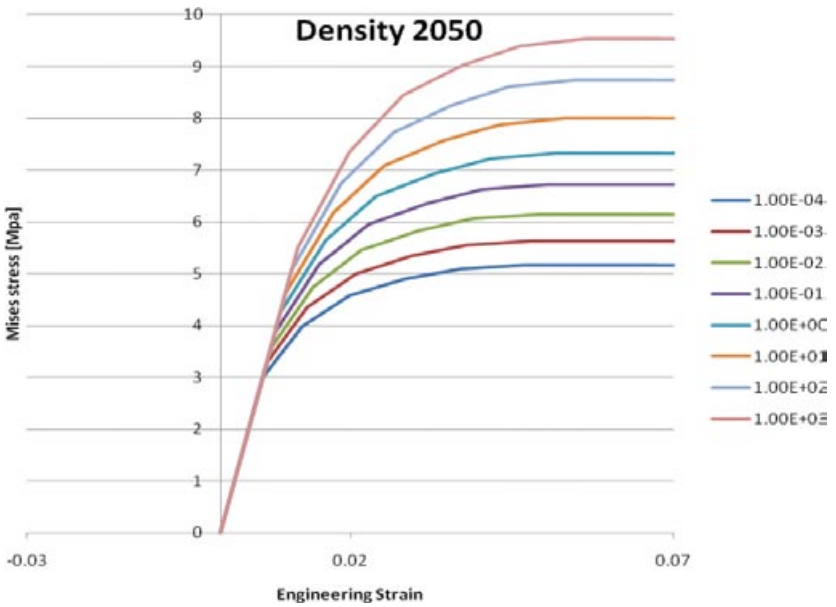

Figure 4-7. *Dimensioning strain-rate dependent stress-strain relation for the calcium converted MX-80 buffer material with maximum density according to the model used in ABAQUS analyses for rock shear /Hernelind 2010/.*

5 Canister shape and dimensions

The canister's size and shape was derived based on the space needed for the actual spent fuel assemblies, the mechanical strength, the chemical durability (corrosion resistance), sub-criticality and radiation protection (max dose rate at the outside surface about 1 Gy/h) referenced in /SKB 2009/. The reference geometry of the canister is documented in /SKBdoc 1203875/.

Shown in Figure 5-1 to Figure 5-6 and in Tables 5-1 to 5-4 are the dimensions required in order to (a) be able to accommodate the fuel elements, (b) have the required strength and (c) prevent criticality in the fuel. In addition, the steel lid of the insert shall be designed in order to permit replacement of the atmosphere inside canister. This is done by inserting a valve into the steel lid.

All nominal dimensions specified are the final canister dimensions and apply at room temperature, +20°C.

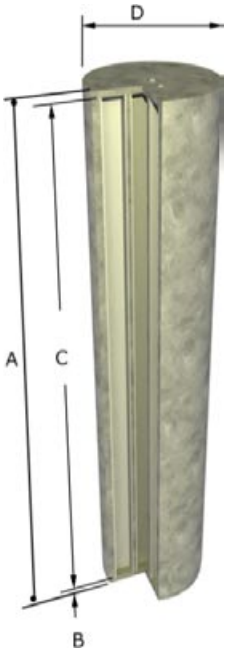

Figure 5-1. *Insert.*

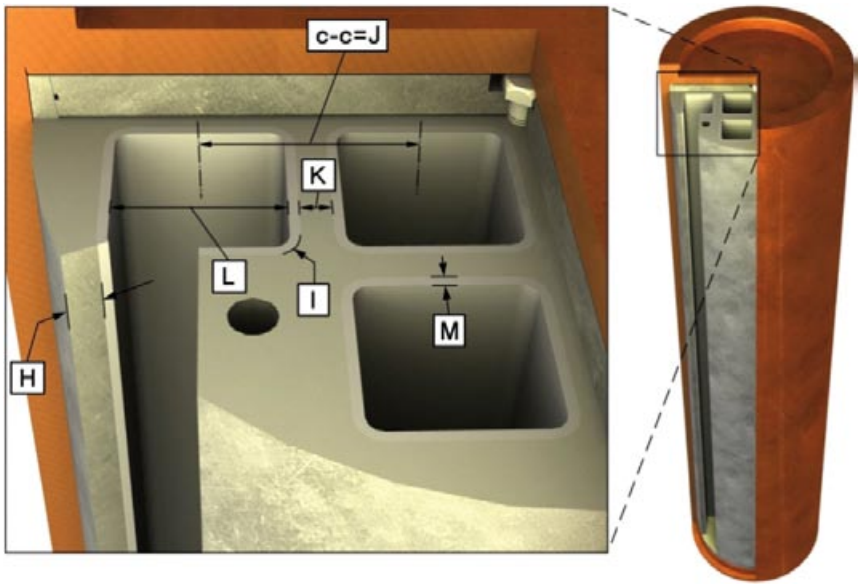

Figure 5-2. *Cross section of insert with channel tubes.*

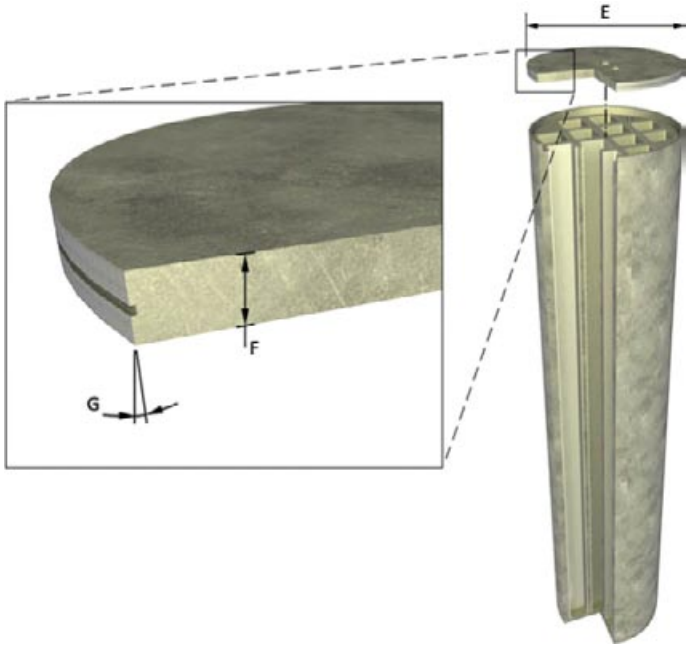

Figure 5-3. *Steel lid.*

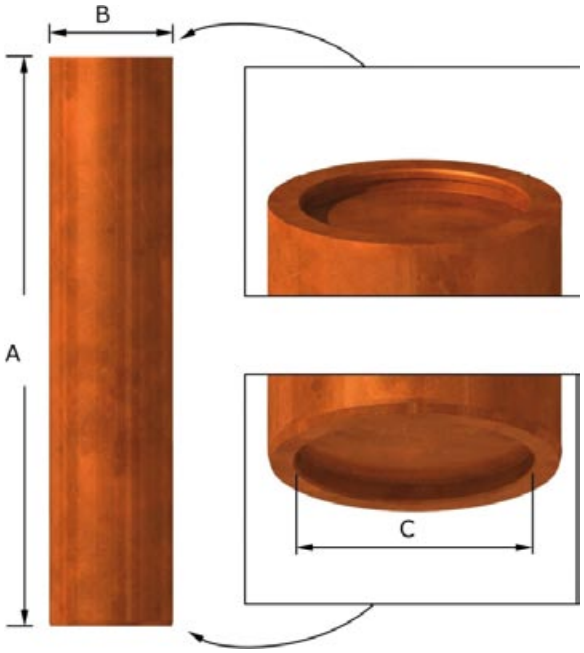

Figure 5-4. *Copper shell.*

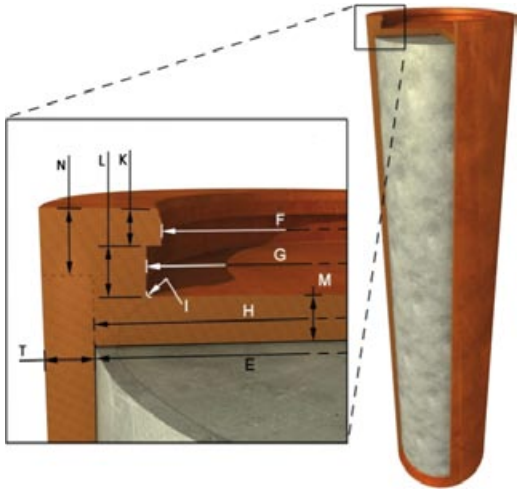

Figure 5-5. *Copper shell lid.*

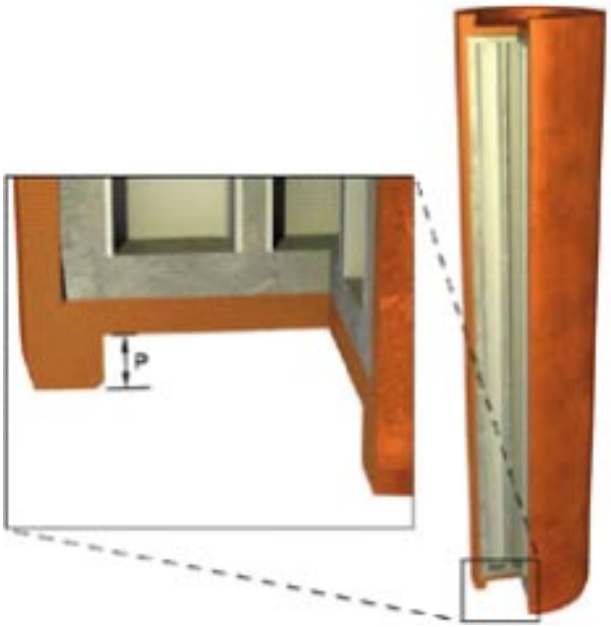

Figure 5-6. *Copper shell bottom.*

Table 5-1. Common dimensions for BWR- and PWR-insert.

Figure no and dimension designation	Designation	Nominal value mm	Tolerance mm
	Insert common dimensions		
5-1 A	Length of insert	*4,573*	*+0/–0.5*
5-1 D	Insert diameter	*949*	*+0.5 /–0*
	Steel lids		
5-3 E	Diameter	*910*	*h7*
5-3 F	Lid thickness	*50*	*+0.1/–0.1*
5-3 G	Bevel angle	*5°*	

Table 5-2. Dimensions for BWR-inserts.

Figure no and dimension designation	Designation	Nominal value mm	Tolerance mm
	BWR-Inserts		
5-1 B	Thickness of bottom	*60*	*+10.1/ –5.6*
5-1 C	Interior length	*4,463*	*+5/–10*
5-2 H	Edge distance	*33.3*	
	BWR-Insert channel tubes		
5-2 I	Ext. channel tube corner radius	*20*	*+5/–5*
5-2 K	Distance between channel tubes	*30*	*+2.7/–4.6*
5-2 Calculated	C-C distance between channel tubes	*210*	*+1/–4*
5-2 L	Int. cross-section	*160 × 160*	*+3.8 /–3.8*
5-2 Calculated	Channel tube thickness	*10*	*+1/–1*
5-2 Calculated	Channel tube size, outer	*180*	*+1.8/–1.8*

Table 5-3. Dimensions for PWR-inserts.

Figure no and dimension designation	Designation	Nominal value mm	Tolerance mm
	PWR-Inserts		
5-1 B	Thickness of bottom	*80*	*+10.1/–5.6*
5-1 C	Interior length	*4,443*	*+5/–10*
5-2 H	Edge distance	*37.3*	
	PWR – Insert channel tubes		
5-2 I	Ext. channel tube corner radius	*20*	*+5/–5*
5-2 K	Distance between channel tubes	*110*	*+6.2/–6.2*
5-2 L	Int. cross-section	*235 × 235*	*+5.1/ –5.1*
5-2 Calculated	Channel tube thickness	*12.5*	*+1.25/–1.25*
5-2 Calculated	Channel tube size, outer	*260*	*+2.6/–2.6*

Table 5-4. Dimensions for copper shells.

Figure no and dimension designation	Designation	Nominal value mm	Tolerance mm
	Copper shell		
5-4 A	Total length	*4,835*	*+3.25/–2.75*
5-5 T	Wall thickness	*49*	*+0.3/–0.3*
5-4 B	Outer diameter	*1,050*	*+1.2/–1.2*
5-4 C	Inner diameter	*850*	*+0.8/–0.8*
5-5 E	Inner diameter	*952*	*+0.5/–0.5*
5-5 F	Inner diameter	*821*	*+0/–0.5*
5-5 G	Inner diameter	*850*	*+0.8/–0.8*
5-5 H	Diameter, lid	*953*	*d8*
5-5 H	Diameter, pipe	*953*	*H8*
5-5 I	Corner radius	*10*	–
5-5 K	Dimension	*35*	*+0.5/–0.5*
5-5 L	Dimension	*50*	*+0.2/–0.2*
5-5 M	Thickness	*50*	*+0.6/–0.6*
5-5 N	FSW position top	*60*	–
5-6 P	Dimension	*75*	*+0.3/–0.3*
5-6	Thickness bottom	*50*	*+1/–1*
5-6	FSW position bottom	*50*	–
5-5 Calculated	Inner free length	*4,575*	*+0.6/–0.1*
5-5 Calculated	Axial gap between lids	*2*	*+1.1/–0.3*
5-5 Calculated	Radial gap between shell and insert	*1.5*	*+0.25/–0.5*

6 Analysis results

6.1 Insert strength

The insert is the principal load carrying part of the canister. All the dimensioning loads act on the canister from outside. Usually they are of isostatic pressure type, but in special cases also unevenly distributed swelling pressure or rock shear may occur. The rock shear load from the deposition hole surfaces is transferred onto the canister surface through the bentonite buffer.

6.1.1 Loads before full bentonite water saturation

The first load phase after disposal of the canister is the start of bentonite buffer wetting. The buffer is wetted randomly from the water bearing fractures that intersect the deposition hole. The process time-scale may be from 0 to more than 100 years until full saturation is reached, depending on the configuration of fractures in contact with the deposition hole or tunnel.

The worst case scenarios of bentonite swelling load evolution are described in /SKBdoc 1206894/.

During the water saturation phase of the buffer the temporary stresses that are critical to the iron insert are estimated. These load cases are derived from uneven horizontal stresses where the canister acts as a freely supported beam. The worst case that may occur, if requirements on the buffer and deposition hole are fulfilled, is a curved hole. Simplified calculations of the stresses in the canister insert yield a maximum bending stress σ_b = 105 MPa /SKBdoc 1206894/.

The resulting bending stresses in the cast iron insert are in all calculated cases lower than the yield strength, thus the insert will withstand them elastically, without plastic deformation or risk for damage. The crack sensitivity at the most stressed location (insert surface) has been estimated and the allowable crack size is larger than in limiting load cases, /Dillström et al. 2010/. These load cases exist only before water saturation of the bentonite buffer and thus they need not be combined with any other loads.

The less-stiff (lower Young's modulus) copper shell will be supported by the insert so long as the pressure is acting locally only on some sections of the shell. When the bentonite wetting process continues, the load will become more symmetric and extend more widely around the canister and thus the bending effect will be reduced.

6.1.2 Loads after full bentonite water saturation

Bending of canister due to uneven swelling

The load cases regarding permanent stresses in the buffer that are critical for the cast iron insert are derived from uneven horizontal stresses where the canister acts as a freely supported beam. The worst case derived in /SKBdoc 1206894/ is a curved hole and a local rock fall out of 3.75% of the cross section area. Simplified calculations of the stresses in the canister insert give a maximum **bending stress** of 111.5 MPa.

This bending stress of 111.5 MPa is a little higher than the highest bending stress during water saturation phase. The full analysis is given in /SKBdoc 1206894/.

The resulting bending stresses in the cast iron insert are in all calculated cases lower than the yield strength, thus the insert will withstand them elastically, without plastic deformation or risk for damage. These load cases are acting after bentonite saturation for a very long time. The probability of occurrence for these extreme load cases is very low, which means that they should not be combined with other low probability cases.

External pressure

As seen from the Table 2-1 earlier in Section 2, the design isostatic load case is the summed pressure of bentonite swelling, the normal ground water hydrostatic pressure at the repository depth and, during glacial period, the additional pressure caused by the ice sheet floating on the groundwater.

The design pressure of the canister is 45 MPa external pressure and the operating temperature (in that load condition) during glacial period will be between 0 and 20°C. The load case will affect all the canisters in the repository. Thus the reliability of the canister mechanical integrity needs to be high against this load case, because the possible risk concerns all the canisters in the repository.

The canister insert is the load bearing component of the canister structure. The cast iron insert is analysed using finite element models taking into account, to varying extent, the variation of material properties, geometry and also the effect of postulated defects. The stability of the structure, interaction with the steel tubes and with the copper shell is analysed. A separate analysis is made for the steel lid from the insert. The analyses are made for both types of inserts, BWR and PWR. The BWR-insert is the governing case of the two. The basic bench marking of the canister insert, insert lid, and bottom against the governing pressure load are presented in /Dillström et al. 2010, SKBdoc 1177857, SKBdoc 1207429/.

The external collapse loads for nominal insert cylinders are 99 and 128 MPa for BWR- and PWR-inserts (using the procedure given in ASME III, Div. 1, NB-3228.3 and NB-3213.25), /ASME 2008a/, respectively, and even more for the steel lids in both constructions according to /SKBdoc 1177857, Dillström et al. 2010/. In /SKBdoc 1207429/ the analyses of the bottoms for the BWR- and PWR-inserts are presented. The bottom analyses were made with manufacturing tolerances, according to Section 5, giving the maximum stresses in the bottoms. The collapse loads were then calculated to 105 MPa and about 100 MPa for the bottom ends of BWR- and PWR-inserts, respectively. The required limit load in ASME Code (ASME III, Div 1, NB-3200), /ASME 2008a/ nomenclature is 1.5 times the design pressure, i.e. 67.5 MPa. According to the design calculations, the actual safety factor against limit load is 2 at the design pressure, as a minimum.

During manufacturing of the insert it might happen that the steel tube cassette is positioned somewhat off-set in relation to the centre of the insert. This will cause a decrease of the edge distance of the insert, dimension *H* in Figure 5-2. The effect of this has been analysed in /Dillström et al. 2010/ and probabilistically evaluated in /SKBdoc 1207426/. The result is that a 10 mm reduction of the edge distance can be tolerated with remained low probability of local plastic collapse and low probability of initiation of crack growth.

The basic design analyses show that the collapse load of the insert including the integral bottom and screw-fastened steel lid is clearly more than 1.5 times the design pressure 45 MPa. The high external pressure load capacity of the canister structure was also verified by two model tests described as follows.

Pressure tests

Two destructive pressure tests were made on two BWR-canisters with insert length of 700 mm; the diameter was the actual one according to Section 5. The tested inserts were covered by normal thickness copper shell and lids. The first sample was a knowingly poor cast sample, it contained large defects and the machining was made with 12 mm off-set (eccentric) so that the steel cassette was not placed centrally. The second one was of the best available samples at that time (2004–2005). The first one was pressurized in a pressure chamber until large plastic deformation of 20 mm at external pressure of 130 MPa and the second one until full plastic collapse and rupture at external pressure of 139 MPa. The testing was documented and reported in /Nilsson et al. 2005/.

The pressure tests were simulated with pre- and post-simulation with various FEM-analysis programmes with good consistency. This showed that actually the collapse pressure of the canister is remarkably high and secondly that the strength of the canister insert can be predicted and simulated by numerical methods with good accuracy and reliability. The pressure tests and the verification strength analyses are widely reported and summaries of them are given in /SKBdoc 1207426, Martin et al 2009/. A probabilistic strength analysis of the canister was made already in 2004–2005 as a part of the pressure test programme. However, the results were updated in 2009 in /SKBdoc 1207426/, when additional fracture resistance data of the inserts was available.

An independent collapse load analysis for the canister /Martin et al. 2009/ was made in 2008. The pressure test results and the calculated collapse load results are very close to each other and thus verify the analysis models and the reliability of the calculation methods in this type of analysis.

For the BWR-insert the isostatic load case has been handled in a probabilistic analysis in /SKBdoc 1207426/. The analysis shows that the risk of failure of the insert is extremely low in all presented cases up to the design pressure of 45 MPa. For an insert with nominal geometry and centred steel cassette the risk for failure has been calculated to be $<1\times10^{-50}$ in /SKBdoc 1207426/.

Fracture resistance analyses

The allowable defect size and other types of deficiencies in various locations (Figure 6-1) in the insert were examined by fracture resistance analysis that is also reported in /Dillström et al. 2010/ and in /SKBdoc 1207429/ for the insert bottom. The analysis was made in the 'normal' way in that the stress intensity factor K_I was calculated in various locations for postulated cracks and the stress intensity was compared, using a safety factor of $\sqrt{10}=3.16$, to a reference value of the tested material property K_{Ic} at a temperature 0°C. In this load case the insert material behaves everywhere linear-elastically, thus K_I-method can be used instead of a non-linear J-integral analysis to assess the risk of fracture. In the isostatic load case (45MPa) the allowable defect sizes for axial crack-like defects in various locations were according Table 6-1 /Dillström et al. 2010/. For the BWR insert bottom the allowable crack depth was calculated to be >80% of the bottom thickness.

The inserts were also analysed against design pressure where axial boreholes were postulated in various zones. The analyses were based on the limit load method using a safety factor of 1.5 according to ASME rules. The allowable hole sizes are given in Table 6-2. Also, other types of material deficien-

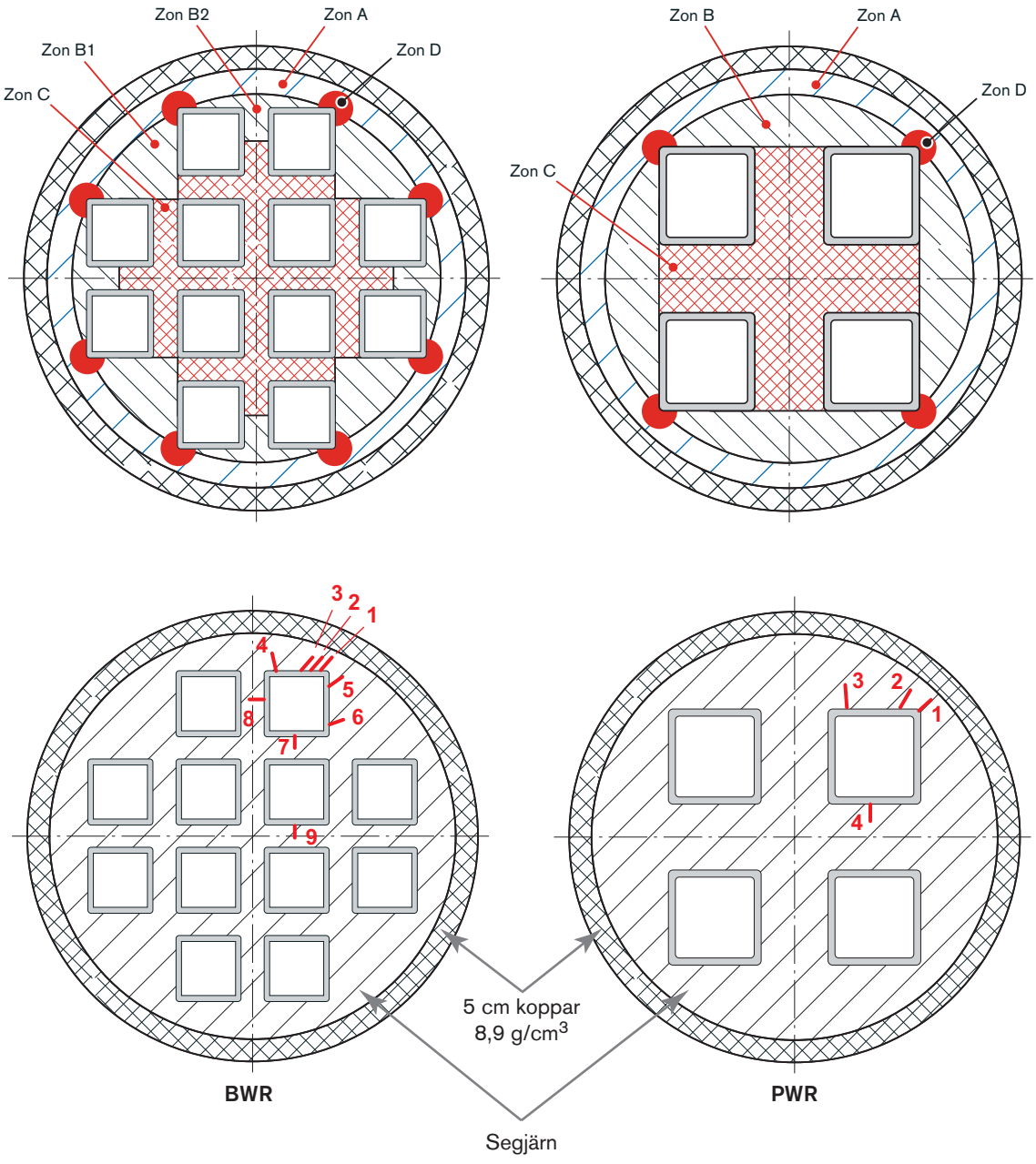

Figure 6-1. *Top: The analysed locations of postulated defects in BWR- and PWR-inserts, Bottom: Positions of analysed crack-like defects /Dillström et al. 2010/.*

Table 6-1. Allowable defect sizes a_c [mm] (c/a-ratio 3 according to ASME reference defect, /ASME 2008b/) in various locations of canister inserts when loaded by dimensioning external pressure load of 45 MPa or with bending stress of 111.5 MPa from uneven bentonite swelling. Safety factor against K_{Ic} iS 3.16.

Zone	Load type	Postulated crack orientation	BWR-insert Defect size a [mm]	PWR-insert Defect size a [mm]
A	External pressure	Axial	37	53
B	External pressure	Axial	–	112
B1	External pressure	Axial	65	–
B2	External pressure	Axial	50	–
C	External pressure	Axial	24	104
D	External pressure	Axial	32	31
A, D	Axial bending stress	Circumferential	48*	–**

*) The extreme value for axial bending stress case is classified as rare load case. A lower safety factor (1.41) is used.

**) Not analysed, because the section modulus of BWR-canister is less than that of PWR-canister. See 6.1.4 for details of section modulus.

Table 6-2. Allowable axial hole sizes D_c [mm] in various locations of canister inserts when loaded by dimensioning external pressure load of 45 MPa. Safety factor against limit load is 1.5.

Zone	Load type	BWR-insert Hole diameter D_c [mm]	PWR-insert Hole diameter D_c [mm]
A	Design pressure	40	80
B	Design pressure	–	100
B1	Design pressure	60	–
B2	Design pressure	20	–
C	Design pressure	20	100
D	Design pressure	20	20

cies are analysed in /Dillström et al. 2010/, and the results show that the insert structure is insensitive to many kinds of material imperfections. The most extreme case that is analysed in /Dillström et al. 2010/ is when all material within zone C for the BWR-insert is removed. Applying the ASME safety factor like for allowable hole sizes, the acceptable axial length for removal of all material within zone C became 412 mm. In Figure 5-2 a hole can be seen. This is a threaded hole (M45) used for lifting the insert. The hole is located to zone B1 for BWR-inserts and zone B for PWR-inserts (see Figure 6-1). Table 6-2 confirms that the holes are smaller than the allowable hole sizes.

The extreme value for the bending load from uneven bentonite swelling is considered as a low probability load case. Based on this the allowable defect size has been calculated with lower safety factors according to ASME rules, e.g. 1.41 was used for K_{Ic} instead of 3.16 as used above. The maximum allowable crack depth (a) of a semi-elliptic surface defect oriented in tangential-radial direction is of size a=48 mm, when the elliptic c/a-ratio iS 3. Symbols 'a' and 'c' stand for the shorter and longer semi-axles of an ellipse. For definition of dimensions 'a' and 'c', see Figure 8-1. The analysis is given in /Dillström et al. 2010/. Later it will be seen that the rock shear case will lead to even smaller allowable defect sizes, which will thus become the governing case. The bending load case has not been combined with an isostatic pressure. This is judged for the tensile stresses as conservative since previous calculations have shown that the maximum tensile stresses caused by the bending will decrease when an isostatic pressure is applied /Dillström et al. 2010/. This is also the case for the rock shear load where the addition of a glacial load decreases the stresses in the insert; this is presented further in Section 6.1.3.

In general, the minimum of allowable defect sizes of all load cases in various zones will be set as the acceptance limit for the NDT-testing of samples after insert manufacture in respective zones. However, the results presented in Table 6-1 are limited by in the range of applicability of the analysis. The maximum defect size, *a,* that can be analysed corresponds to 80% of the material thickness. All given defect sizes in Table 6-1 correspond to this 80% limitation. This limitation originates from the limited range of applicability of the applied computer model. Even deeper cracks may be allowable.

Copper shell creep analysis

The results for iron insert obtained from glacial pressure load creep analysis are reported in /Hernelind 2010/ and could be summarized for the iron insert as follows:

- The glacial pressure load does not generate any plastic strains in the insert.
- The stresses in the insert are shown later in Figure 6-15 – mostly in compression and much below the yield stress.
- The insert will have displacements less than 1 mm, see Figure 6-14. The displacements due to creep in the shell do not seem to affect the initial geometry used for a following earthquake induced rock shear analysis.

The results for the copper shell in this analysis are given in 6.2.5.

6.1.3 Rock shear with or without glacial pressure load

The rock shear case was analysed in two subsequent steps. The first step used a global model of the canister including the surrounding bentonite /Hernelind 2010/. Also the bentonite will have some creep (not included in the model). However, due to very short time of the shear load action, the possible creep in the bentonite does not have time to affect the short time result. The creep in bentonite relaxes the residual stress condition in the bentonite buffer later. This first model generated deformations that were used as input for a more detailed damage tolerance analysis /Dillström 2010/ using sub models. The damage tolerance analysis was the second step of rock shear analyses.

Rock shear analysis using a global model

The global model rock shear analysis was done with a 3D-finite-element model using ABAQUS. A symmetric half of the bentonite buffer, copper canister and cast iron insert was modelled with 8-noded hexahedral and a few 6-noded wedge elements. The rock shear load was introduced by an applied displacement at the outer boundary of the bentonite buffer. All interfaces between bentonite, copper shell and iron insert interacted through contact surfaces with modelled friction of 0.1 times the contact pressure. In cases where contact was lost, the friction was set equal to 0. The rock shear analyses are reported in /Hernelind 2010/. When not otherwise stated the simulations have been done based on the geometry for the BWR-insert.

The shear plane was varied. The temperature of the materials was assumed conservatively to be constantly 300 K (+27°C) for the copper and 273 K (0°C) for the cast iron. The density of the bentonite was varied, with the values set to 1,950, 2,000 and 2,050 kg/m^3, which mean that different material models for the bentonite were used. The swelling pressure of bentonite and the hydrostatic pressure of groundwater (normal 4 MPa or under glacial period up to 32 MPa) have been added in various analysis cases with the actual shear load. The glacial pressure load combined with rock shear load is not, however, the governing load combination, but the combination of normal hydrostatic pressure + bentonite swelling pressure + rock shear. For details of all analysed combinations, see /Hernelind 2010/.

For each analysis a large amount of results are available and to have an indication only a few values are reported. The reported values all correspond to the case of 5 cm rock shear. However, results are available also for larger shearing amplitudes in /Hernelind 2010, Dillström 2010/. For the **short term rock shear analyses** (the analyses include only a short time frame of a few seconds, creep is not included) the cross sectional average and peak values for Mises effective stress and effective plastic strain (PEEQ) are summarized in Table 6-3. A short description of each model name in Table 6-3 is given below. The highest peak value for PEEQ in the copper shell, 23%, occurs for rock shear perpendicular to the canister axis at ¾ of the height from bottom. The full glacial pressure existing after a rock shear gives the highest value 23% but in case of ½ height and without glacial pressure the highest PEEQ in copper shell is almost equal, 21%.

This means that neither the effect of glacial pressure load existing after the rock shear nor the intersection point of the rock shear make big difference in the dimensioning results.

Table 6-3. Summary of insert results for short term rock shear analyses, 5 cm shear case.

Model name Model6g_xx	1 – iron insert 2 – steel channel tubes	PEEQ/CEEQ [%]		Mises stress [MPa]		S33 stress*) [MPa]	Comment
	Shearing [cm]	5		5		5	
	Insert material	1	2	1	2	1	
normal_quarter_2050ca3		0.5	0.9	321	470	333	
normal_quarter_creep_2050ca3		0.4	0.4	314	455	336	
normal_quarter_creep_ggr5_2050ca3		0.4	0.4	314	455	336	
normal_quarter_glacial3_2050ca3		0	0.003	335	475	102	
normal_quarter_pressure_2050ca3		1.0	1.9	340	551	295	After glacial load
normal_quarter_halffrict_2050ca3		0.5	0.5	319	463	333	
normal_quarter_doublefrict_2050ca3		0.7	1.5	336	468	332	
normal_quarter_slow_2050ca3		0.5	0.8	312	462	327	
normal_quarter_steel_2050ca3		0.3	0.4	305	476	330	
thick_normal_quarter_2050ca3		0.1	0.1	301	455	304	
normal_half_2050ca3		0.1	0.3	299	464	212	
normal_half_creep_2050ca3		0.01	0.1	292	441	192	
22_quarter_tension_2050ca3		0	0.2	290	495	126	Stops after 9.2 cm
22_quarter_tension_creep_2050ca3		0	0	139	287	119	Stops after 5.1 cm
22_mid_tension_2050ca3		0.03	0.2	295	491	177	
22_mid_tension_creep_2050ca3		0	0.1	259	493	197	Stops after 5.5 cm
full_hori_quarter_2050ca3		0.4	0.3	300	545	64	
full_hori_quarter_creep_2050ca3		0.3	0.3	301	550	80	Stops after 6.4 cm
full_hori_mid_2050ca3		0.5	0.7	309	558	82	
full_hori_mid_creep_2050ca3		0.5	0.7	312	551	100	
normal_quarter_2000ca3		0.2	0.3	309	457	324	
22_mid_tension_2000ca3		0	0.04	213	488	130	
22_quarter_tension_2000ca3		0	0	199	474	98	Stops after 6.6 cm
normal_quarter_1950ca3		0.1	0.1	301	452	310	
22_mid_tension_1950ca3		0	0	155	392	98	Stops after 8.9 cm
22_quarter_tension_1950ca3		0	0	149	342	95	Stops after 7.1 cm
PWR_normal_quarter_2050ca3		0.5	0.3	318	416	325	
PWR_normal_quarter_creep_2050ca3		0.3	0.2	313	414	324	Copper shell creep only

*) S33 is the maximum axial stress component used for indication of postulated crack location.

The highest equivalent stress in the insert occurs when the rock shear is perpendicular to the canister axis at ¾ of the height from the bottom. The PEEQ is 1% and the von Mises stresS 340 MPa. This maximum is reached with the rock shear followed by the glacial pressure. In case the glacial pressure is not affecting simultaneously, the maximum stress iS 321 MPa and the plastic strain 0.5%. For all results, see Table 6-3 or the analysis report /Hernelind 2010/. The highest axial principal stress (S33) case is used for fracture resistance analysis and that load case is the normal rock shear case without glacial pressure.

The square steel tubes are modelled separate in this set of analyses. The highest reported von Mises stress is 558 MPa and the maximum strain some 2%, which is some 10% less than the ultimate strength of the steel (UTS=613 MPa) and the ultimate elongation in one-dimensional stress-strain testing is generously 20% at minimum. For material model of steel, see Table 4-3.

Table 6-3 also contains results when the maximum hydrostatic pressure caused by the glacial ice sheet is applied or not by using pore pressure elements. Furthermore, the Table contains results when using the creep model instead of plasticity for the copper shell – in this case the effective creep strain (CEEQ) is reported.

For the canister insert, the effective stress (von Mises) in rock shear case (5 cm) is always less than UTS (456 MPa) and even remarkably less than the allowable 395 MPa in the insert. The results fulfil the stress criteria set out in 3.3.2. The maximum occurring effective stress (340 MPa) corresponds to the strain of 2.55% in the static uniaxial stress-strain curve for the insert iron. Static strength is conservative, if compared to rate-dependent (dynamic) strength. According to Figure 6-2, the actual maximum stresS 340 MPa is far from the maximum allowable stresS 395 MPa due to the plastic character of the stress-strain curve. The actual equivalent strain 2.55% is only about 2/5 of the allowable strain 6.3% and about 1/5 of the strain at rupture. This means that there is a lot of deformation capacity left in the insert structure during the shear load case. Figure 6-2 gives a clear picture of the ratio between actual, allowable and the ultimate tension stress and strain. Allowable strain is more than two times higher than the actual strain.

Figure 6-2. *The actual stress/strain (blue lines) in rock shear case in comparison to allowable stress/strain (green lines) and to ultimate stress/strain (red lines). The reference stress-strain curve is conservative, because it is based on static tests in room temperature, whereas the rock shear is dynamic load and the actual temperature is close to 0°C.*

The stresses and strains induced in the canister insert and copper shell are, on average, relatively low in the cross sections of the canister components. High values only exist locally in notches, geometric transitions or corners, where geometric stress concentration cause "peak stresses". Peak stresses are deemed relevant only in case of fatigue analyses according to ASME Code practice. No canister load is cyclic over a sufficient number of cycles that fatigue analysis would become necessary.

The numbers in Table 6-3 to 6-5 should be used with care and used in combination with the corresponding plots shown in the appendixes of the analysis report, /Hernelind 2010/. Each of the models referenced in Table 6-3 to 6-5 describes the load and the material properties as follows.

All geometry models are version 6g. They correspond to BWR insert with nominal dimensions. In some cases the analysis is made for PWR insert geometry. This is indicated with PWR string. The copper shell has always the same geometry with nominal dimensions and shape. The end of the model name string tells the respective bentonite buffer type and density; for ex. 2050ca3 means that it is question of strain-rate dependent Ca-bentonite with density 2,050 kg/m^3.

Three cases of rock shear directions have been analysed – these directions have been chosen based on the results from previous analysis:

rock shear perpendicular to the axis of the canister

- at ¾ of the height from the bottom (model6g_normal_quarter_2050ca3/2000ca3/1950ca3)
- at ½ of the height (model6g_normal_half_2050ca3/2000ca3/1950ca3)

rock shear in tension inclined with 22.5 degrees to the axis of the canister

- at ¾ of the height from the bottom (model6g_22_quarter_tension_2050ca3/2000ca3/1950ca3)
- at ½ of the height (model6g_22_mid_tension_2050ca3/2000ca3/1950ca3)

rock shear in the horizontal direction through a vertical plane (full model)

- at the symmetry plane (model6g_full_hori_mid_2050ca3)
- at ¾ vertical plane (model6g_full_hori_quarter_2050ca3)

The long term scenario has also been analysed, where creep effects are included for the copper shell. The long term analyses (100,000 years) are performed by using the full symmetric model. The long term creep analysis is identified in the model name by a string "_creep_".

The PWR has been analyzed with rock shear perpendicular to the axis of the canister at ¾ of the height from the bottom using Na-bentonite converted to Ca-bentonite with density 2,050 kg/m^3 (model6g_PWR_normal_quarter_2050ca3).

The hydrostatic pressure caused by the ice sheet (30 MPa) has been simulated by one analysis where pore-pressure elements have been used for the bentonite. Model name is model6g_normal_quarter_glacial3_2050ca3.

In one scenario an earthquake occurs followed by a time period of about 13,000 years, in which case a thick layer of ice is build up corresponding to a pressure load of 30 MPa. The model name is model6g_normal_quarter_pressure_2050ca3.

More details of the large number of analyses made are given in the analysis result report /Hernelind 2010/.

The strain and stress result for the copper shell are given in Tables 6-4 and 6-5 accordingly with the iron insert results in Table 6-3.

Figure 6-3 shows typical plastic strain result plot of the iron insert from the short term analyses (with Model6g_normal_quarter_2050ca3). The figure also shows that the highest strains in the insert are concentrated at the corners of the square openings and that the more strained volumes are very small. The maximum strain value in the rounding of the cast iron insert is less than 1% in the design rock shear load case of 5 cm. In the square tubes made of steel the maximum strain is about 1% accordingly in the rounded corner.

The results obtained from the global model used for rock shear analyses could be summarized as:

Table 6-4. Summary of copper shell strain results for short term rock shear analyses, 5 cm shear case according to /Hernelind 2010/.

Model name Model6g_xx	1 – mid shell 2,3 – top/bottom welds 4,5 – top/bottom discontinuous 6,7 – top/bottom fillets 8,9 – top/bottom reminding	PEEQ/CEEQ [%] 5 cm shearing								
	Copper shell region	1	2	3	4	5	6	7	8	9
normal_quarter_2050ca3		1.0	3.6	2.7	1.5	16	0.4	0.05	2.6	0.8
normal_quarter_creep_2050ca3		0.7	2.6	5.5	1.8	7.2	0.09	0	0.2	0.3
normal_quarter_creep_ggr5_2050ca3		0.7	2.6	5.4	1.8	7.5	0.09	0	0.2	0.3
normal_quarter_glacial3_2050ca3		1.3	12.3	3.1	3.2	16	1.9	0.08	1.9	1.0
normal_quarter_pressure_2050ca3		1.4	3.6	2.8	2.1	23	0.9	0.1	3.1	1.3
normal_quarter_halffrict_2050ca3		1.0	4.0	2.7	1.4	16	0.4	0.8	2.6	0.9
normal_quarter_doublefrict_2050ca3		1.1	2.3	2.6	2.0	17	0.4	0.3	0.7	0.7
normal_quarter_slow_2050ca3		1.0	3.6	2.7	1.5	16	0.4	0.05	2.4	0.8
normal_quarter_steel_2050ca3		0.8	3.4	2.7	1.5	16	0.4	0.2	1.9	1.0
thick_normal_quarter_2050ca3		0.8	3.0	2.8	1.7	12	0.8	1.0	0.8	1.2
normal_half_2050ca3		1.9	4.5	3.3	6.3	21	4.7	1.4	3.0	1.7
normal_half_creep_2050ca3		0.8	4.3	4.5	2.3	6.7	0.2	0.1	0.3	0.4
22_quarter_tension_2050ca3		1.5	14	9.5	2.4	15	9.3	0.9	5.5	1.2
22_quarter_tension_creep_2050ca3		0.1	0.4	6.2	0.1	1.2	0.1	0.1	0	0.09
22_mid_tension_2050ca3		0.7	4.3	5.1	1.8	15	0.9	1.0	0.9	1.2
22_mid_tension_creep_2050ca3		0.6	3.1	9.6	2.1	2.0	0.8	0.1	0.3	0.2
full_hori_quarter_2050ca3		0.7	4.2	5.0	1.1	4.3	2.7	1.4	1.6	1.3
full_hori_quarter_creep_2050ca3		0.6	7.2	10.1	3.3	2.5	0.6	0.1	0.7	0.3
full_hori_mid_2050ca3		0.9	4.1	3.5	1.1	6.9	3.6	1.3	1.7	1.7
full_hori_mid_creep_2050ca3		0.4	6.0	7.3	3.1	2.1	0.5	0.1	1.0	0.2
normal_quarter_2000ca3		0.8	2.8	2.5	1.1	14	0.5	0.1	0.6	1.0
22_mid_tension_2000ca3		0.5	5.0	5.3	1.2	8.1	0.5	0.5	0.8	0.6
22_quarter_tension_2000ca3		0.7	17	9.6	2.1	8.1	4.4	0.7	2.4	0.8
normal_quarter_1950ca3		0.6	2.3	2.6	0.9	12	0.8	0.2	0.5	1.0
22_mid_tension_1950ca3		0.5	4.3	5.3	0.6	3.4	0.4	0.2	0.5	0.3
22_quarter_tension_1950ca3		0.6	18	9.3	1.6	4.0	2.0	0.5	1.2	0.5
PWR_normal_quarter_2050ca3		1.1	3.2	2.7	1.3	17	0.5	0.1	0.8	0.8
PWR_normal_quarter_creep_2050ca3		0.7	2.5	5.3	0.2	9.4	0.2	0	0.2	0.5

Table 6-5. Summary of copper shell von Mises stress results for short term rock shear analyses, 5 cm shear case according to /Hernelind 2010/.

Model name Model6g_xx	1 – mid shell 2,3 – top/bottom welds 4,5 – top/bottom discontinuous 6,7 – top/bottom fillets 8,9 – top/bottom reminding	Mises [MPa] 5 cm shearing								
	Copper shell region	1	2	3	4	5	6	7	8	9
normal_quarter_2050ca3		103	145	147	121	201	81	85	109	103
normal_quarter_creep_2050ca3		237	206	223	308	304	178	141	206	283
normal_quarter_creep_ggr5_2050ca3		233	205	220	309	298	173	139	200	278
normal_quarter_glacial3_2050ca3		102	210	152	121	216	100	87	113	88
normal_quarter_pressure_2050ca3		116	149	142	118	262	85	84	141	119
normal_quarter_halffrict_2050ca3		102	146	97	117	198	82	84	111	88
normal_quarter_doublefrict_2050ca3		111	88	99	115	202	81	85	113	108
normal_quarter_slow_2050ca3		102	146	147	121	201	80	85	109	104
normal_quarter_steel_2050ca3		94	104	144	120	201	81	81	127	88
thick_normal_quarter_2050ca3		102	141	102	109	207	94	92	98	89
normal_half_2050ca3		139	99	149	134	254	130	94	112	95
normal_half_creep_2050ca3		241	227	230	317	310	236	242	228	279
22_quarter_tension_2050ca3		128	268	185	112	133	174	96	179	93
22_quarter_tension_creep_2050ca3		221	181	200	99	174	104	202	115	187
22_mid_tension_2050ca3		92	178	144	128	118	112	94	115	91
22_mid_tension_creep_2050ca3		212	325	259	322	271	235	244	216	218
full_hori_quarter_2050ca3		128	146	146	116	145	108	101	129	94
full_hori_quarter_creep_2050ca3		294	239	256	407	262	223	242	326	220
full_hori_mid_2050ca3		107	98	142	121	171	118	99	115	98
full_hori_mid_creep_2050ca3		239	241	266	400	267	217	235	315	233
normal_quarter_2000ca3		123	131	100	105	187	84	82	117	111
22_mid_tension_2000ca3		94	173	144	109	105	109	88	107	84
22_quarter_tension_2000ca3		93	260	186	112	109	122	93	115	96
normal_quarter_1950ca3		107	121	101	100	174	85	83	120	88
22_mid_tension_1950ca3		82	152	142	100	127	86	88	108	87
22_quarter_tension_1950ca3		95	247	183	120	114	99	91	142	88
PWR_normal_quarter_2050ca3		103	145	144	110	206	103	89	111	90
PWR_normal_quarter_creep_2050ca3		238	212	234	211	301	195	178	206	275

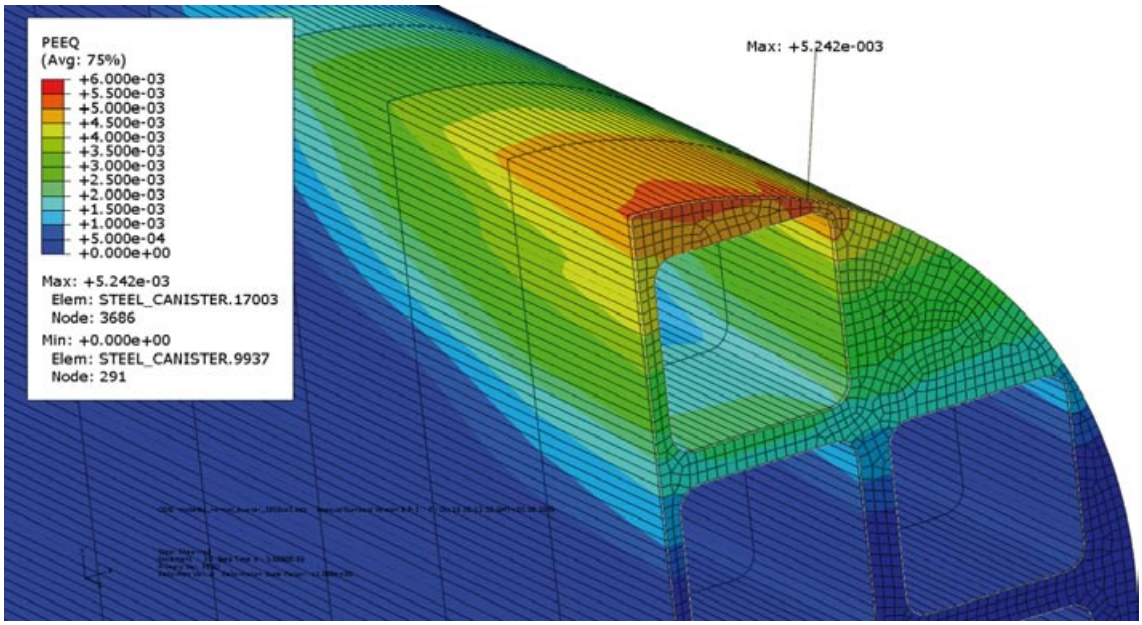

Figure 6-3. *The highest strains in the iron insert are concentrated into the corner radii of the square openings. Generally the plastic strain level is low in insert. The case is "normal_quarter_2050ca3", the maximum strain 0.5% and the rock shear amplitude is 5 cm.*

- The maximum plastic strain in the copper shell occurs in fillet corners. At the global level the plastic strain is much lower, see Figure 6-17.
- The maximum plastic strains and effective stresses in the insert occur at the corners of a specific channel. The steel cassette tubes were modelled separately in the global model.
- Maximum principal stress in the insert mainly comes from bending of the canister – the level depends mainly on material properties for the insert and the buffer.
- Creep seems not to be a concern, since the copper deformation is controlled by the surrounding material, which implies small creep strain rates as soon as the final deformation has been established. Also the bentonite will have some creep, which will lower the remaining stress level in the copper and thus contribute to less creep in the copper.
- Other loads acting simultaneously with the shear load does not influence the result negatively. The other loads increase the compression stresses of the insert, and thus the damage analysis would not lead to smaller allowable defect size.
- Finally, a comparison between the BWR- and PWR-inserts shows that, as expected, the stress and strain magnitudes are lower for the PWR-insert.

Damage tolerance analysis of the canister insert during rock shear case

The displacement results of the rock shear case from the global model are post-processed with more detail using higher order elements in local sub models (20-noded isoparametric elements) including defects - see /Dillström 2010/.

The results, presented below, are obtained using the different sub-models with defects. The ABAQUS domain integral method is used to calculate the *J*-integral. The sub model was placed such that the defect was located where the highest principal stress was identified. The results show that the density of the bentonite clay does have an effect on the results. Higher density gives higher *J*-values. It is also seen, as expected, that the elliptical surface defects give much higher *J*-values than the circular surface defects. The internal defects do not give as high *J*-values as the surface defects. These trends between the different types of defects do correspond to handbook solutions for simpler geometries and loading conditions.

The acceptable and critical defect sizes are calculated for ASME-type reference defects, a semi-elliptical surface defect with *a/c*-ratio of 1/3, for an elliptical subsurface defect (*a/c* = 1/3), a semi-circular surface defect and subsurface circular (coin-shaped) defect. The calculated allowable defect sizes of semi-elliptical surface defects (ASME reference defects, /ASME 2008b/) are shown in Table 6-6. The allowable *J*-integral value is based on the measured J_{2mm} value of 88 kN/m (with 90% confidence) and a safety factor of 2 according to ASME Code practice for postulated emergency or faulted condition (level C or D). The assessment guidance of actual detected indications is given in /Dillström et al 2008/.

If a surface defect is semi-circular the allowable crack depth, *a*, is 8.2 mm for the 5 cm shear load case and bentonite density 2,050 kg/m^3. Ccorrespondingly, for subsurface (buried) defects the allowable size of a circular crack, 2*a,* is >10 mm, and for an elliptical crack, 2*a*, is >10 mm for the ASME-reference defect (*a* being the minor axis of the ellipse).

This damage tolerance analysis is the governing case for the canister insert defects. It means that the maximum allowable surface defect size on the cylinder surface is 4.5 mm deep and 6 times as long reference defect. Presented values are thought to be conservative based on the discussion in Section 7.5. The most important result is to show that the reference canister has sufficient damage tolerance capacity to allow manufacturing and testing.

6.1.4 Strength of PWR insert

Most of the strength analyses are made for the BWR-insert. The PWR-insert is shown to be remarkably stiff against external pressure load and global bending load. Thus it is sufficient to do the more detailed analyses for BWR-insert only. The outside dimensions of the two inserts are identical but the sectional properties are somewhat different.

The basic design verification of the PWR-insert (including lid and bottom) is made in /Dillström et al. 2009, SKBdoc 1177857, SKBdoc 1207429/. The collapse limit load of the PWR insert is 20–30% higher than that of BWR-insert and thus acceptable. The section modulus *W* of PWR-insert (0.066 m^3) is 17% higher than that of BWR-insert (0.056 m^3) – which means that the maximum bending stress from equal force-controlled load in PWR-insert is about 15% lower than in BWR-insert. Section modulus (*W*) is the flexural rigidity (second moment of area) divided by maximum distance from the principal central axis of the section. According to Euler-Bernoulli beam-theory, the maximum bending stress is the maximum bending moment (*M*) divided by the section modulus (*W*). The higher bending strength of PWR-insert was noted also in the few rock shear analyses that were made for the PWR-canister model in /Hernelind 2010/.

The copper shell behaves on a PWR-insert in same way as on a BWR-insert, because of the same shape, dimensions and tolerances. The copper shells for BWR- and PWR-canisters are identical.

In manufacturing tests for the PWR-insert the ductility properties of cast iron have been generally somewhat lower than those of the BWR-inserts. This may depend on the fact that there have been fewer PWR-insert casting tests than BWR-casting tests and, secondly, that the section thicknesses are typically higher in PWR- than in BWR-inserts. In a heavier section the cast iron properties

Table 6-6. The calculated acceptable defect sizes of semi-elliptical surface defects (ASME reference defects, semi-elliptical, c/a=3) and the critical defect sizes. The defects are located in the tangential-radial direction. Load case corresponds to 5 cm shear. Remark the bentonite buffer density variations in different cases that are indicated in the analysis model name.

Model	Acceptable defect depth a (mm)	Acceptable defect length 2c (mm)
model6g_normal_quarter_2050ca3	4.5	27.0
model6g_normal_quarter_2000ca3	8.7	52.2
model6g_normal_quarter_1950ca3	>10	>60
	Critical defect depth a (mm)	**Critical defect length 2c (mm)**
model6g_normal_quarter_2050ca3	>10	>60
model6g_normal_quarter_2000ca3	>10	>60
model6g_normal_quarter_1950ca3	>10	>60

tend to be less ductile than in slender sections. According to test data from manufacturing tests in /SKBdoc 1207576/, the yield strength and ultimate strength of the PWR-inserts have been as good as those for BWR-inserts, but the average elongation at break (8.6%) has been somewhat lower than that of BWR-inserts (14%). However, the average value for the PWR includes inserts with lower toughness properties that are due to changes in the manufacturing process aimed at improving the understanding of the casting process. A recently produced insert that is more representative of what can be produced gave the following elongation at fracture for 90% confidence: $9.3\% < A_5 < 14.5\%$ /SKBdoc 1207576/. This value is closer to the one presented for the BWR-insert. A full batch of the PWR-inserts has not yet been manufactured. To finally establish the quality that can be foreseen a series of as-manufactured tests are needed and will be performed as soon as the manufacturing process is judged to be sufficiently optimised. Then full testing of the fracture toughness properties can also be done in order to confirm the strength of the PWR-insert in all load cases.

From the assessment made above it can be concluded that the PWR-insert most probably fulfils the integrity requirement at least as evidently as the BWR-insert. The slight difference in material properties is not remarkable in postulated load conditions, where an actual safety factor of 1.5, at minimum, against limit load conditions is present.

6.2 Copper shell strength

The copper shell that is surrounding the canister insert is not predominantly a load carrying structure. Its principal function is to be a gastight and waterproof barrier between the insert and the surrounding environment. However, to ensure its function, it must not be penetrated by any of the mechanical loads affecting the canister in long term.

6.2.1 Creep analysis with loads after saturation (symmetric loads)

The geometry of the canister is described in Section 5. The nuclear fuel waste is placed in a cast iron insert that is placed in the copper shell. The copper, Cu-OFP, to be used in the shell is specified in Section 4. The canister is exposed to an external pressure of about 15 MPa at a temperature of about 75°C after the disposal. The influence of these conditions will be discussed below. These conditions have been simulated with FEM-modelling.

The creep model applied is given by Equation 4-6. For the translation to multiaxial stresses, Equation 4-7 was used. First conditions with constant pressure along the shell will be considered below.

The outer dimensions of cast iron inserts are somewhat smaller than the inner dimensions of the copper shells to allow for safe assembly and thermal expansion of the insert in heat-up phase. The lid and the bottom of the copper shell can be described as clamped disks. When the external pressure is applied, inward deflection occurs. For the cylindrical part of the copper shell an inward deformation will also take place except at the lid and the bottom. The shell becomes slightly hourglass shaped.

When sufficient plastic deformation has taken place the shell establishes contact with the insert at the lid and bottom as well as along the cylindrical part of the copper shell. To represent the contact between the shell and the insert, the penalty-barrier method is used /Jin and Sandström 2008/. According to this method, non-linear springs connect the surfaces, giving additional stiffness. During non-contact, this stiffness is low and has little effect on the deformation. At predefined distances between the contacting surfaces the springs are activated and resist further closure.

The creep rate as a function of radius in the copper shell is illustrated in Figure 6-4. For convenience in the interpretation of Figure 6-4, the translation of seconds to more handy units is given:

Initially the effective stress (von Mises) is much higher at the inner radius than at the outer radius. This is the initial elastic stress state. This is the reason why the creep rate is larger at the former position. As a consequence stress redistribution takes place. After about 1×10^8 s (about 3 years), the creep rate distribution is more or less horizontal. This is a result of the high creep exponent $n = 65$. For a detailed discussion, see /Jin and Sandström 2008/. This can be considered as a space stationary state. Once the cylindrical part of the copper shell is in contact with the insert, the stress and the creep rate drop. A horizontal strain rate distribution is reached after 1×10^8 s and the strain rate begins to drop at 3×10^8 s.

1.0E+04 s	2.8 hours
1.0E+05 s	28 hours
1.0E+06 s	12 days
1.0E+07 s	4 months
1.0E+08 s	3 years
1.0E+09 s	32 years

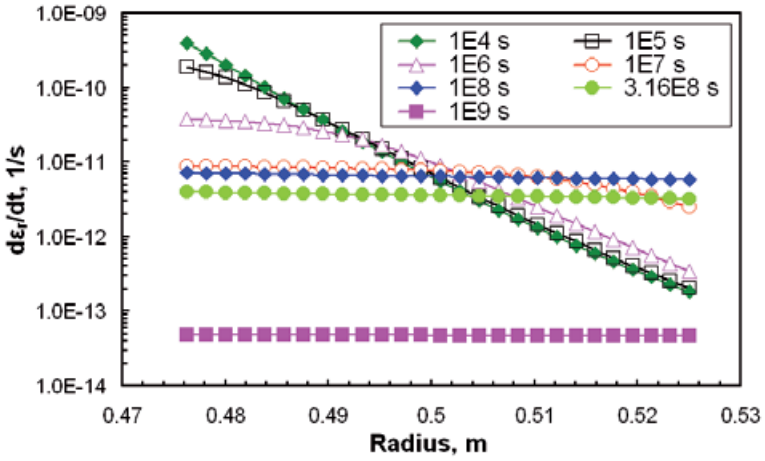

Figure 6-4. *Creep rates across the wall of canister shell in r direction at times between 10^4 and 10^9 s.*

In Figure 6-5 the displacements in the radial direction along the length of the cylindrical wall of the copper shell are shown. The z-axis is along the canister cylinder, starting from the bottom. Initially an elasto-plastic deformation takes place. After 10^7 s creep deformation starts to appear. Not until 1×10^8 s is there any significant displacement due to creep. After 3×10^8 s contact has occurred with the insert along most of its length and the creep deformation is essentially complete. The creep strain is then 0.27% at the inside and 0.21% at the outside of the wall /Jin and Sandström 2009b/.

The displacements in the lid and the bottom at different times are shown in Figures 6-6 and 6-7.

Elasto-plastic deformation takes place directly upon loading and represents the major part of the straining. The deflections at the centres of the lid and bottom immediately get in contact with the insert, reaching the specified maximum values. Only after about 1×10^8 s does some creep deformation appear. There is a slight continuous creep due to the rotation of the corners of the shells, which will be discussed below. The magnitude of the displacements remains limited due to the contact with the cast insert at the lid and bottom and along the cylindrical wall of the copper shell.

The maximum creep strains appear at the corners at the radii in the lid and bottom. These strains are given as a function of time in Figure 6-8. After 3.16×10^8 s the maximum strain is less than 12%.

The magnitude of the creep strain in Figure 6-8 is considerably larger than in the cylindrical wall of the copper shell, which is less than 0.3%, see above /Jin and Sandström 2009b/. At the corners there are initially very large stresses, Figure 6-9.

They are due to the presence of bending moments. Consequently the creep strains are large. A rapid relaxation of these stresses takes place. The maximum stress is reduced linearly with the logarithm of time. If this behaviour continues, the contribution to the strain decreases by more than a factor of 10 for each extra decade in time. The contribution for much longer times than in Figures 6-8 and 6-9 can therefore be expected to be small.

In a previous analysis the constitutive equations only took secondary creep into account /Jin and Sandström 2008/. In that analysis the time to close the gap between copper shell and insert was several order of magnitude larger than in the analysis presented here. It demonstrates that primary creep plays an important role.

For the climb-glide model, Equation 4-7, the creep rate is reduced approximately by an order of magnitude if the temperature is decreased by 10ºC. Thus if the temperature in the copper is 65ºC rather than 75ºC, the gap along the cylindrical wall of the copper shell will be closed after 3×10^9 s, i.e. 100 years. On the other hand if the temperature is 85ºC, the gap will be closed already after one year after full load has been applied. The influence of the stress level is even more dramatic due to the high creep exponent $n = 65$. If the saturation stress is increased 1 MPa, the cylindrical gap will be closed in less than 1/10 of the time for 15 MPa. On the other hand if the stress is reduced by 1 MPa the time will be increased by more than a factor of 10. If the new basic model for primary creep mentioned in Section 4 is used, this sensitivity is expected to be much reduced. The reason is that the basic model gives a larger contribution for the initial elasto-plastic straining, and this effect is known to be significant. This can be seen in Figures 4-5 and 4-6.

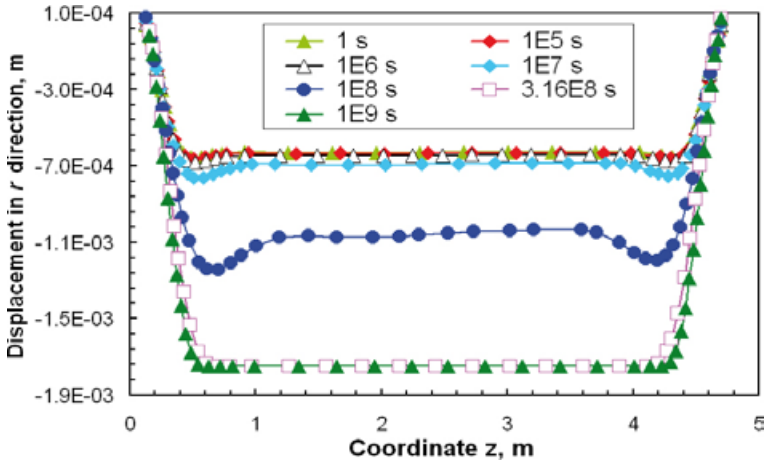

Figure 6-5. *Displacements for the inner wall of canister shell in the radial direction at times up to 10^9 s.*

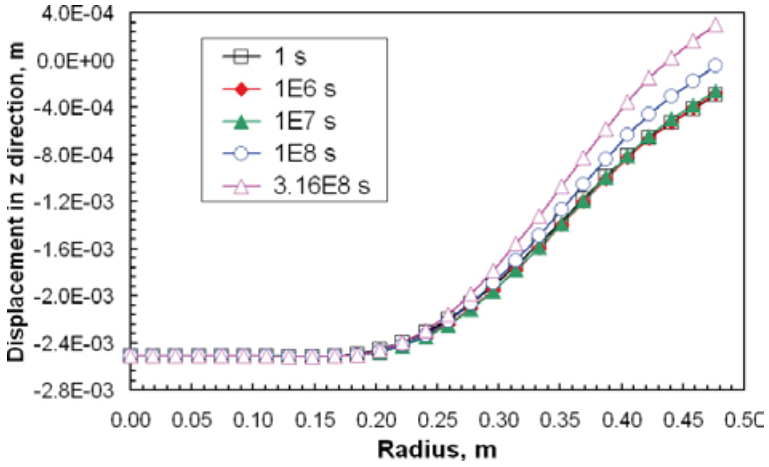

Figure 6-6. *Displacements of inner side of lid in the axial direction at times up to 3.16×10^8 s.*

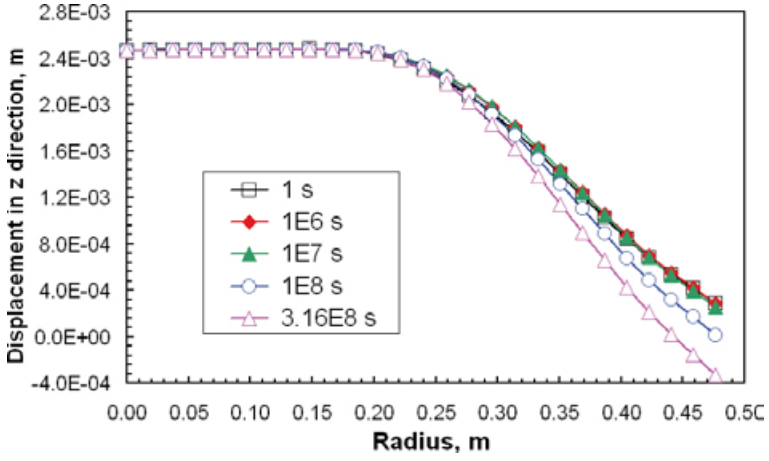

Figure 6-7. *Displacements of inner side of bottom in the axial direction at times up to 3.16×10^8 s.*

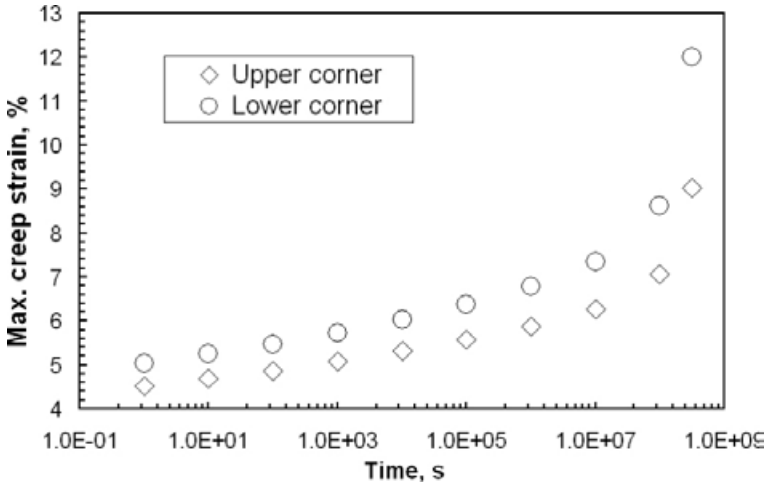

Figure 6-8. *Maximum equivalent creep strain at inner corners.*

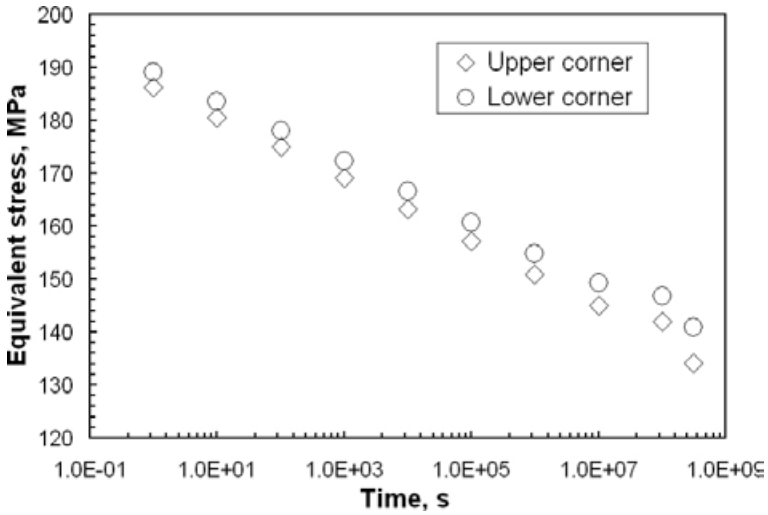

Figure 6-9. *Equivalent stress at corners as a function of time.*

6.2.2 Effects of uneven swelling pressure

Due to uneven wetting, rock contours and bentonite density distribution, uneven swelling pressure on the canister can appear. In Section 2 load cases are identified that can be expected to have the largest impact on the canister shell and insert, see also /SKBdoc 1206894/. With reference to the effect on the canister an analysis was performed in /Andersson-Östling and Sandström 2009/. It turned out that the only load case listed in /SKBdoc 1206894/ that is of direct relevance for the copper shell is where there is an uneven loading in the axial direction. This may occur if the density of the buffer at the bottom of the deposition hole just below the canister is 2,050 kg/m^3 and the density at the top of the deposition hole just above the canister is 1,950 kg/m^3, see Figure 2-3. This case can be considered possible since there may be rock fall out in the upper parts and upwards swelling of the buffer against a dry backfill, which will cause a decrease in buffer density in the upper part. This load case, see Figure 2-3, gives a maximum stress in the copper shell of 167 MPa /Andersson-Östling and Sandström 2009/. Effective stresses above 120 MPa that can give rise to creep are highly localised and appear only at radii in the structure. Creep tests on notched bars demonstrate that such stress distributions do not give rise to cracking /Andersson-Östling and Sandström 2009/.

6.2.3 Stresses and strains in slits and their role in copper shell integrity

In the copper canisters, slits exist between the cylinder and the lid as well as between the cylinder and bottom after welding. They cannot be avoided due to the manufacturing tolerances. When the copper shell is loaded, these slits may contact each other and close, giving rise to stress concentrations. The slits have not been taken into account in the computations presented in Section 6.2.1. In the present section the stresses and strains in these slits will be analysed.

A displacement-controlled elasto-plastic model is used. The material model for the stress strain curves is the one presented in Section 4.2. The geometry modelling for the copper shell utilises axial symmetry. For the contact modelling the penalty barrier method in Section 4.3 is used.

When 15 MPa pressure is applied to the outer surface of the copper shell contact occurs in the slits and some local stresses there become quite high due to the stress concentrations. The small contact area cannot sustain such high stresses and will immediately undergo plastic deformation. Elasto-plastic modelling has been performed at 75ºC, assuming isotropic strain hardening. The results are presented in Figures 6-10 and 6-11. Figure 6-10 shows that the maximum equivalent stress emerges at the initial contact point, the magnitude being 198 and 207 MPa in the upper and lower corners, respectively. The corresponding maximum effective plastic strains become 23.4 and 30.2%, Figure 6-11.

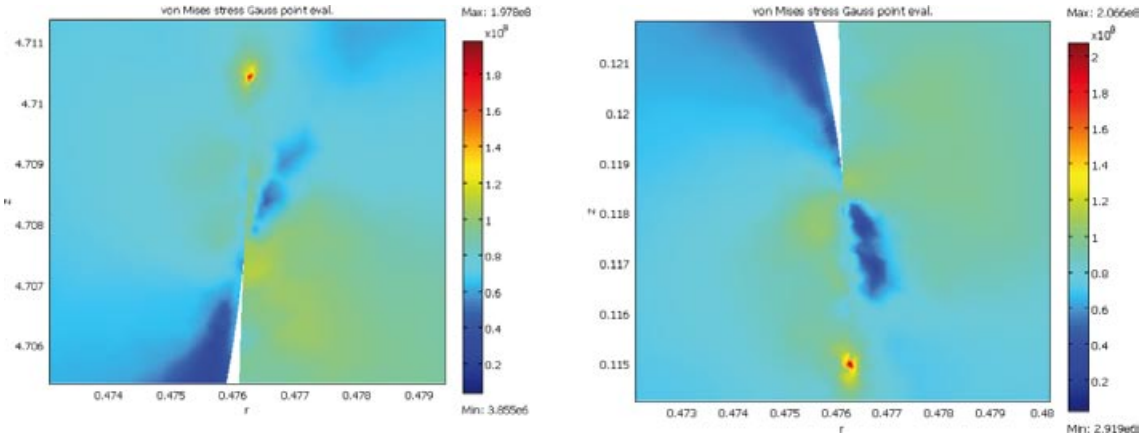

Figure 6-10. *Equivalent stress distribution in the slit at the a) upper corner and b) lower corner of the copper shell determined with elasto-plastic modelling /Andersson-Östling and Sandström 2009/.*

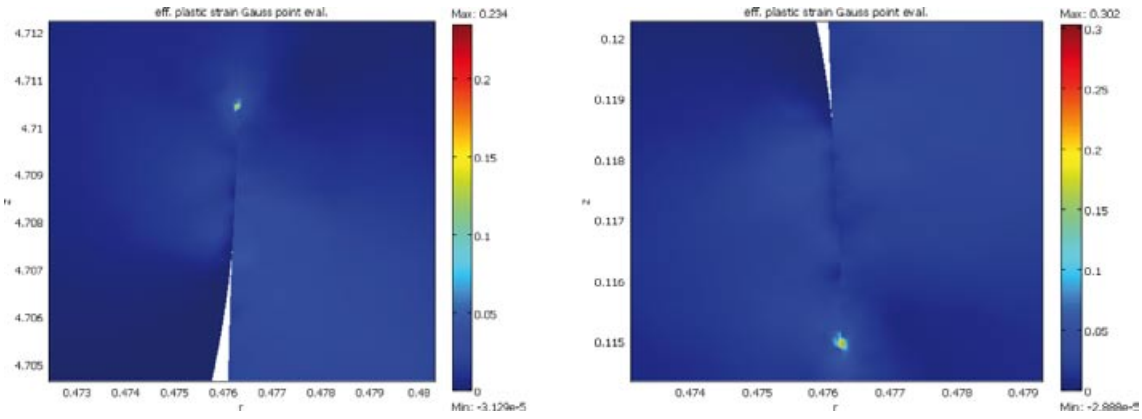

Figure 6-11. *Equivalent plastic strain distribution in the slit of a) upper corner and b) lower corner determined with the help of elasto-plastic modelling /Andersson-Östling and Sandström 2009/.*

The high stresses are strongly localised; 0.1 mm from the max positions the magnitude of the stresses and strains have dropped by more than 20%. To assess the potential failure risk at these stress concentrations, a comparison to circumferentially notched creep specimens is made. These specimens have also highly localised strains. The notch in such a specimen is illustrated in Figure 6-12. The creep test was run at a net section stress of 215 MPa at 75ºC, which is much higher than a uniaxial specimen can withstand. The specimen failed after 9,701 h. For the slit notches, the von Mises stress presented in Figure 6-10 shows that after the initial plastic deformation, the stresses lie at a level of 190–210 MPa. This stress level is thus comparable to the net section stress in the creep specimen.

The plastic strain of 20 to 30% that appears in the slits can be compared with the creep specimens in Figure 6-12. The maximum strain is somewhat larger in the creep specimen. The creep tests demonstrate that large local strains can be present without rupture taking place directly. Considering that the notch in the creep specimen is exposed to tensile stresses, this represents a much more critical situation than for the slits with compressive loading. Thus, the localised stresses and strains in the slits will not give rise to failure.

6.2.4 Blunting of notches during creep

To check whether creep crack growth can take place in copper, CT-specimens have been exposed to long term loading /Andersson-Östling and Sandström 2009/. The crack geometry is closely monitored. Two examples are shown in Figure 6-13, one at 20°C and one at 75°C. The reference stresses are 165 and 150 MPa, respectively.

Initially the notch has a radius of 0.15 mm. Already during the loading the radius increases to 1 mm. Extensive plastic deformation also takes place directly. The subsequent testing gives only a smaller addition to the plastic deformation. After longer time testing, the notch radius has increased to about 2 mm, Figure 6-13. The Figure illustrates still running tests. By now 10,000 and 3,000 h have been reached in the two tests without any cracks appearing. The plastic deformation is so large that it is visible directly, Figure 6-13. A large amount of plastic deformation in a CT-specimen verifies that the toughness is very high. The slow propagation of the notch takes place by blunting of the notch and plastic deformation of the specimen. Creep tests for notched bars at 75°C also demonstrate that creep in copper is not notch sensitive /Wu et al. 2009/.

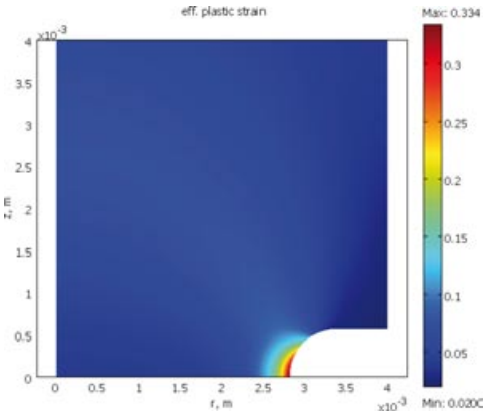

Figure 6-12. *Effective plastic strain distribution after rigid-plastic deformation on notched creep specimen with acuity 5 and net section stress 215 MPa at 75ºC. Cylinder symmetry and symmetry around z = 0, /Andersson-Östling and Sandström 2009/.*

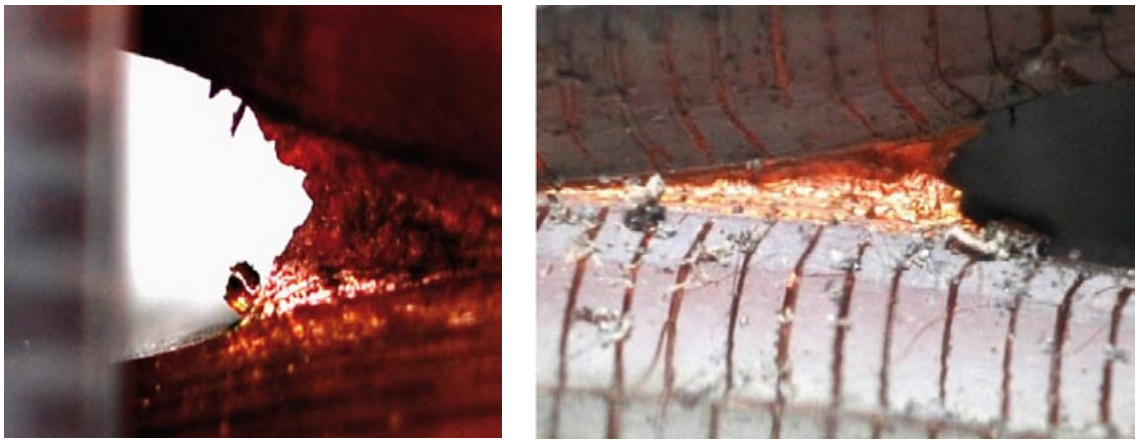

a b

Figure 6-13. *Creep crack growth tests with CT-specimens. An initial crack radius of 0.15 mm has been blunted to a radius of about 2 mm. mm markings in the images. a) 20°C, 165 MPa, 6,527 h, b) 75°C, 150 MPa, 721 h.*

6.2.5 Creep analysis results with glacial load

The behaviour of the copper shell at a higher external pressure of 45 MPa and 27ºC, simulating the situation during a glacial period has been analysed /Hernelind 2010/. The assumed temperature is conservative, actual temperature may be close to 0°C. Creep strains above 3% only appear at the slit between the lid and the cylindrical part of the shell. The climb-glide Equation 4-7 was used to compute the creep deformation. All creep deformation above 3% is concentrated to elements at the slit. The initial plastic deformation there is 11%. Then a slow logarithmic increase in the creep strain is observed as a function of time. After more than 10,000 years 2% additional creep strain is found, for details, see Figures 29 and 32 in /Hernelind 2010/. Since the higher creep deformation is very locally concentrated all the time, it is not technically important.

The results obtained from glacial load creep analysis are reported in /Hernelind 2010/ and could be summarized for the copper shell as follows:

- The maximum strain (13%) in copper shell that includes the plastic strain and the creep strain components occurs after 100,000 years at the geometrically singular point at the root of the weld. At the global level the strains are much lower. The singular point peak creep strain value cannot cause any global damage since the loading is displacement controlled.
- The copper shell will deform when the glacial load is applied and the initial gaps between copper shell and iron insert will be closed if this has not taken place already.

The results for iron insert in this analysis are given in the end of Section 6.1.2.

6.2.6 The role of notches in the copper for creep rupture

In Sections 6.2.3 and 6.2.5 it was demonstrated that high local stresses and strains can appear in the slits between shell tube and lid or bottom, in particular if fully sharp notches with a radius of 0.15 mm are assumed.

– It was demonstrated in Section 6.2.4 that creep crack growth will not take place even under tensile loads of a magnitude that give rise to significant plastic deformation. The cracks will simply blunt.

– Creep rupture cannot be initiated because a section through the shell would then have to creep simultaneously, and this does not take place since the high stresses and strains are local. Thus the design criterion in Section 3.3.1 is satisfied, since an essentially constant stationary creep stress is not established.

It has clearly been demonstrated that the parent metal is not sensitive even to severe defects as notches. Since the creep ductility of the different parts of the friction stir welds are about the same as for the parent metal, the weld will not be sensitive to defects.

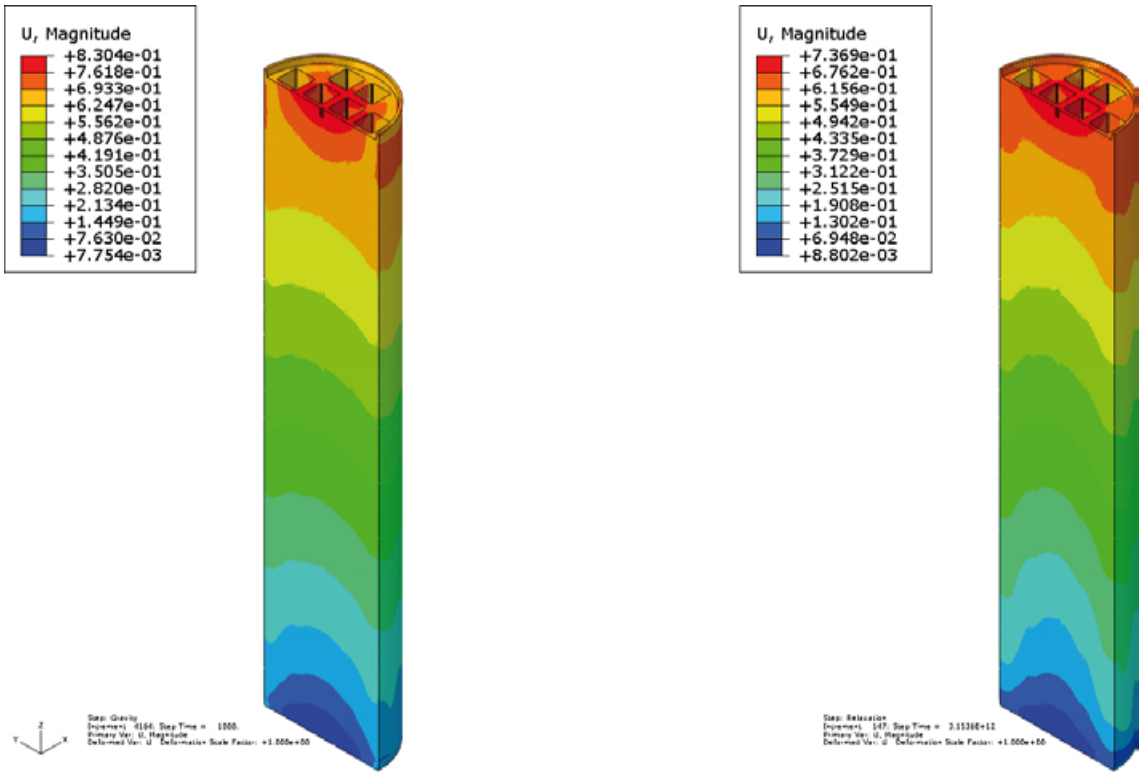

Figure 6-14. *Magnitude of displacement (length of displacement vector) of the insert after applied glacial load (left) and after relaxation (right).*

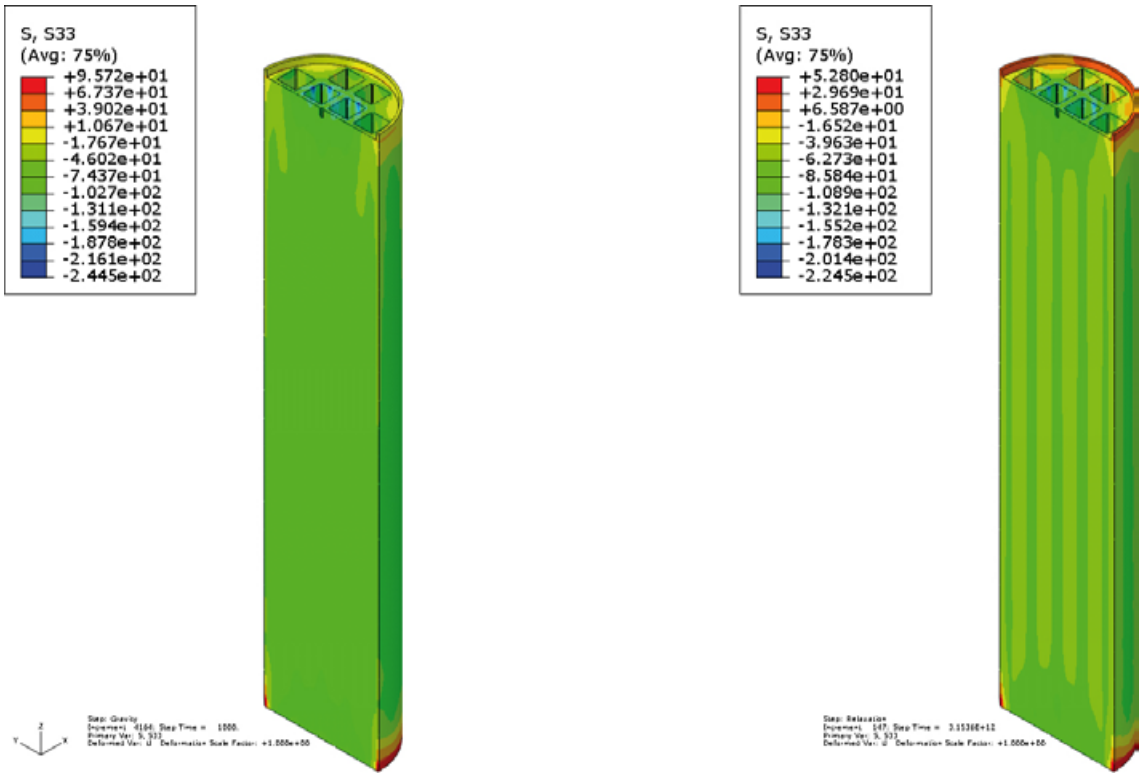

Figure 6-15. *Insert stresses in axial direction after applied glacial load (left) and after relaxation (right), mostly in compression and much below the yield stress.*

6.2.7 Copper behaviour during rock shear case

The rock shear case in analysed in /Hernelind 2010/. The results are discussed also in 6.1.3 in this report. Figures 6-16 and 6-17 show typical plastic strain result plot from the short term analyses. The load is 5 cm rock shear perpendicular to the axis of the canister at ½ of the height from the bottom and calcium bentonite density is 2,050 kg/m^3. Figures 6-16 and 6-17 show that the higher strains are concentrated into the geometric discontinuities of the copper lid and the maximum plastic strain of copper is here about 21%.

In a series of following **creep analyses** reported in /Hernelind 2010/, the maximum creep strain was observed to be only about 2%, see Table 6-4. This means that the most of copper strain is caused by the immediate plasticity during the rapid rock shear load case and the creep after the shear case will only relax the stresses in the bentonite-copper-iron construction.

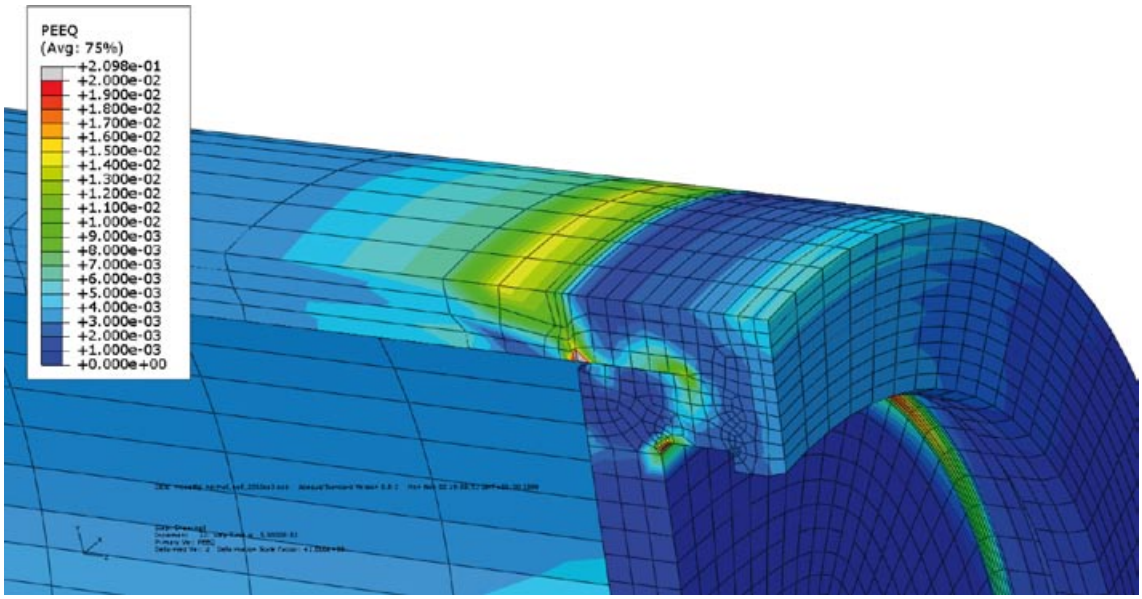

Figure 6-16. *Plastic strain of copper in canister shell top lid corner. The load is 5 cm rock shear at midnormal compression. The model is "normal_half_2050ca3". Maximum strain is 21% but it is very local.*

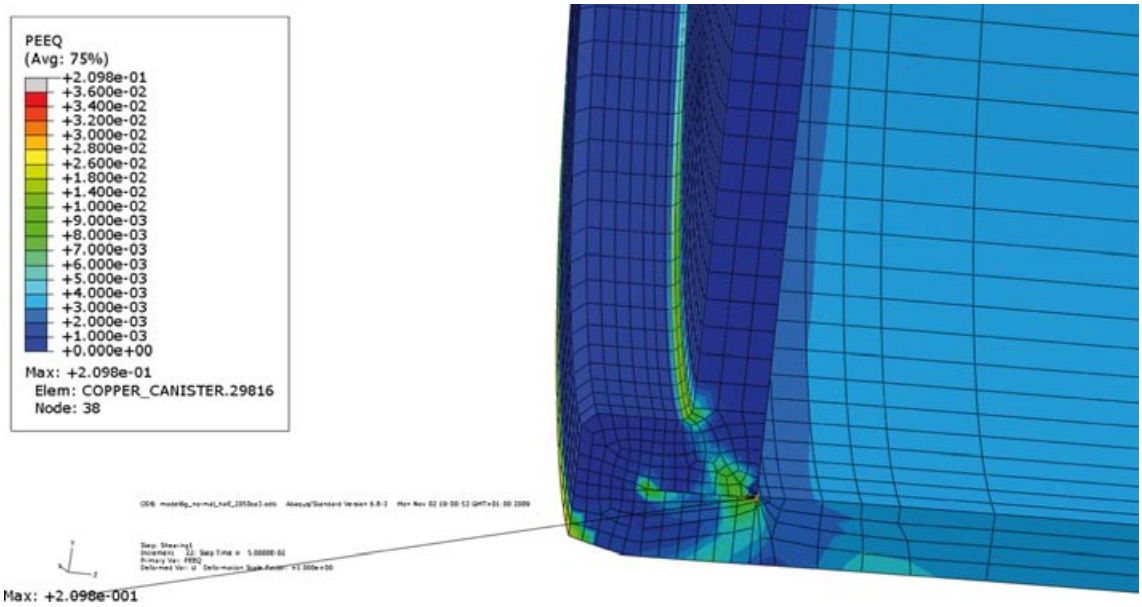

Figure 6-17. *Plastic strain of copper in canister shell bottom lid corner. The load is 5 cm rock shear at mid normal compression. Maximum strain is 21% but it is very local.*

6.2.8 Strength and damage tolerance analysis with operational handling loads

A damage tolerance analysis by limit load analysis has been conducted for the copper shell of the PWR and BWR canisters in /SKBdoc 1206868/. The geometry of the region of interest is shown in Figure 6-18.

The copper shell has been shown to have a very large margin to the collapse load for the most severe load case during handling of the canister. The structural integrity can be verified for the copper shell by limit analysis according to ASME. The load cases are according to Section 2.1 for (a) the unexpected braking during lift of canister and (b) the emergency braking of the lift after a free fall from the height of the deposition hole.

Limit load analyses have also been conducted for models containing large (width of 18–40 mm in radial direction) circumferential defects. For modelling details see Figure 6-19. It has been shown that the copper shell is very robust to defects. The copper shells structural integrity could be verified with limit analyses according to ASME even with large defects present.

The results from the limit load analyses for the copper shell without defects show very large margins between the load cases and the failure criteria of 2/3 of the collapse load. Hence the loads the copper shell is subjected to during the handling of the canister are not considered to be of any major concern. The copper shell can be said to have very large margins to the collapse load for the most severe load during handling of the canister. The corresponding limit load analyses with large postulated material defects showed accordingly that the required safety margins are available. Even during the worst case loading scenario the stresses in the copper are low, below 100 MPa.

6.2.9 Effect of indentations on the copper shell

In the manufacturing as well as during the further handling of the canisters, cold work can be introduced by accidental deformation of the copper shell. Both experimental studies and FE-modelling of indentations with a spherical, cylindrical and conical shape have been performed. The results are summarised by Unosson /SKBdoc 1205273/. The results show that strains up to 50% can easily be reached. This is supported by complementary FE computations of indentations created by a cylindrical punch with a diameter of 20 mm which generates 23% plastic strain when the depth of the indentation is 2 mm. The results are illustrated in Figures 6-20 and 6-21. If the depth of the indentation is almost doubled to 3.9 mm the plastic strain generated will be 53% /Andersson-Östling and Sandström 2009/.

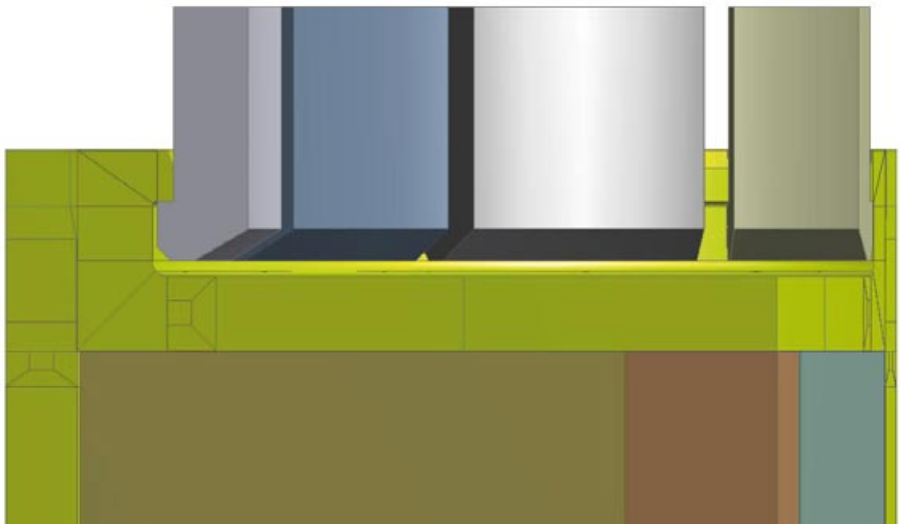

Figure 6-18. *The geometric model of the top part of the canister shell and the gripper.*

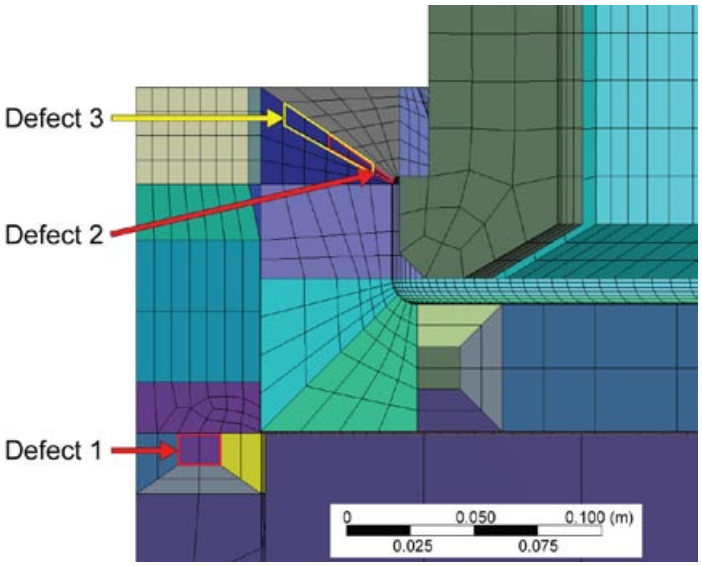

Figure 6-19. *The modelling of the material defects in the canister shell.*

Plastic strains generally reduce creep strain and creep rate. Reductions in creep rupture elongation down to 10% have been observed for copper material subjected to at least 10% homogenous cold work /Andersson-Östling and Sandström 2009/. Cold work (plastic) strains might consequently jeopardise the copper shell integrity during creep if the strains are on a global level. However, minor indentations (local cold work) to the surface are not judged to jeopardise the integrity of the copper shell at the creep strains expected under repository conditions. The basis for this judgement is that general creep strains at the outer surface of the copper shell, that could experience damage during handling, are below 3% as reported in Section 6.2.5. Further experimental studies and modelling of effects from indentations and local plastic strain are however required to better assess this kind of damage and, if required, develop acceptance criteria.

6.2.10 Residual stresses in the copper shell

The interest of residual stresses in copper shells is primarily related to the possibility that stress corrosion might appear for unforeseen reasons or that elastic deformation might take place.

After welding and other high temperature processes, residual stresses appear in the material. There are many factors that influence the distribution and magnitude of these stresses: physical and mechanical properties of the material, structural dimension, restraint conditions, and welding parameters such as heat input. It must also be taken into account that the material properties vary across the welds and that the properties are temperature dependent. A number of these parameters are simply not fully known. As a consequence fully reproducible measurements and accurate computations of the residual stresses cannot be expected. This is even more characteristic for copper than for steels where most work on residual stresses has been performed, because of the low yield strength of copper.

Measurement on copper shells have been performed with two techniques: X-ray diffraction /SKBdoc 1040350, SKBdoc 1040347/ and hole drilling /SKBdoc 1072169/. Both methods are well established.

A summary of the observations are given in /SKBdoc 1196484/ see Table 6-7.

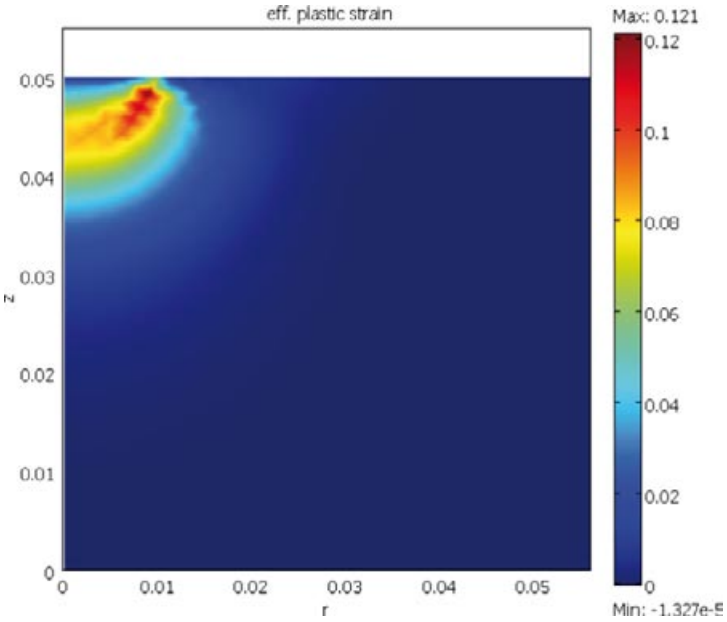

Figure 6-20. *Effective plastic strain below an applied punch Φ 20 mm with a stress 500 MPa (load 0.157 MN) /Andersson-Östling and Sandström 2009/.*

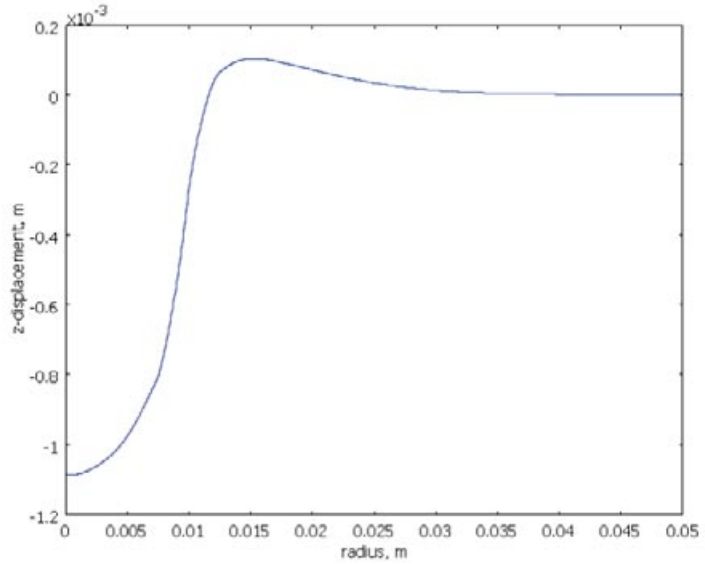

Figure 6-21. *The displacement below the punch for the case in Figure 6-20 /Andersson-Östling and Sandström 2009/.*

Table 6-7. Measured residual stresses in copper shells, MPa.

Position	FSW X-ray diffraction /SKBdoc 1040350/	FSW Hole drilling /SKBdoc 1072169/
Lid centre, outside	–57 to –45	–29 to 5
Lid centre, inside	–56 to 2	
Bottom centre, outside		–31 to –24
Shell outside		–41 to 5
Lid weld metal surface, 0 – 360°	–36 to 6	–24 to 11
Lid weld metal below surface, 7 – 30 mm, /SKBdoc 1040347/	–8 to 39	
Bottom weld HAZ		–47 to –3

As can be seen from Table 6-7, the stresses for FSW (Friction Stir Welding) are modest and rather evenly distributed.

In the FSW welds all values obtained have an absolute value below 60 MPa. Most values are compressive on the outside of the shell. Below the surface some tensile stress values are observed. The two measuring techniques give similar results when they are comparable. Due to scatter in the measurements as well as differences between individual weldments, full agreement is not to be expected.

The distribution of residual stresses has been computed using a procedure described for example in /Deng and Murakawa 2006/. In these computations the heat conduction and transfer as well as plastic deformation during the friction stir welding is taken into account. Results are illustrated in Figure 6-22.

As is evident from Figure 6-22, the computed results are in the same range as the observations. Thus, their absolute values are less than the yield strength. This is not surprising since if the yield strength would be significantly exceeded, plastic deformation would take place which would immediately reduce the stresses. In addition the yield strength is lower at elevated temperature than at room temperature which explains why the yield strength level at room temperature is not reached.

It is interesting to note that the predicted residual stresses are lower at the outside of the shell than below the surface in Figure 6-22. This is fully consistent with the observations. It should be emphasized that the computed results depend on a number of parameters that are not fully known as was explained above. A detailed quantitative prediction is therefore not possible.

For analyzing the potential risk for stress corrosion, it is of interest to make a comparison between primary and residual stresses. The principal stresses in the shell after creep has taken place are illustrated in Figure 6-23 /Jin and Sandström 2009b/.

At two positions on the outside of the shell the first principal stress is larger than the yield strength in Figure 6-23. These stresses are tensile. It is at the lower notch at the top of the lid and around the weld at the shell. The corresponding positions can be found at the bottom of the shell. It can be concluded that the primary stresses are more important for analyzing stress corrosion than the secondary residual stresses.

Apart from these positions the absolute values of the principal stresses are lower than the yield strength and comparable in magnitude to the residual stresses. The largest compressive stresses are represented by the second principal stress. This can be seen in Figure 6-23 b. The lowest compressive stresses are about –70 MPa.

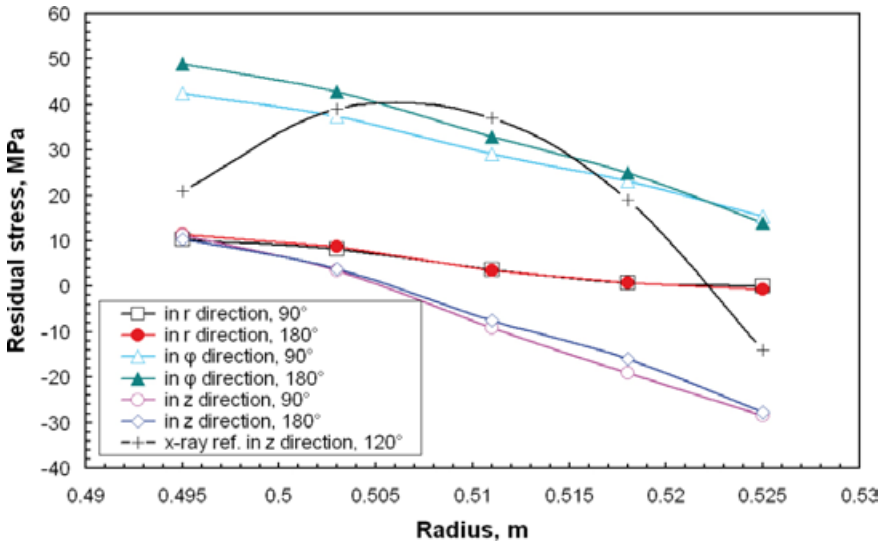

Figure 6-22. *Residual stresses in a FSW weld in the lid as a function of radius. Values in the radial (r), tangential (ϕ) and the axial direction (z) are given at two positions on the canister circumference (90 and 180°). For comparison experimental data from /SKBdoc 1040347/ are included (L-Z Jin unpublished results, 2009).*

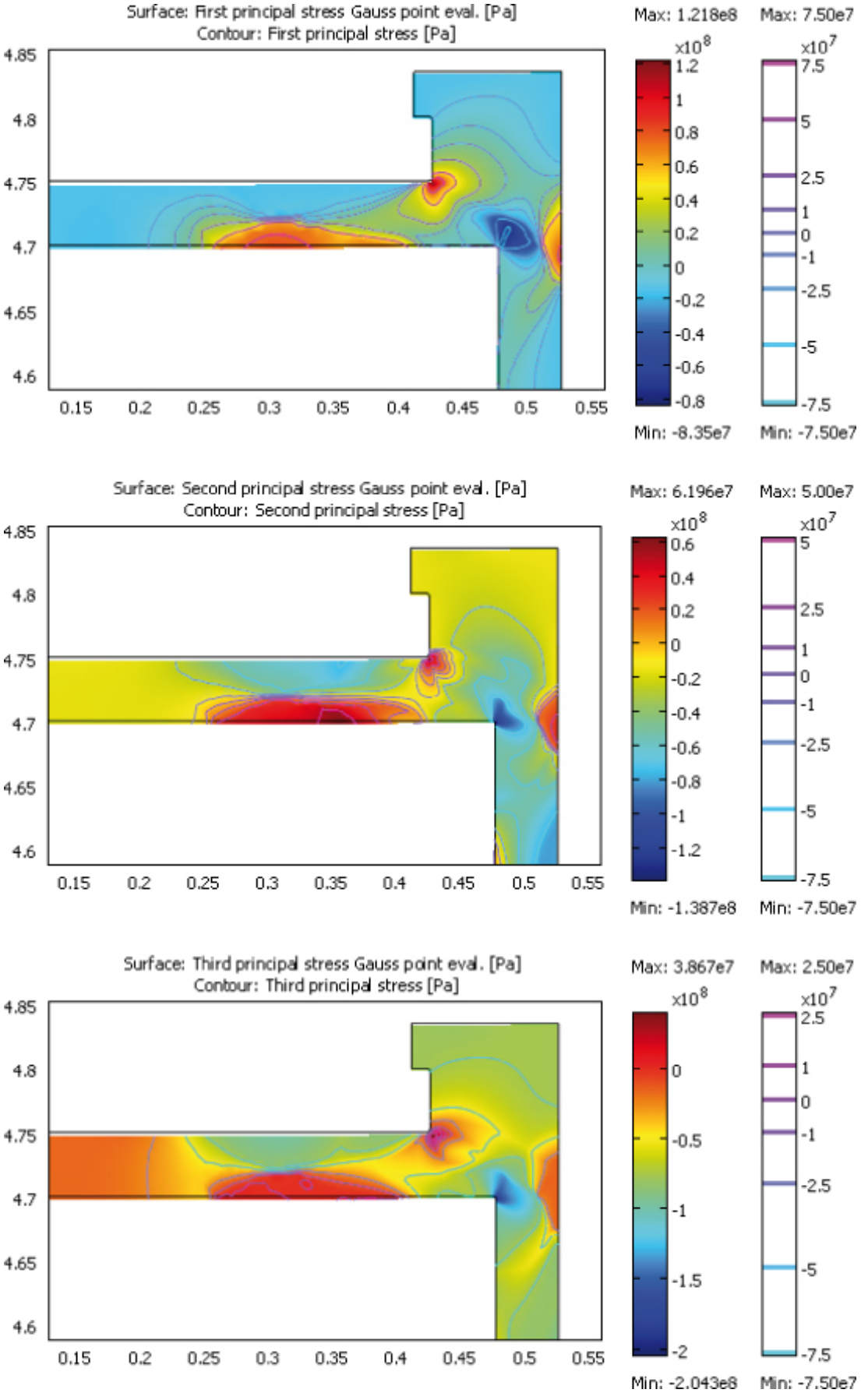

Figure 6-23. *First (a), second (b) and third (c) principal stress in Pa at the top of the canister shell, /Jin and Sandström 2009b/.*

7 Results uncertainties accounted for in this report

The uncertainty analyses are carried out by assessing:

- Uncertainties in input, typically materials data, geometries and assumptions.
- Uncertainties in the analysis methodology.
- Uncertainties in results.

Table 7-1 gives an overview of uncertainty analysis of the results presented in this report including references to sections for results and the corresponding uncertainty analysis.

7.1 Uncertainty analysis, uneven swelling loads, insert

These load cases are aimed at reflecting the worst case scenarios. If analysis results are found to be critical a more elaborate analysis will be motivated. The load analysis results are given in Sections 6.1.1 (water saturation effects) and 6.1.2 (permanent asymmetric loads).

The full backgrounds of these loads are presented in /SKBdoc 1206894/. The resulting stresses in the insert are determined by a simplified calculation method using beam theory, thereby calculating the maximum bending moment that can occur. The assumptions made in the calculations are based on a worst case scenario and hence reflects a very low probability event.

7.1.1 Uncertainties in input

Assumptions regarding the load distribution

The uncertainty in the assumption can be set to zero on the high side as the worst scenario philosophy is applied. The bentonite density distribution, deposition hole deviation and temporary swelling distribution is combined in the most unfavourable way.

7.1.2 Uncertainties in the analysis methodology

Calculation method for the load distribution

The pressure build-up is both simplified and pessimistic.

Calculation method for the stresses

Possible errors in determining the section modulus W (BWR insert) are not given in /SKBdoc 1206894/. Calculation of W is based on the nominal geometry of the insert cross section. The allowable deviations of the geometry are insignificant, when calculating W. Possible errors in the calculations of bending moment and bending stress are not given, but maximum error can be estimated to be ±2%. The same error will be transferred to stress results also. Possible axial pressure components, which will reduce the main tensile stress component, are not taken into account in Section 6.1.2.

The uncertainty in the damage tolerance analysis (allowable defects) is discussed in Section 7.3.

7.1.3 Estimation of uncertainties in results

The consequences of simplifications in the analysis method are not given in /SKBdoc 1206894/. However, the pessimistic approach in the assumptions will give pessimistic results that consequently have a low probability for occurring. The accuracy of analysis method is much better than the accuracy of load assumption.

Table 7-1. Overview of uncertainty analysis of the results presented in this report including references to sections for results and the corresponding uncertainty analysis, respectively. Coloured boxes correspond to the possible periods for the load case (1…5) in question.

Uncertainty analysis Repository evolution phase Years after closure of the repository Load #)	Deformation rate	Water saturation 0–100 y	Temperate 100 a–20 ka	Permafrost 20 ka–50 ka	Glacial 50 ka–60 ka	Subsequent permafrost and glacial periods 60 ky. → 1 My.
Canister temperature (°C)		**< 125/100 (Fe/Cu)**	**20 < T < 125/100**	**0 < T < 20**	**0 < T < 20**	**0 < T < 20**
1) Asymmetric loads due to uneven water saturation and imperfections in deposition hole geometry. No simultaneous hydrostatic pressure. Uneven water saturation effects will decay and be replaced by permanent loads 2) and 3) acting in saturated condition.	**Insert** Static	Results in 6.1.1. Uncertainty in 7.1				
	Copper shell Creep or static	No critical case identified				
2) Permanent asymmetric loads due to uneven bentonite density and imperfections in deposition hole geometry.	**Insert** Static		Results in 6.1.2 Uncertainty in 7.1.		Results in 6.1.2. Uncertainty in 7 1	
3) Ground water hydrostatic pressure + even isostatic swelling pressure of bentonite.	**Copper shell** Creep or static		Results in 6.2.2. Uncertainty in 7.2		Results in 6.2.2. Uncertainty in 7 .2	
4) Glacial pressure (additional isostatic pressure, only during glacial period).	**Insert** Static				Results in 6.1.2. Uncertainty 7.3	
	Copper shell Creep or static				Results in 6.2.5. Uncertainty in 7.4	
5) Shear load due to rock displacement. Amplitude 5 cm, shear velocity 1m/s.	**Insert** Short-time forced displacement					Results in 6.1.3. Uncertainty in 7. 5
	Copper shell Short-time forced displacement					Results in 6.2.7. Uncertainty in 7.6

7.2 Uncertainty analysis, uneven swelling loads, copper shell

In /SKBdoc 1206894/ no significant load case under water saturation has been identified. After water saturation however, an unfavourable pressure distribution possibly occurs. This load case is further evaluated in Section 6.2.2 and found not to be harmful to the copper shell integrity.

7.2.1 Uncertainties in input

The uncertainty in the assumptions in /SKBdoc 1206894/ can be set to zero on the high side as the worst case scenario philosophy is applied. The bentonite density distribution and, hence swelling distribution, is combined in the most unfavourable way.

7.2.2 Uncertainties in the analysis methodology

The used copper creep model for uneven swelling loads is the same as the one used in /Hernelind 2010/. Therefore the uncertainties in the model are the same, giving an uncertainty of the creep rate by a factor of five.

7.2.3 Estimation of uncertainties in results

The uncertainty has not been explored in detail as worst case scenario philosophy is applied, as explained above. However, the influence of the uncertainty in the creep model concerning the creep rate has been investigated elsewhere /Hernelind 2010/. The influence has been shown to be small on the final result, see also Section 7.4.2.

7.3 Uncertainty analysis of the canister under glacial load, insert

The results regarding glacial load are given in Section 6.1.2 and can be summarised as follows. For the cylindrical part of the insert the actual safety factor at design pressure against limit load is 2, at minimum. This has also been confirmed in pressure tests /Nilsson et al. 2005/ that showed a margin well above 2. The basic design verification analyses show also that the limit load of the insert, including the integral bottom and screw fixed steel lid, is clearly higher than 1.5 times the design pressure of 45 MPa, which is the code requirement for the safety factor.

It is also concluded in 6.1.2 that the inserts have been analysed against design pressure having axial boreholes and other types of loss of material in various zones. The analyses are based on the limit load method using the 1.5 safety factor according to ASME rules. Damage tolerance to volumetric defects has been analysed. The allowable hole sizes are given in Table 6-2. Also, calculations are made for other types of material deficiencies and acceptable and critical defect sizes for ASME-type reference defects. The results show that the insert structure is insensitive to different kinds of material imperfections.

7.3.1 Overview over uncertainties in analysis methodology and results

An overview of the extensive analysis presented in /Dillström et al. 2010/ is given in Table 7-2 where also the uncertainty is judged with short justifications. In Table 7-3, a summary of different sensitivity analyses for different input parameters to /Dillström et al. 2010/ is given. Table 7-4 and Table 7-5 give an overview of the uncertainty analyses for the insert bottom and the steel lid, respectively.

Table 7-2. Uncertainty analyses, glacial load on insert, cylindrical part.

#	Purpose	Task	Subtask	Analysis methodology	Safety factors	Input Data (BWR)	Uncertainty in result
1	Analyse dimensioning of insert	Determine limit load		Elastic-plastic stress analysis, 2D and 3D	Design pressure SF 1.5	Rp0.2 = 270 MPa σ_{UTS} = 478 MPa	Result judged to be reliable, margin >2 to limit load
2	Define acceptance criteria	Find acceptable defect sizes	Postulate volumetric defects, spherical holes and slits	Elastic-plastic stress analysis 2D	Design pressure SF 1.5 45*1.5 =67.5 MPa	Rp0.2 = 270 MPa σ_{UTS} = 478 MPa	Result judged to be pessimistic.
3	Define acceptance criteria	Find acceptable defects sizes	Postulate crack like defects, semi-elliptical	Linear analysis	Safety factor brittle fracture SF_K=3.16. Safety factor for plastic collapse is SF_L=2.4	K_{1C} 79.4 MPa $(m)^{1/2}$ Rp0.2 = 270 MPa σ_{UTS} = 478 MPa *Old data set at room temperature. Comparison to new data at 0° C gives no difference in result. Pessimistic use of data 2 mm growth not allowed.*	Results judged to be pessimistic.
4	Define acceptance criteria	Handle limitations in inspectability.	Determine acceptable shadowed area. Remove material in central area and determine allowable size on fictive slits	Elastic-plastic stress analysis 2D	Design pressure SF 1.5 45*1.5 =67.5 MPa		Result judged to be pessimistic.
5	Effect from asymmetric loads	Find acceptable defects sizes	Postulate crack like defects, semi-elliptical	Linear analysis	Safety factor brittle fracture SF_K=3.16. Safety factor for plastic collapse is SF_L=2.4	K_{1C} 79.4 MPa $(m)^{1/2}$ Rp0.2 = 270 MPa σ_{UTS} = 478 MPa *Old data set at room temperature. New data at 0° C gives no difference in result. Pessimistic use of data 2 mm growth not allowed.*	Results judged to be pessimistic.

Table 7-3. Sensitivity analysis to estimate possible errors due to simplifications and idealizations in the analysis of the insert, cylindrical part.

#	Purpose	Task	Subtask	Comments
1	Sensitivity analyses; geometry and canister components	Sensitivity analysis, structural components	Analyse: A) Only insert B) Insert + Cu shell C) Insert + Cu shell + insert tubes	Additional structural components give only marginal increase on load capacity
2	Sensitivity analyses; geometry and canister components	Sensitivity analysis channel cross section size	Compare old and new PWR- design	No effect can be traced
3	Influence from assumption regarding friction coefficient between components	Sensitivity analysis friction copper shell/insert		At interesting stress levels the possible errors are small
4	Uncertainty analysis methodology	Validate 2D approach	Compare analysis 2D-3D at 45MPa	At interesting stress levels 2D is marginally pessimistic
5	Uncertainty analysis methodology	Validate simplified tension model	Compare to generalized tension model.	No effect can be traced

Table 7-4. Uncertainty analysis of insert bottom. The analysis follows the same methodology as for the cylindrical part of the insert.

#	Purpose	Task	Subtask	Analysis strategy and methodology	Safety factors	Input Data	Uncertainty in result
1	Analyse dimensioning of bottom	Determine limit load		Elastic-plastic stress analysis, 2D	Design pressure SF 1.5	σ_s =270 MPa σ_B = 478 MPa	Result judged to be reliable, margin >1.5 to limit load
2	Define acceptance criteria	Find acceptable defect sizes	Postulate crack like defects, semi-elliptical	Linear analysis	Safety factor brittle fracture. SF_K=3.16. Safety factor for plastic collapse is SF_L=2.4.		Analysed in 6.1.2. Acceptable crack size >80% of bottom thickness.
3	Geometry and insert geometries	Least favourable tolerances chosen					
4	Other conditions: Fuel element mass included in analysis						
5	Material model of channel tubes does not take into account the possible softening during casting						Judged to have minimal influence on the results

Table 7-5 Uncertainty analysis insert lid (steel lid).

#	Purpose	Task	Subtask	Analysis strategy and methodology	Safety factors	Input Data	Uncertainty in result
1	Analyse dimensioning of insert	Determine limit load		Elastic-plastic stress analysis, 2D	Design pressure SF 1.5 according to ASME VIII.	According to SS-EN10025 minimum values	Result judged to be reliable, margin >2 to limit load
2	Geometry and insert geometries	Least favourable tolerances chosen					
3	Material model for the channel tubes does not take into account the possible softening of the material during casting						Judged to have minimal influence on the results

7.3.2 Residual stresses

Residual stresses induced in the material during manufacturing processes like casting, hot-deformation, welding or machining, are secondary stresses. They do not have any external driving force that would continue their existence after yielding or thermal stress relief treatment of the material. The residual stresses in inserts are investigated by core drilling method in /SKBdoc 1208266/. The testing was made on a BWR-type insert, manufacturing number I56, which is a typical sample from the "serial manufactured" inserts, whose material fulfils the current specifications. The measurements were made from 9 locations on the cylindrical surface of the insert, far from the ends. The results show that the surface stress state is slightly in compression, in the range 50–100 MPa, but 1 mm deeper from the surface the compression stresses are increased typically to 100–200 MPa. This means that the residual stresses are lower (partly relaxed) close to free surface and that is why the cutting of the test pieces from the large cast body also may decrease the original residual stresses to be measured. The core drilling method is very sensitive to use and the scatter of the results is wide. Further information for greater depths was not practically available using this specific equipment. The origin of this type of residual stress is the casting process, where the cylindrical surface is solidified first and later the shrinking of the melt iron inside the thicker sections cause tension, which causes compression in the surface areas as a balancing reaction.

The compressive residual stresses on component surfaces are beneficial for surface cracks due to a crack closing tendency, as well as for global bending loads due to a larger applied tensile stress required to cause yielding. The residual stresses have no practical influence on limit load or other higher loads that cause yielding, because the manufacturing-based residual stresses are expected to vanish when the material yields. As for postulated cracks, residual stresses might increase the load assumption in case of brittle fracture, but in case of plastic tearing or stable crack growth the loading effect of residual stresses is low due to the secondary character of the load. Canister inserts including postulated allowable cracks do not behave in a brittle manner in any load case or condition assessed in this report.

7.3.3 Summary of analysis of canister under glacial load; insert, bottom and base

BWR-type insert, cylindrical part

The calculations are based on statistically well documented data and well established analysis procedures made in a careful way; the uncertainties are judged to be small in comparison to the design load of 45 MPa. This is further supported by a probabilistic analysis /SKBdoc 1207426/ and two pressure tests Nilsson et al. 2005/. Residual stresses are judged to be secondary and not to affect the limit loads.

BWR bottom

The calculations are based on statistically well documented data and well established analysis procedures made in a careful way; the uncertainties are judged to be small in comparison to the design load of 45 MPa.

PWR-type insert, cylindrical part

The calculations are not based on statistically well documented material data (BWR data are used). The lack of data are reflecting that SKB have not yet established a completely stable PWR manufacturing process and have therefore decided that the current process is not mature enough to perform a demonstration series – which is necessary to collect adequate data. More optimization of the process is needed to avoid deformation of the channel tubes. The current status in the PWR development is however close to BWR in terms of tensile strength and yield strength which most likely will give similar compression data as for BWR. Due to lack of statistical, well documented, data the results for PWR must be judged as uncertain.

Steel lid for BWR and PWR inserts

The calculations are based on minimum standard requirements and well established analysis procedures made in a careful way; the uncertainties are judged to be small in comparison to the design load of 45 MPa.

7.4 Uncertainty analysis of the canister under glacial load, copper shell

The results for the copper shell are given in Section 6.2.5 and can be summarised as:

- The maximum cumulative strain (13%) in copper shell that includes both the initial plastic strain and the successive creep strain that occurs after 100,000 years at the geometrically singular point at the root of the weld. Generally, at the global level, the strains are much lower. The singular point peak creep strain value cannot cause any global damage, since the loading is displacement controlled.
- The copper shell will deform when the glacial load is applied and the initial gaps between copper shell and iron insert will be closed, if this has not taken place before. The insert will have deformations less than 1 mm.

7.4.1 Uncertainties in input

The following assumptions in input data that can influence the final results have been identified:

- The temperature is assumed to be constant, 27°C. This assumption is conservative since the creep rate increases with increasing temperature. The temperature in the repository during this condition will be close to 0°C.
- Initial nominal geometry of the canister is used in the analysis. In practice bentonite swelling and water pressure will initiate creep at an earlier stage and thus reduce the creep strain under glaciation.
- The used bentonite properties correspond to sodium bentonite converted to calcium bentonite. This is a realistic assumption.
- The time period used in the analysis is 100,000 years. This is a pessimistic assumption since no glacial period is expected to last for such a long period of time.

7.4.2 Uncertainties in calculation

The uncertainty in the used creep model is reported in /Hernelind 2010/ regarding creep rate and is estimated to be a factor of five. Therefore, in /Hernelind 2010/ the creep model has been used with a factor of five regarding the creep rate when used in conjunction with a rock shear. The result of this is valid also for other results using the same copper creep model.

In Section 4.3 the creep model has also been compared to a newly developed model without fitting parameters, called basic model. The comparison showed good agreement and this gives further support to the used copper creep model. However, more development of the basic model is needed before it can be fully used for creep analysis of the canister.

7.4.3 Uncertainties in results

The use of a factor five for the creep rate gives no significant influence on the result /Hernelind 2010/. Overall the result is judged to be pessimistic. This is based mainly on the assumptions listed in Section 7.4.1 and the fact that the influence of the uncertainty in creep rate is small.

7.5 Uncertainty analysis of the damage tolerance analysis of the insert during rock shear

The rock shear analyses consist of a series of subsequent analyses where the final one, the damage tolerance analysis /Dillström 2010/, sets the input to this Design Analysis report. An overview description of the data and analysis flow is given in Figure 7-1. This uncertainty analysis treats the uncertainties given in /Hernelind 2010/ as input uncertainties and deals with the uncertainty in the results given by /ASM handbook 1990/.

The analysis is divided into two parts for the copper and insert, respectively, as can be seen from Figure 7-1.

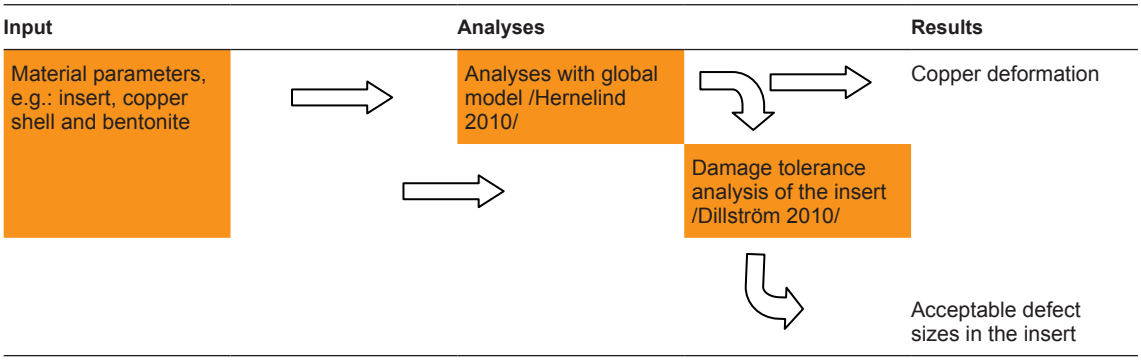

Figure 7-1. *Schematic flow of data and analyses in the rock shear case.*

7.5.1 Uncertainties in the input to the damage tolerance analysis of the insert

In /Hernelind 2010/ a number of uncertainties are given that generate uncertainties in the input to /Dillström 2010/. These are:

- The stress-strain relationship of the bentonite has a great effect on the outcome from /Hernelind 2010/.
- All canister materials, and the bentonite, experience strain rate effects, i.e. the stress-strain relationship is changed when the strain rate is changed. This has not been fully implemented for the copper shell in all analyses in /Hernelind 2010/.
- The coefficient of friction to define the interaction between different parts used in /Hernelind 2010/ might influence the result and has therefore been subjected to a sensitivity analysis.
- The natural scattering in the material data for the canister materials that exist in reality has not been considered in the input to /Hernelind 2010, Dillström 2010/. Conservative values for fracture toughness, and statistically averaged values for stress-train relationship are used.

There are uncertainties connected to that fact that data based on testing of material from BWR-inserts are used also for the PWR-insert analyses in /Hernelind 2010/. As the development of the PWR progresses the validity of this assumption will be evaluated. Especially, the fracture toughness of the material in the PWR-insert needs to be evaluated when a full data set becomes available. No separate damage tolerance analysis has been so far been done for the PWR-insert.

7.5.2 Uncertainties in the analysis methodology

The analysis methods used are well established but some uncertainties can be identified:

- Displacements from /Hernelind 2010/ are used as input to /Dillström 2010/. The uncertainty in the data transfer has been analysed in /Dillström 2010/ where principal stresses generated in /Hernelind 2010, Dillström 2010/ are compared. The differences are considered so small as not to significantly influence the results.
- The special case of the contact between the channel tubes and the cast iron is commented in /Dillström 2010/; the tubes are considered as welded to the cast iron. This is not the case in reality and the assumption might have an influence on the result.

7.5.3 Estimation of the uncertainties in results for the damage tolerance analysis

Uncertainties in the damage tolerance analysis will result in uncertainties in the acceptable defect sizes:

- In /Dillström 2010/ a sensitivity analysis is presented that shows that the density of the bentonite has a major influence on the acceptable defect size. In /Hernelind 2010/ it is stated the used stress-strain relationship probably has been slightly overestimated (i.e. used values corresponds to somewhat higher densities then the actual ones), also when including strain rate effects. This gives that the presented values for the acceptable defect size are judged to be slightly conservative /Hernelind 2010/.

- Including the strain rate effect also for the copper can influence the results in /Dillström 2010/. However, analysis results in /Dillström 2010/ where the strain rate effect is included show that the maximum effective stress level and the maximum strain level decrease while the maximum axial stress, that is detrimental, is almost unchanged. The influence on the final result is therefore judged as small.
- The influence of the coefficient of friction defining the interaction between different parts is shown in /Hernelind 2010/ to have a negligible influence on the detrimental axial stress (S33) level in the insert.
- Scatter in the experimental stress-strain data for the canister materials will always be present.

The used values are thought to be representative for the materials at present conditions but no sensitivity analysis for the results in /Hernelind 2010, Dillström 2010/ have been done.

- The scatter in the fracture toughness in terms of *J*-integral is handled by conservatively using the lower value of the calculated confidence interval (90%) for the *J*-integral.

One uncertainty that might influence the results in /Hernelind 2010, Dillström 2010/ and that has not been analysed is the combination of bending stresses in the canister in combination with a rock shear. This is not regarded to give any uncertainties in the results, when considering the maximum bending as given in Section 6.1.2, since this is a very rare case. However, bending stresses of lower magnitude might occur more frequently and the effect of interfering stresses has not been investigated. More data about the bending stress distribution is needed in order to evaluate this effect.

Altogether, the uncertainties given here imply that the acceptable defect sizes as given in Section 6.1.3 are conservative.

7.6 Uncertainty analysis of the deformation in the copper during rock shear

7.6.1 Uncertainties in the input parameters

- The deformation of the copper shell during a rock shear load has been evaluated by using /Hernelind 2010/ as seen in Figure 7-1. The results are based on the copper creep model presented in Section 4. Therefore, most uncertainties in the results for the copper shell depends on the accuracy of the used model.
- The assumption made for the coefficient of friction between the copper and the surrounding materials might influence the deformation of the copper shell.

7.6.2 Uncertainties in the analysis methodology

- As stated earlier in Section 7.6.1 the copper creep model presented in Section 4.3 has been used for some rock shear analyses in /Hernelind 2010/. As given in /Hernelind 2010/ there are uncertainties connected to the copper creep model that may affect the creep strain rate by a factor 5.

7.6.3 Estimation of the uncertainties in results regarding deformation in the copper

- Analyses where the creep strain rate has been increased by a factor of five are presented in /Hernelind 2010/. The change in the results is very small for both short term and long term shear load analyses.
- A sensitivity analysis of the influence of the coefficient of friction in /Hernelind 2010/ shows that the influence is negligible for both stress and strain levels in the copper shell after rock shear.

8 Assessment of analysis results against failure criteria

The basic design verification of the canister as a load carrying component has been conducted according to mechanical design codes where applicable. As an example, the ASME Boiler and Pressure Vessel Code, /ASME 2008a, ASME 2004, ASME 2008b/, gives methods and application rules for design verification of reactor pressure vessels. The code gives practical guidance to make the integrity assessment. The only problematic area in the design verification and strength verification is that the engineering materials of the canister are non-typical for customary vessels and shells. Thus the examination of the properties of the construction material (cast iron and oxygen-free copper) has been emphasized. The material testing and analysis of test data that have been carried out are comprehensive and extensive, and the experimentally determined properties used in the design verification analyses are considered very reliable.

As for acceptability of the calculated results, the failure criteria defined in Section 3 are used as a reference. All the set criteria are assessed separately in the following sub-sections.

8.1 Plastic collapse criteria

The basic design verification of the canister against the design pressure (external pressure of 45 MPa) has been conducted according to the ASME Code guidance utilising the limit load method. The canister is modelled using both 2 and 3-dimensional finite-elements, where all the components, gaps, tolerances and materials are modelled as realistically as possible and the limit load is estimated. The stress acceptance criterion is that the design load shall not exceed 2/3 of the limit load. Separate analyses are made for insert cylinder, insert bottom and the steel lid on the top end of the insert. All these analyses fulfilled the design criteria.

In addition to basic design verification analyses, the strength was also investigated with modelled deviations in nominal geometry, tolerances, lack of material or inclusions in the cast, eccentric installation of steel cassette and rounding radii. The canister was shown to be insensitive to these types of imperfections.

The pressure load capacity of the canister was demonstrated earlier by two model tests, when 700 mm long sections of actual canisters were pressure tested up to the limit load. The pressure tests showed that the collapse pressure was in both cases between 130 and 140 MPa; that is roughly 3 times the design pressure. The pressure tests have been used also for calculation method's validation.

8.2 Stress/strain criteria

The **operational loads** for the copper shell have been analysed. The strength is adequate in all the analysed cases.

For cases involving an **external pressure load** and design conditions the strains and stresses are low. Also the bending effect of the postulated **uneven bentonite pressure load** does not lead to any risk of excessive stress or strain values in the insert. For the strength analyses of the insert, the plastic collapse load method, with a safety factor 1.5, was applied according to /ASME 2004/.

The only load case that may locally lead to significant yielding and plasticity of the insert is the **rock shear case**. Rock shear is, however, a "displacement-controlled load" that causes secondary stresses only according ASME nomenclature. If load is secondary, the possible local yielding or cracking leads to decreasing stiffness and increasing deformation in the structure and, consequently, the load would decrease. That is why additional safety factors are not needed in displacement-controlled load cases. However, the analysis results for rock shear case show, that in case of 5 cm shear the plastic deformations and strains in the canister insert are low and material rupture is not expected to take place. For the square steel tubes the stresses are higher than for the cast iron part, but the steel has higher ductility and higher ultimate strength, so both of the insert materials fulfil the criteria.

The measured ductility /SKBdoc 1207576, SKBdoc 1203550/ from manufactured inserts is clearly sufficient for the insert in the postulated 5 cm rock shear case, as far as the allowable size of existing cracks is concerned, /Dillström 2010/. The applied metric was allowable equivalent stress (von Mises). What most evidently justifies the analysis as a whole is that if the effective plastic strain exceeds the ductility limit, a crack can be expected to initiate. Both linear and non-linear fracture mechanics analyses do however show that the integrity of the insert structure is not at jeopardy in postulated load cases, even if very large cracks are postulated in critical locations and orientations.

For the description of the behaviour of the copper shell during governing load cases, Section 6.2 is referred to. High strains are observed only at geometric discontinuities. These do not threaten the global integrity or leak tightness of the copper shell. Extensive copper creep is limited either by the supporting effect of the insert in the pressure load cases or by the relaxation of the applied displacement boundary condition in the bentonite buffer in the rock shear case. The results are shown to be acceptable.

One important fact to keep in mind when assessing the allowable stresses and strains is that in case of the canister, the loads are not variable or cyclic in nature, but stable and unique in character, and there is no need for fatigue studies.

8.3 Fracture resistance criteria/allowable defect sizes

For the copper shell, no kind of postulated crack, defect or cavity of reasonable size has proven to be critical. The operational loads for the copper shell have been analysed with postulated large circumferential cracks or with a lack of material. The copper shell withstands the design loads with a good margin even with these large postulated defects. The material testing has shown that the copper cracks blunt under tension load and no kind of crack growth is detected at applicable temperatures.

The insert was analysed for postulated cracks and other types of material deficiencies. With design pressure load the allowable ASME-type reference defect became a 32 mm deep semi-elliptic crack in the BWR-insert and 31 mm in the PWR-insert, respectively. The safety factor used waS 3.16 according to ASME-requirements for normal operation condition loads as expressed in stress intensity factor value K_{Ic}, according to practice described in /ASME 2008b/. The crack sizes are however limited to a maximum 80% of the material thickness and deeper cracks are thought to be possible without exceeding the allowed K_{Ic}.

The dimensioning load case with respect to allowable defect size proved to be the rock shear case. This load is a rare case that will occur only for very few canisters or none at all. The load will be very short lived and there is extremely low probability that the shear movement will occur more than once on the same single canister. The temperature is assumed conservatively be at 0°C and a safety factor of 2 is used when defining the allowable *J*-parameter value from the fracture test results corresponding the stable crack growth of 2 mm at 0°C. The rock shear is classified as a level D load case (emergency condition) according to ASME Code /ASME 2008b/ practice and the safety factor is determined respectively. The maximum allowable surface defect size on the cylinder surface is a 4.5 mm deep and 27 mm long reference defect laying in a circumferential orientation. This damage tolerance analysis is the governing case for the canister insert for close-to-surface volumes. The definition of the ASME reference defect is shown in Figure 8-1.

The reference canister withstands the specified loads with an applicable safety factor even if the material has the allowable sized defects.

8.4 Essential design parameters

Essential design parameters that have an influence on the canister integrity have either an effect on the static strength or damage tolerance of the canister. The essential parameters are collected into Table 8-1. Table 8-1 also contains the processes on which the parameter has an effect on, estimate of the qualitative sensitivity and a reference to possible manufacturing specification values.

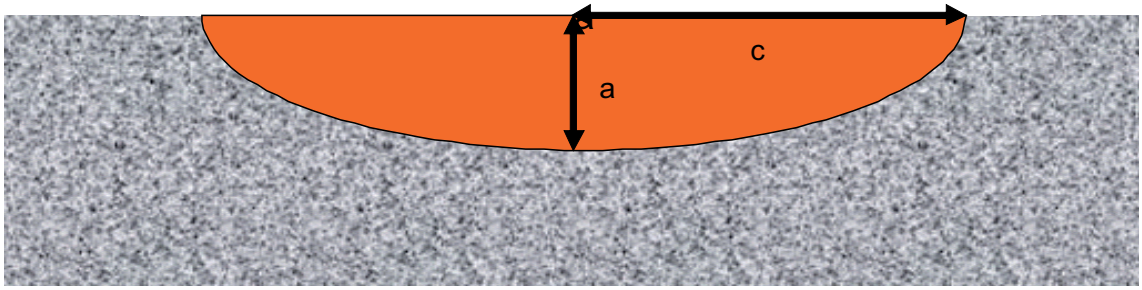

Figure 8-1. *The definition of ASME reference defect as a semi-elliptic surface crack.*

Table 8-1. Essential design parameters.

Parameter	Effects on	Sensitivity	Value derived from the Design analysis
Yield strength of cast iron in compression	Plastic deformation and strain	Important but adequate in practice	≥ 270 MPa (statistical requirement)
Yield strength of cast iron in tension	Plastic deformation and strain	Less important for any load case as far as the lower limit is satisfied	≥ 267 MPa, upper limit to be determined (shear load case)
Ultimate elongation of cast iron	Risk of rupture	Important but adequate in practice	≥ 12.6 (As defined in Section 4.1.1, statistical requirement)
Fracture toughness of cast iron	Risk of ductile fracture	Important in low-temperature-high-load condition	K_{1c} >78 MPa $(m)^{1/2}$ $J_{2\,mm}$ > 88.1 kN/m statistical requirement)
Minimum ligament thickness of the insert wall around square openings (dimension H in Figure 5-2)	Strength and stability	Collapse load is directly ruled by the weakest load carrying member of the insert	10 mm deviation from nominal value
Ultimate elongation of copper	Risk of rupture	Important but adequate in practice	≥ 40% in uniaxial tests
Creep ductility of copper	Risk of creep rupture	Important	≥ 15%
Cold work copper	Reduce creep ductility	Important	Requires further investigations
Gap dimensions between insert and copper shell	Limits the plastic or creep deformation of the copper shell	Sensitive and important, but strictly set tolerances keep the effect within acceptable limits	Axial gap 1.7–3.1 mm, radial 1.25–2.0 mm
Wall thickness of copper shell	Corrosion resistance	Non-dimensioning in the Design analysis	Nominal 5 cm

9 Summary

The mechanical strength of the canister (BWR and PWR types) has been studied. The loading processes are taken from the design premises report /SKB 2009/ and some of them, especially the uneven bentonite swelling cases, are further developed in this study and in its references. The canister geometry is described in detail including the manufacturing tolerances of the dimensions. The canister material properties are summarised and the wide material testing programmes and model developments are referenced.

The combination of various load cases are rationalised and the conservative combinations are defined. Also the probabilities of various load cases and combinations are assessed for setting reasonable safety margins. The safety margins are used according to ASME Code principles for safety class 1 components.

The governing load cases are analysed with 2D- or global 3D-finite-element models including large-deformation and non-linear material modelling and, in some cases, also creep. The integrity assessments are partly made from the stress and strain results using global models and partly from fracture resistance analyses using the sub-modelling technique. The sub-model analyses utilize the deformations from the global analyses as constraints on the sub-model boundaries and more detailed finite-element meshes are defined with defects included in the models together with elastic-plastic material models. The J-integral is used as the fracture parameter for the postulated defects. The allowable defect sizes are determined using the measured fracture resistance curves of the insert iron as a reference with respective safety factors according to the ASME Pressure Vessel Code requirements.

Based on the BWR canister analyses, the following conclusions can be drawn. The 45 MPa isostatic pressure load case shows very robust and distinct results in that the risk for local collapse is vanishingly small (10^{-50}) according to /SKBdoc 1207426/. The probabilistic analysis of plastic collapse only considers the initial local collapse of the ligament. This is a conservative assumption since the final collapse of the insert will be at a much higher external pressure. Further, the copper shell will remain intact after such expected events despite that a number of worst case events are taken into account. The corresponding analyses for PWR are not yet completed, as relevant test data for PWR material are not yet available. In general the design of the PWR inserts is more robust than the BWR inserts. The analyses of the BWR copper shell are also valid for the PWR case.

For the shear load case the stresses and strains in the canister are high, depending on the shear amplitude, shear angle and the intersection point. The governing case for the insert is perpendicular to the canister main axis at about ¾ of its length while the governing case for the copper shell is 22.5º to the main axis.

The corrosion protection layer, the copper shell, is made of soft (hot-deformed) copper and thus its ability to tolerate deformation is especially high. The design case of the 5 cm rock shear leads to equivalent plastic strains typically between 5 and 23%, predominantly in locations of geometrical discontinuities (or even at geometric singularities). This observation applies directly to the short term analysis and roughly the same results also apply to the creep analysis. This means that creep has no important role in the rock shear case and that the plastic and creep elongation in copper is so high that the copper shell will manage the applied deformation. The insert also experienced slight plastic deformation due to shear load, but the effective stress remained below the ultimate tensile stress even in and around geometric discontinuities; thus no damage is expected.

The combined load of isostatic pressure and rock shear is also analysed in /Hernelind 2010/ in two alternative sequences; either the glacial load is existing prior and during the rock shear or it is introduced after the rock shear. The results show that in both cases the maximum von Mises stress in the insert is slightly increased and the maximum plastic strain in copper shell is also slightly increased, if compared to rock shear case without additional glacial pressure load. However, in both analysed cases the maximum principal stress (in tension) was decreased. This means that the damage tolerance of the insert is increasing, if we have pressure loads combined with the rock shear case. This can easily be understood from the fact that external pressure load adds compressive stresses in all orientations in the insert and this decreases the maximum tension stress level caused by the bending of rock shear case. Thus the allowable faults become larger, if the isostatic pressure load is on when the rock shear takes place. The insert maintains its pressure-bearing properties also to all postulated isostatic loads acting during or after a rock shear case.

The damage tolerance analysis for the different load cases leads to a number of requirements on inspection of the insert where the most rigorous requirements are derived from the shear load case. The inspection requirements from the 45 MPa case are however more modest. For the copper shell it is important to avoid even smaller impact damage or other cold work in the regions of the bottom and lid in order not to jeopardize the creep ductility, this most likely needs to be confirmed by appropriate inspections. The lifting safety puts very modest requirements on inspection of the lifting flange.

The asymmetric loads that may exist due to the uneven wetting process during the first decades and due to density or geometry variations of the bentonite buffer later in the saturated condition were shown not to be a governing load case.

When using established methods, and some newly developed analysis methods (e.g. creep), it is shown that the reference BWR canister can withstand all given load cases in the design premises with moderate safety factors. The canister has also been shown to have a good tolerance against material defects.

For the PWR reference canister it can be stated that the design seems acceptable, since the construction gives lower stresses and strains compared to BWR. However, due to lack of extensive statistical material data for PWR inserts, this cannot yet be established for certain. Thus more production trials and material-testing are needed for the PWR type inserts.

10 References

SKB's (Svensk Kärnbränslehantering AB) publications can be found at www.skb.se/publications. References to SKB's unpublished documents are listed separately at the end of the reference list. Unpublished documents will be submitted upon request to document@skb.se.

Andersson-Östling H C M, Sandström R, 2009. Survey of creep properties of copper intended for nuclear waste disposal. SKB TR-09-32, Svensk Kärnbränslehantering AB.

ASM handbook, 1990. Vol. 2, Properties and selection: nonferrous alloys and special-purpose materials. 10th ed. Materials Park, Ohio: ASM International.

ASME Boiler & Pressure Vessel Code, 2004. Section VIII – Pressure Vessels – Division 2 – alternative rules. New York, NY: American Society of Mechanical Engineers.

ASME Boiler & Pressure Vessel Code, 2008a. Section III – Rules for construction of nuclear power plant components – Divisions 1 and 2. New York, NY: American Society of Mechanical Engineers.

ASME Boiler & Pressure Vessel Code, 2008b. Section XI – Rules for inservice inspection of nuclear power plant components. New York, NY: American Society of Mechanical Engineers.

Börgesson L, Dueck A, Johannesson L-E, 2010. Material model for shear of the buffer. Evaluation of laboratory test results. SKB TR-10-31, Svensk Kärnbränslehantering AB.

Deng D, Murakawa H, 2006. Numerical simulation of temperature field and residual stress in multipass weld in stainless steel pipe and comparison with experimental measurements. Computational Materials Science, 37, pp 269–277.

Dillström P, Bergman M, Brickstad B, Zang W, Sattari-Far I, Andersson P, Sund G, Dahlberg L, Nilsson F, 2008. A combined deterministic and probabilistic procedure for safety assessment of components with cracks – Handbook. SSM 2008:01, Strålsäkerhetsmyndigheten.

Dillström P, 2010. Damage tolerance analysis of canister inserts for spent nuclear fuel in the case of an earthquake induced rock shear load. SKB TR-10-29, Svensk Kärnbränslehantering AB.

Dillström P, Alverlind L, Andersson M, 2010. Framtagning av acceptanskriterier samt skadetålighetsanalyser av segjärninsatsen. SKB R-10-11, Svensk Kärnbränslehantering AB.

Hernelind J, 2010. Modelling and analysis of canister and buffer for earthquake induced rock shear and glacial load. SKB TR-10-34, Svensk Kärnbränslehantering AB.

Jin L-Z, Sandström R, 2008. Creep of copper canisters in power-law breakdown. Computational Materials Science, 43, pp 403–416.

Jin L-Z, Sandström R, 2009a. Modified Armstrong-Frederick relation for handling back stresses in FEM computations. In: Shibli I A, Holdworth S R (eds). Creep & fracture in high temperature components – design & life assessment issues. Proceedings of the 2nd international ECCC conference. Dübendorf, 21–23April 2009, pp 836–847.

Jin L-Z, Sandström R, 2009b. Non-stationary creep simulation with a modified Armstrong-Frederick relation applied to copper canisters. Computational Materials Science, 46, pp 339–346.

Martin O, Nilsson K-F, Jakšić N, 2009. Numerical simulation of plastic collapse of copper cast-iron iron canister for spent nuclear fuel. Engineering Failure Analysis, 16, pp 225–241.

Nilsson K-F, Lofaj F, Burström M, Andersson C-G, 2005. Pressure tests of two KBS-3 canister mock-ups. SKB TR-05-18, Svensk Kärnbränslehantering AB.

Sandström R, Andersson H C M, 2007. Creep during power-law breakdown in phosphorus alloyed copper. In: Hasegawa K, Scarth D A (eds). Proceedings of the ASME Pressure Vessels and Piping/Creep8 Conference. San Antonio, Texas, 22–26 July 2007. New York, NY: American Society of Mechanical Engineers, p 4.

Sandström R, Andersson H C M, 2008. Creep in phosphorus alloyed copper during power-law breakdown. Journal of Nuclear Materials, 372, pp 76–88.

Sandström R, Hallgren J, Burman G, 2009. Stress strain flow curves for Cu-OFP. SKB R-09-14, Svensk Kärnbränslehantering AB.

SKB, 2009. Design premises for a KBS-3V repository based on results from the safety assessment SR-Can and some subsequent analyses. SKB TR-09-22, Svensk Kärnbränslehantering AB.

SKB, 2010. Design, production and initial state of the canister. SKB TR-10-14, Svensk Kärnbränslehantering AB.

Wu R, Seitisleam F, Sandström R, 2009. Creep properties of phosphorus alloyed oxygen free copper under multiaxial stress state. SKB R-09-41, Svensk Kärnbränslehantering AB.

Yao X, Sandström R, 2000. Study of creep behaviour in P-doped copper with slow strain rate tensile tests. SKB TR-00-09, Svensk Kärnbränslehantering AB.

Unpublished documents

SKBdoc id, version	Title	Issuer, year
1040347 ver 1.0	X-ray diffraction measurements of residual stresses in welded copper canister lids	CSM Materialteknik, 2005
1040350 ver 1.0	X-ray diffraction measurements of residual stresses in welded copper canister lids	CSM Materialteknik, 2004
1072169 ver 1.0	Residual stress measurement according to ASTM E837	SP Technical Research Institute of Sweden, 2007
1173031 ver 1.0	Compression experiments addressing canister inserts I24 and I25: interim report	JRC, 2004
1175208 ver 5.0	Tillverkning av kapselkomponenter	SKB, 2010
1177857 ver 1.0	Designanalys av stållock till kapsel för använt kärnbränsle – geometriuppdatering	Inspecta, 2009
1187725 ver 1.0	Fracture toughness testing of copper cylinder T31 and lid weld FSWL27	Bodycote, 2008
1196484 ver 2.0	Restspänningar i kopparkapselns locksvets	SKB, 2009
1201865 ver 1.0	Dragprovning av gjutjärn. KTH PM SKB0903c	KTH, 2009
1203550 ver 1.0	Brottmekanisk provning av gjutjärn. KTH PM SKB0903	KTH, 2009
1203875 ver 1.0	Ritningsförteckning	SKB, 2009
1205273 rev 2.0	Intryck i koppar	SKB, 2009
1206868 ver 1.0	Damage tolerance analysis of the copper shell in PWR and BWR canisters during handling of the entire canister	Inspecta, 2009
1206894 ver 1.0	Uneven swelling pressure on the canister – simplified load cases derived from uneven wetting, rock contours and buffer density	SKB, 2009
1207426 ver 1.0	Updated probabilistic analysis of canister inserts for spent nuclear fuel Inspecta	Inspecta, 2009
1207429 ver 1.0	Canister bottom structural integrity	Inspecta, 2009
1207576 ver 2.0	Test of mechanical properties on cast iron inserts for encapsulation of nuclear waste, summary report	SKB, 2009
1208266 ver 1.0	Residual stress measuring by incremental hole drilling technique	SP Technical Research Institute of Sweden, 2009